NASA TECHNICAL
MEMORANDUM

NASA TM X-52579

CADMIUM SULFIDE THIN-FILM
SOLAR CELL REVIEW

June 11-12, 1968
NASA Lewis Research Center
Cleveland, Ohio

CADMIUM SULFIDE THIN-FILM

SOLAR CELL REVIEW

June 11-12, 1968

NASA Lewis Research Center
Cleveland, Ohio

Edited by

A. F. Forestieri
A. E. Spakowski
H. W. Brandhorst, Jr.

PREFACE

In June 1968 a review meeting was held at the Lewis Research Center. Personnel from Clevite Corporation, Lincoln Laboratories and Lewis were present. The purpose of the meeting was to review the data and results of a program on CdS thin-film solar cells, discuss the significance of those results and revise the program to incorporate new ideas.

The purpose of this report is to record the information and opinions presented in the meeting. The editors did not attempt to check back with the attendees on whether or not their opinions had changed during or since the meeting. Opinions and interpretations expressed at the meeting may not have been subscribed to by other participants, and may not be held any longer even by the originator. Also, there was no attempt to make a coherent, consistent point of view through editing. Prepared text by the session reporters is presented herein; discussion and across-the-table talk is not included. The organization of this report follows the agenda.

CONTENTS

E-5000

I. INTRODUCTION

D. T. Bernatowicz, NASA-Lewis

The NASA-Lewis Research Center has sponsored both internal and contractual programs on cadmium sulfide thin-film solar cells since 1961. The interest in CdS is based primarily on the low cost potential of the cells. However, flexibility, light weight and radiation resistance are other considerations. Since the first CdS thin-film solar cells were made, the efficiency of the cells has increased steadily. Presently, cells can be made with about 55 cm^2 area with an efficiency of 3.5 percent AMO, 25° C, Kapton covered.

In September 1967, the results of the programs on CdS were reviewed. The programs were then redirected to attempt to uncover the cause or causes for the erratic behavior observed in cadmium sulfide thin-film solar cells. Some of the phenomena observed were: the cells degraded and sometimes recovered; there was a large amount of scatter in the data; cells were not reproducible. The most likely cause for these observations was attributed to mechanical faults in the cells, and the most likely suspect was the grid attachment. The redirected program plan included: maintain a "standard" cell design for the pilot line production so as not to introduce new variables by design changes; improve cell reproducibility by improved quality control and standardized fabrication techniques; check and improve measurement techniques; design experiments and special cells to determine the effect of grid attachment; attempt to determine the electronic model for electrical behavior of the cell; use new diagnostic techniques to characterize the cell and search for degradation causes.

Since the program review much new data has been obtained and many new diagnostic techniques have been developed. The purpose of this meeting is to review and discuss the results, decide on new tests and approaches and determine if a better understanding of the CdS solar cell problem has been achieved.

II. STATUS OF CELL MANUFACTURING

F. A. Shirland, Clevite

The present design of the CdS thin-film solar cell as fabricated by
Clevite has been in use for about two years. The pilot line began producing
the cells at a rate of 5 cells per day. The production rate increased
steadily and about eighteen months ago the cells were placed on the open
market. At that time the maximum rate was 20 cells per day.

About one year ago revisions were made in the pilot line to allow a
production rate of 100 cells per day. However the average rate achieved
has been between 20 and 30 cells per day. In this interim more inspection
steps were included in the pilot line and some quality control steps were
added. Work on improving the efficiency of the cells and cost reduction
were not emphasized; instead, more work was done on cell stability problems.

Figure 1 is a histogram giving the distribution of cell efficiencies
for 563 Kapton covered cells produced for NASA from December 1966 to Decem-
ber 1967. The cells were tested at 25° C AM1 sunlight equivalent. The
efficiencies given in figure 1 should be reduced by about 30 percent to
obtain AM0, 60° C test conditions. Figure 2 is a histogram for 508 cells
produced from December 1967 to May 1968. Table I indicates the yields
obtained from the pilot line for the past eighteen months. CdS film starts
and cell rejects are listed. The major cause for rejection was due to pin-
holes in the CdS films. In the gridding and laminating operation the major
cause for rejection was because of voids in the epoxy cement used to attach
the cover plastic. At final testing cells were rejected for low output,
electrical shorts, and cosmetic reasons.

Figure 3 shows the fabrication steps and inspection points in the pro-
duction of CdS thin-film solar cells. There are six major steps in the
fabrication process. These are 1) substrate preparation, 2) cadmium sulfide
evaporation, 3) barrier formation, 4) grid attachment, 5) cover plastic
attachment, and 6) final cell preparation. Quality assurance inspections
are carried out by a full time inspector and these steps are indicated in
figure 3. The steps where the inspection is done by the pilot line operators
are also indicated.

TABLE I

YIELDS FROM STANDARD CELL FABRICATION LINE
3" x 3" CELLS
For NASA, Lewis Research Center

Month	CdS Film Evap Total	Rejects	Barriers Total	Rejects	Grid & Laminate Total	Rejects	Final Testing Total	Rejec
1967								
1	164	3	161	22	139	1	138	37
2	195	12	183	7	176	5	171	70
3	271	16	255	18	237	15	222	122
4	267	42	225	44	181	4	177	77
5	366	93	273	27	246	7	239	139
6	412	60	352	13	339	14	325	225
7	313	64	249	53	196	8	188	108
8	240	1	239	27	212	21	191	91
9	178	0	178	36	142	6	136	36
10	144	0	144	14	130	0	130	30
11	302	14	288	85	203	0	203	38
12	248	9	239	65	174	3	171	33
Total	3100	314 10%	2786	411 15%	2375	84 4%	2291	1006 44%
1968								
13	310	22	288	140	148	3	145	45
14	458	63	395	156	239	8	231	131
15	306	3	303	147	156	10	146	46
16	432	0	432	155	277	15	262	162
17	515	3	512	145	367	0	367	267
Total	2021	91 5%	1930	743 38%	1187	36 3%	1151	651 57%

DISTRIBUTION OF STANDARD
PROCESS CELL EFFICIENCIES FOR
KAPTON COVERED 3"X3" CELLS
FABRICATED OVER 12 MONTH
PERIOD.

TESTED AT 25°C, AM I SUNLIGHT
EQUIVALENT.

CALENDAR YEAR 1967
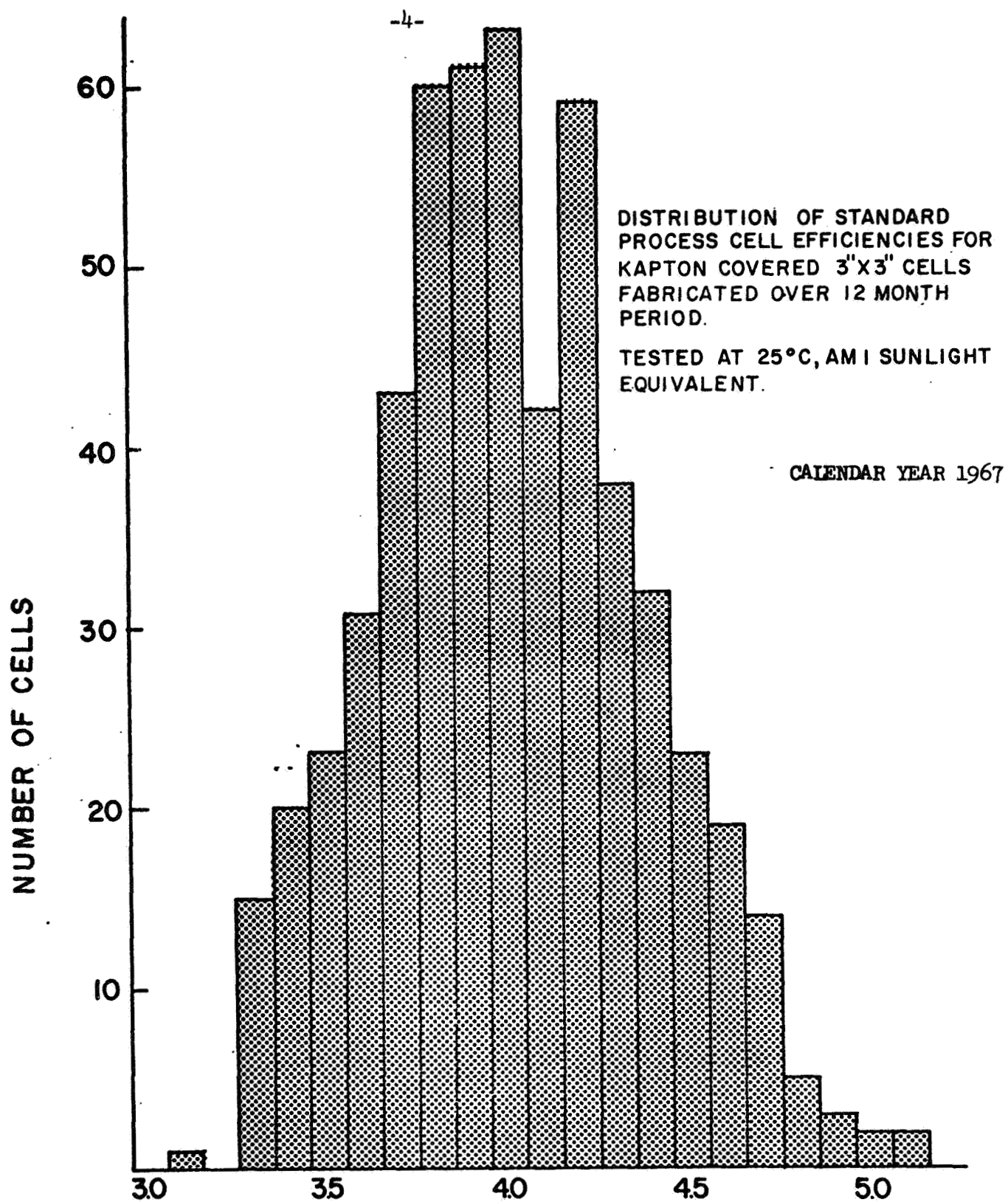
STANDARD PROCESS CELL EFFICIENCIES – KAPTON CELLS.

FIGURE 1

Distribution of Standard
Process Cell Efficiencies for
Kapton Covered 3" x 3" Cells
Fabricated over 5 Month Period
in 1968

Tested at 25°C, AM1
Sunlight Equiv.
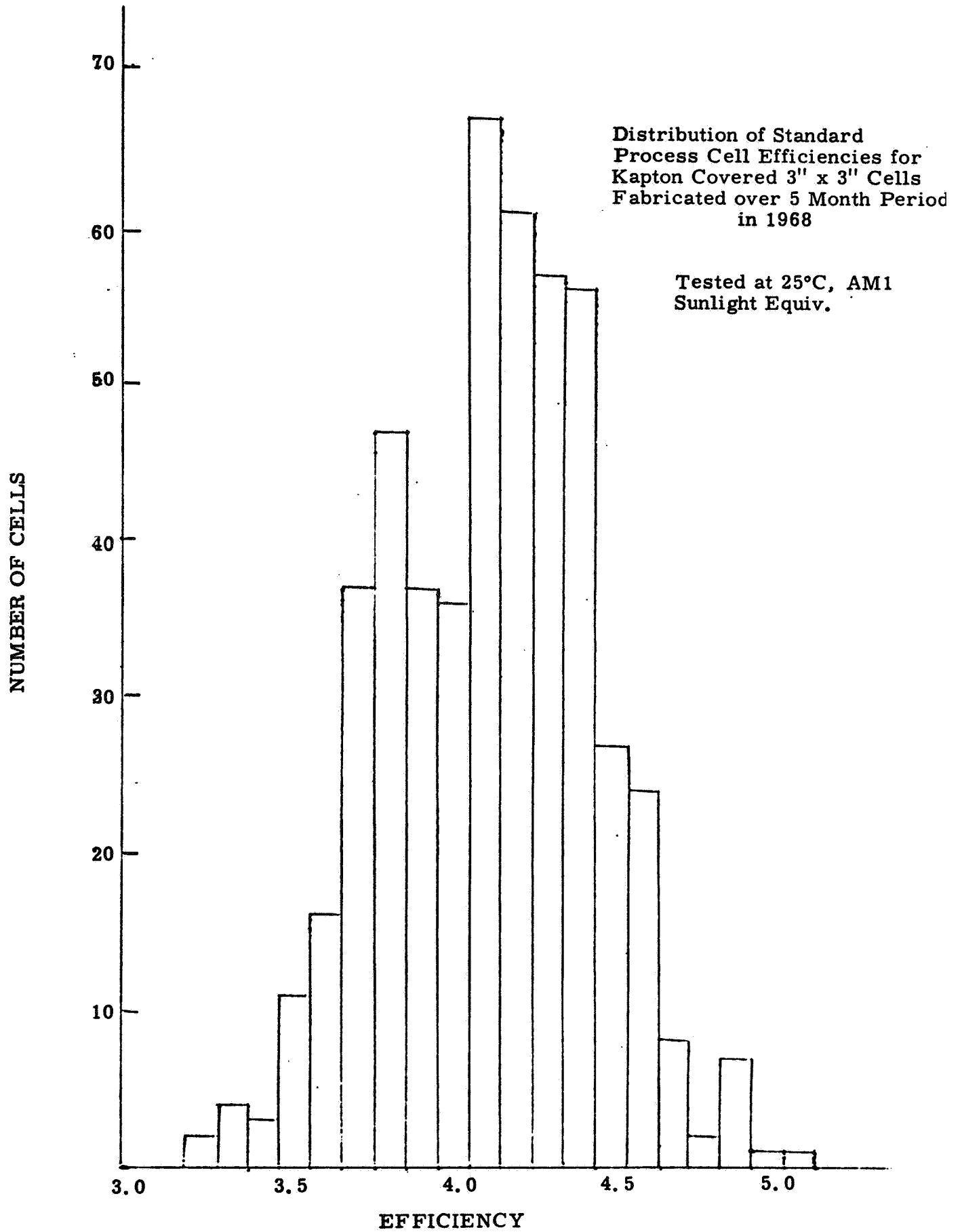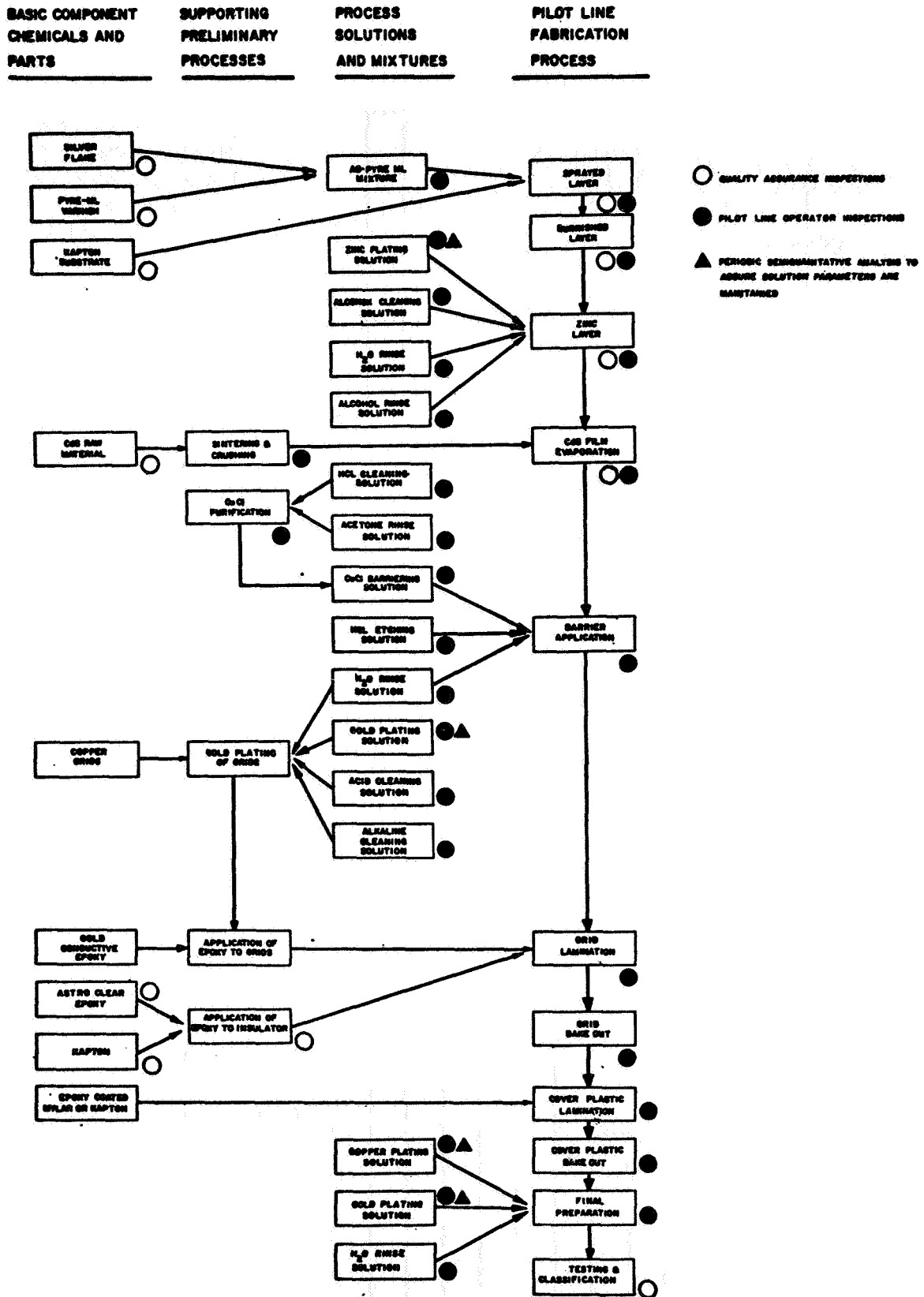
NUMBER OF CELLS

EFFICIENCY

FIGURE 2

FIGURE 3

FABRICATION STEPS AND INSPECTION POINTS

III. FUNDAMENTAL MEASUREMENTS AND MECHANISM

MECHANISM

H. W. Brandhorst, Jr., NASA-Lewis

One of the major steps in the fabrication of high efficiency CdS cells is a heat treatment at 250° C for two minutes. During this heat treatment copper will diffuse from the Cu_2S layer into the CdS layer. It was of interest, therefore, to examine that copper diffused region of the cell shown in figure 4. The only technique that can easily be used to examine this region is to measure the capacitance of the cell as a function of applied bias.

As shown in figure 5 two parameters of interest can be determined from such measurements. Equation 1 shows that the thickness of the depletion region (equivalent to the depth in the CdS layer) is inversely proportional to the capacitance. From equation 2, the impurity concentration, N_D, at any depth for any doping profile can be simply obtained from the slope of a plot of $1/C^2$ versus applied bias for any given depth λ. Finally, if the layer is uniformly doped, the barrier height, V_D, is obtained by extrapolation of the $1/C^2$ versus V plot to its intercept with the voltage axis.

Capacitance-voltage plots for the CdS cell are rather difficult to make, requiring that approximately 100 ma of current be passed through the cell in the forward direction for several hours before reproducible curves can be obtained. A large number of cells failed to complete the measurement cycle because of this extreme treatment. However, when cells did pass this "conditioning," capacitance-voltage plots such as shown in figure 6 were obtained. The curve is complex showing two distinct linear regions. It is therefore necessary to analyze the curve with equation 2 of figure 5.

A typical impurity profile so obtained is shown in figure 7. Copper is an acceptor in CdS and will reduce the carrier concentration. This is clearly shown in figure 7 as the carrier concentration has been decreased from about 2.6×10^{18} cm^{-3} to 8.5×10^{15} by the infusion of copper during the heat treatment. The profile is quite abrupt and the interface comes

at a depth of about 0.26 μm. This corresponds well to the depth expected from diffusion coefficients determined by Shiozawa.

In order to show that the profile occurred as a result of the heat treatment, the cell was heated for 10 minutes at 200° C and the profile shifted as shown in figure 8. Two things are noteworthy in this figure -- first, the interface moved to a greater depth and second, the degree of compensation of the CdS layer also increased. Copper diffusion in the CdS would cause both of these effects.

A study was also made of the effect of various wavelengths of light on this impurity distribution and the data are tabulated in figure 9. Essentially identical profiles are obtained in the dark and under illumination by infrared light (0.8 to 1.2 μm). However, when white light or intense blue light is used the profile changes drastically. It can be seen that the strongly absorbed blue light (or the blue region of white light) reduces the amount of compensation of the CdS. Because the compensation decreases, the resistance of the copper doped CdS layer should also decrease. This means that the measured properties of the cell will strongly depend on the spectrum of the illuminating source.

This is clearly shown in figure 10 where the I-V curve of a cell has been measured under equal intensities of infrared (0.8-1.2 μm) and white light. Under red illumination the series resistance of the cell is considerably greater than under white light as expected from the data of figure 9. This effect can also be seen from figure 11 which shows spectral responses as measured under no additional illumination and under 20 mw/cm^2 white illumination. The known trap behavior of copper in CdS plus the effect of white (or blue) light on the compensation of the CdS explain the effects seen in this figure. It is quite necessary, therefore, to measure all spectral responses under intense white light bias to obtain reproducible curves.

From the carrier profiles obtained from the capacitance measurements and from Hall data it is possible to assemble a band structure for the Cu$_2$S-CdS heterojunction as shown in figure 12. The bulk CdS layer has a carrier concentration between 10^{17} - 10^{18} cm^{-3}. The capacitance data

indicate about 10^{18} cm^{-3} while Hall data show about 10^{17} cm^{-3}. It is
possible that the capacitance data are high because the area factor of the
cell is hard to determine. The geometric area may be too small by a factor
of 2-3 because of the many convolutions formed in the film by the etching
process. The capacitance data has therefore been reduced to correspond to
Hall measurement for the band structure of figure 12. The Fermi level in
the bulk CdS lies about 0.08 eV below the conduction band. In the next
region where the copper compensation has taken place the Fermi level is
about 0.24 eV below the conduction band and essentially all the band bending
in the junction region takes place in this layer. The amount by which the
bands are bent is the barrier voltage, V_D, and equals about 0.85 V. This
figure was obtained by extrapolation of the capacitance-voltage plot to
intercept the voltage axis. A value for V_D of 0.87 V is obtained from
the data of figure 6.

The remaining two regions of the band structure occur in the Cu_2S
layer. No extreme discontinuities have been shown at the interface because
data on electron affinities in Cu_2S are lacking. The Cu_2S layer is about
0.3 μm thick and is formed by chemical reaction in an aqueous bath of Cu^+
ions. Because of this type of forming process, some Cd^{++} ions are left in
the Cu_2S after the dip and some more probably diffuse into the Cu_2S from
the CdS on heating. Cd^{++} will compensate the Cu_2S layer and it has been
estimated that the Fermi level in the Cu_2S:Cd region is about 0.1 eV above
the valence band. The bulk of this layer is $p + Cu_2S$ with a carrier con-
centration of about 10^{20} cm^{-3} thus pinning the Fermi level essentially at
the valence band edge. The band gap of Cu_2S is 1.2 eV and it is quite
certain that it is this layer which is responsible for the response of the
cell to energies lower than the CdS band gap. Further confirmation comes
from the onset of response in the red at about 1.0 corresponding to the
band gap of Cu_2S. Also, from the absorption coefficients of Cu_2S it can
be seen that a layer 0.3 μm thick absorbs nearly 90 percent of the incident
light. It is therefore apparent that the cell could more aptly be called
a "Cu_2S cell" and indicates that considerable additional effort should be
devoted to studying this layer to obtain further improvement in the cell.

PLASTIC COVER

METAL
COLLECTOR
GRID

$p^+ Cu_2S$

≤ 0.5 μm

COPPER DIFFUSED
REGION

METALLIZED
KAPTON SUBSTRATE
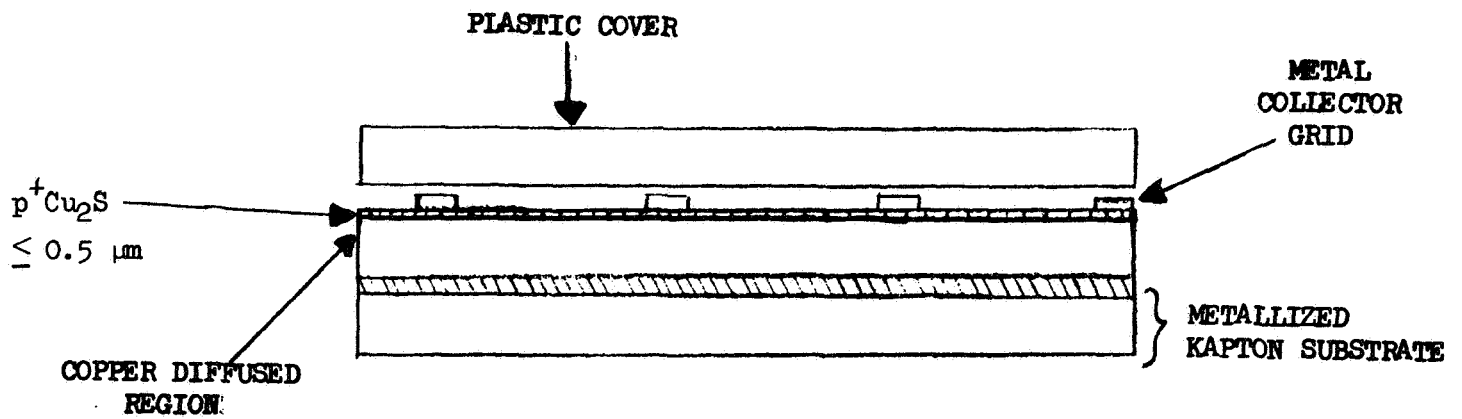
FIGURE 4.   CROSS SECTION OF CADMIUM SULFIDE
THIN-FILM SOLAR CELL

1. DEPTH INTO CdS , λ

$$\lambda = \frac{K\epsilon_o A}{C}$$

K = DIELECTRIC CONSTANT

ϵ_o = VACUUM PERMITTIVITY

A = CELL AREA

C = CAPACITANCE

2. IMPURITY CONCENTRATION (ANY DOPING PROFILE), $N_{D,A}$

$$\frac{d\,\dfrac{1}{(C/A)^2}}{dV} = \frac{2}{K\epsilon_o e N_{D,A}}$$

3. BARRIER HEIGHT (UNIFORM DOPING PROFILE), V_D

$$N_{D,A} = \frac{2}{K\epsilon_o e}\,(V_D - V)(C/A)^2$$

FIGURE 5. EQUATIONS GOVERNING CAPACITANCE MEASUREMENTS
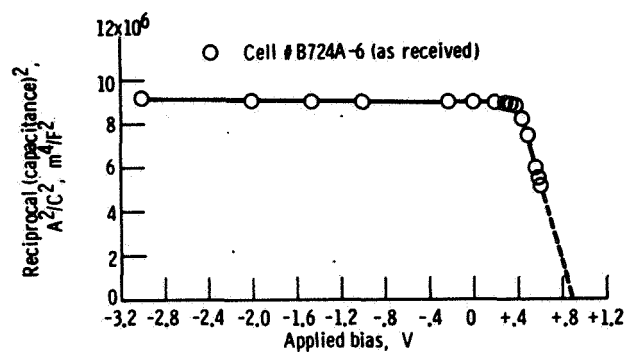
Figure 6 - Capacitance-voltage plot for Cu₂S-CdS thin film solar cell.
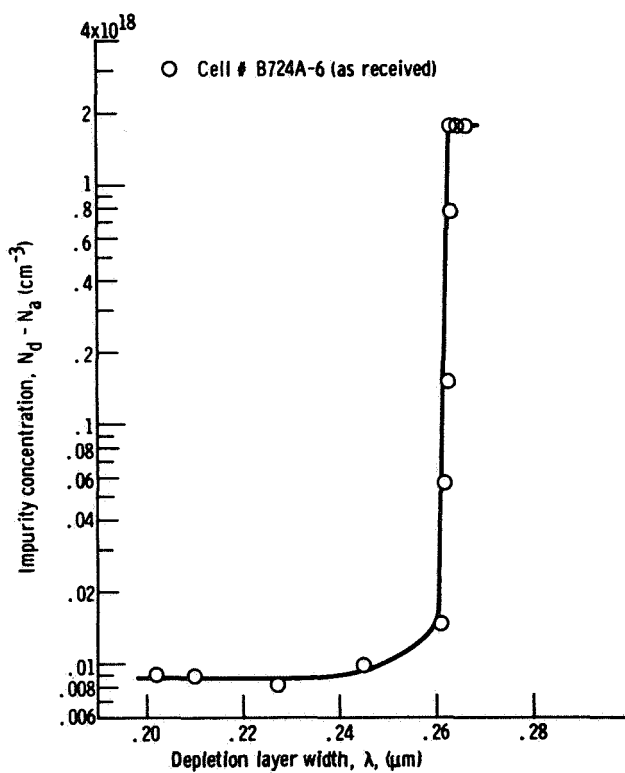
Figure 7 - Impurity distribution in the CdS layer.

Figure 9 - Effect of illumination on the impurity distribution in the CdS layer.

Cell # B724A-1

○ No illumination
□ Blue light (5 mw/cm²)
◇ White light (20 mw/cm²)
△ Infrared light (10 mw/cm²)

Impurity concentration, $N_d - N_a$ (cm^{-3})

Depletion layer width, λ, (μm)

Figure 8 - Effect of heat treatment on the impurity distribution in the CdS layer.

Cell # B724A-6

○ (As received)
□ (Heated 10 min at 200° C)

Impurity concentration, $N_d - N_a$ (cm^{-3})

Depletion layer width, λ, (μm)

FIGURE 10. CURRENT-VOLTAGE CURVES OF CdS CELL ILLUMINATED
WITH RED AND WHITE LIGHT
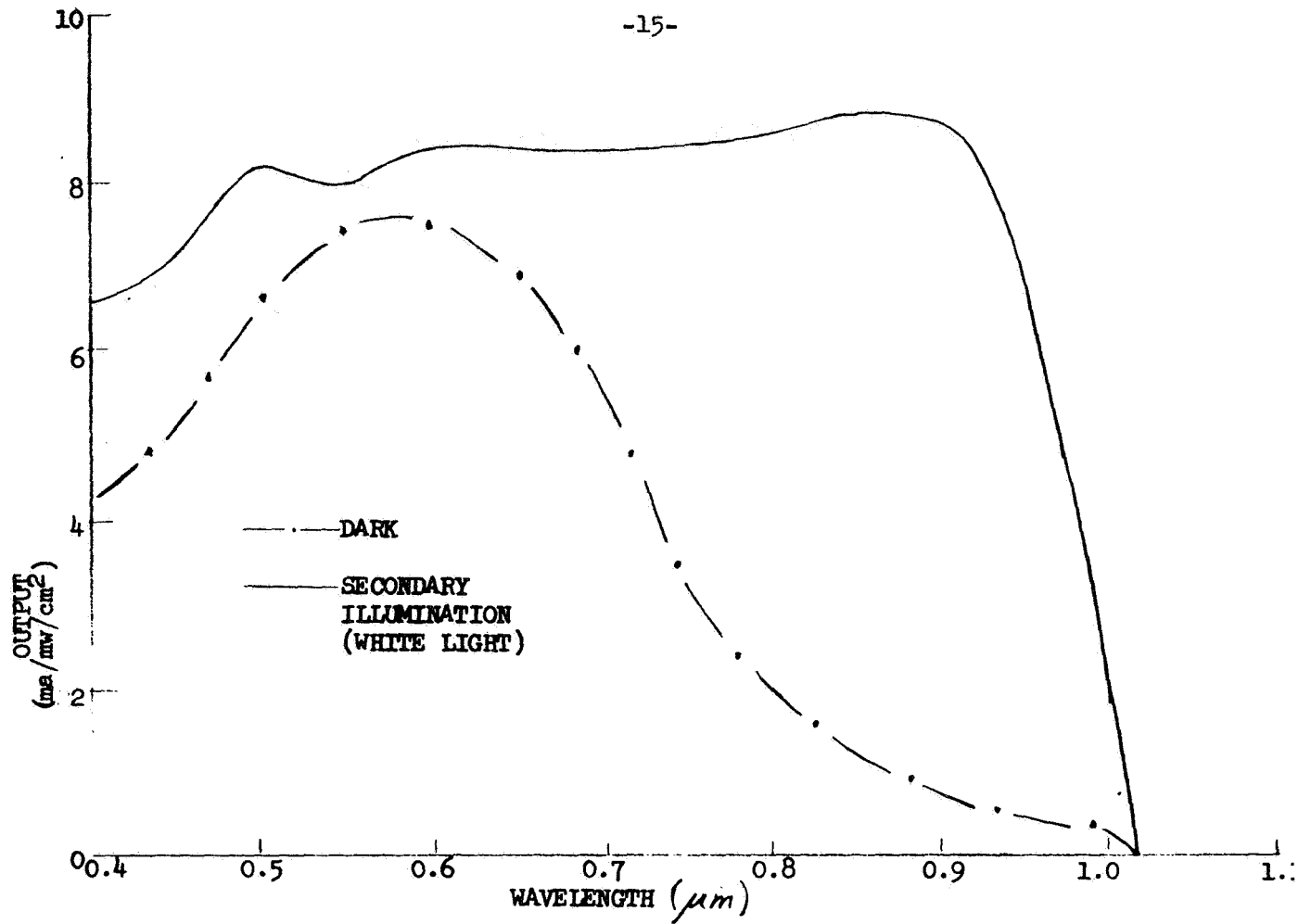
FIGURE 11. SPECTRAL RESPONSE OF A TYPICAL CdS CELL
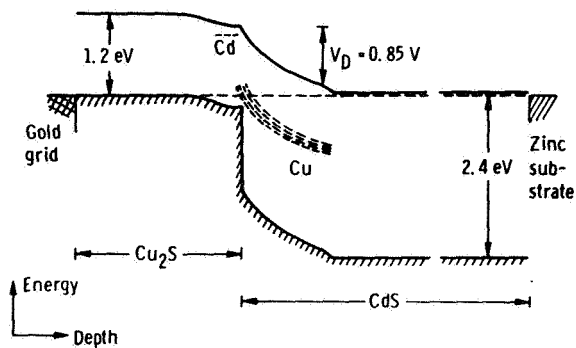
Figure 12 Band structure for the Cu_2S-Cds heterojunction.

MECHANISM OF THE PHOTOVOLTAIC EFFECT IN
HIGH EFFICIENCY CdS THIN-FILM SOLAR CELLS

L. R. Shiozawa, Clevite

We have proposed[1-4] a physical model to explain the operation of the CdS solar cell. Earlier arguments have been strengthened by new experimental findings. The strong photovoltaic response in the extrinsic range of CdS is shown to arise from intrinsic absorption of light in a thin surface layer of epitaxially formed p-type Cu_2S. The minority electrons generated in this layer diffuse to and are collected by a Cu_2S:CdS heterojunction. The CdS immediately adjacent to the Cu_2S is compensated by Cu acceptors that diffuse into the n-type base layer during cell f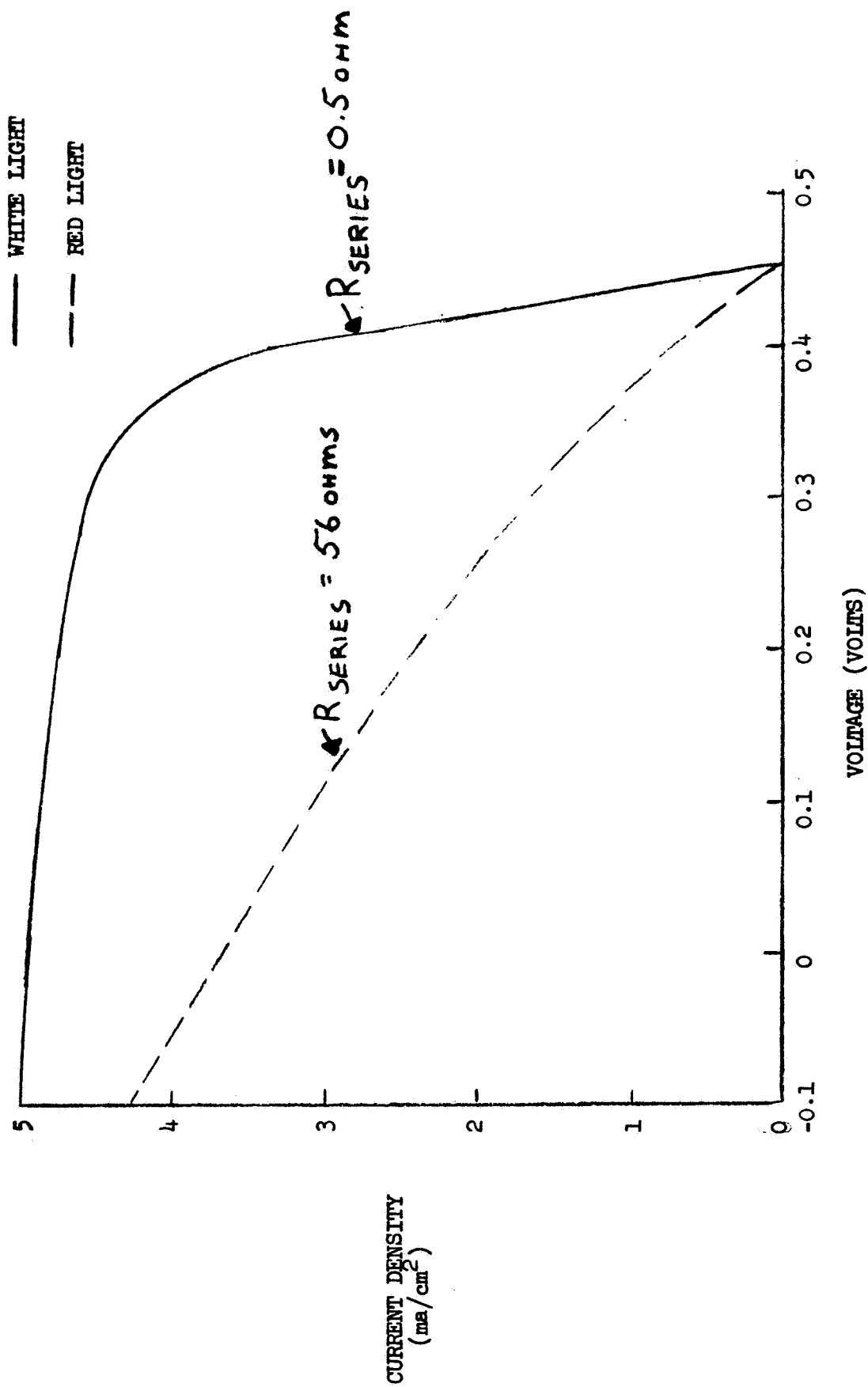abrication. Capacitance measurements indicate that this layer is approximately 0.5 µm thick, in agreement with independent measurements of Cu diffusion in CdS crystals. The strong photoconductivity of this dark-insulating layer accounts for the absence of appreciable series resistance under strong illumination and also accounts for the wavelength dependence of the observed enhancement effects of biasing light.

Absorption measurements on CdS crystals saturated with Cu at 250° C show that the extrinsic absorption is much too weak to account for the

[1] Shiozawa, L. R.; Sullivan, George A.; and Augustine, Frank: Research on the Mechanism of the Photovoltaic Effect in High-Efficiency CdS Thin-Film Solar Cells. Clevite Corp.(ARL-67-0190,DDC No. AD-661557), Sept. 1967.

[2] Shiozawa, L. R.; Sullivan, George A.; and Augustine, Frank: Research on the Mechanism of the Photovoltaic Effect in High-Efficiency CdS Thin-Film Solar Cells. 5th Quart. Rep., Clevite Corp. (Contract AF33(615)-5224), Oct. 27, 1967.

[3] Shiozawa, L. R.; Sullivan, George A.; and Augustine, Frank: Research on the Mechanism of the Photovoltaic Effect in High-Efficiency CdS Thin-Film Solar Cells. 6th Quart. Rep., Clevite Corp. (Contract AF33(615)-5224), Dec. 15, 1967.

[4] Shiozawa, L. R.; Sullivan, George A.; and Augustine, Frank: Research on the Mechanism of the Photovoltaic Effect in High-Efficiency CdS Thin-Film Solar Cells. 7th Quart. Rep., Clevite Corp. (Contract AF33(615)-5224), Apr. 15, 1968.

observed photovoltaic current. On the other hand, measurements of the thickness of the Cu_2S layer ($\sim 3 \times 10^{-5}$ cm) and its absorption coefficients ($\sim 10^5$ cm^{-1}) demonstrate that approximately 90 percent of the photons in the solar spectrum, which have energy greater than the 1.2 eV band gap of Cu_2S, are absorbed in this layer. This is consistent with the near unity quantum efficiency observed in the visible range. The minority carrier (electron) diffusion length in Cu_2S is inferred to be $\sim 3 \times 10^{-5}$ cm from the observed decrease of the short-wave response relative to the long-wave response as the thickness of the Cu_2S layer is increased beyond this value. The electron-hole pairs created by the more energetic photons are generated closer to the surface of the Cu_2S and hence suffer more recombination losses than do those generated by the less energetic photons.

The barrier height between the p^+Cu_2S and the n-CdS base during illumination is estimated as ~ 0.8 eV from low temperature open circuit voltage measurements performed in this laboratory. Similar barrier heights have been inferred from capacitance versus voltage measurements performed at NASA[5]. The i-n CdS homojunction which prevails in the dark is almost erased under illumination due to the rise of the quasi-Fermi level of electrons in the compensated layer. The same effect gives rise to the Cu_2S-CdS heterojunction when the cell is illuminated.

Figure 13(a) shows a band structure for the Cu_2S-CdS heterojunction with an indicated barrier height of 0.85 eV. The open circuit voltage is shown as 0.49 volts as a reasonable maximum value obtained to date. Figure 13(b) shows the heterojunction between p-Si and n-CdS as reported by Okimura et al.[6] The reported V_{oc} is 0.50 volts and the barrier height is about 0.9 eV. This device makes a very useful intermediate between the Cu_2S-CdS heterojunction and the well understood silicon solar cell p-n homojunction shown in figure 13(c). In this case the barrier height is 1.0 eV and the observed open circuit voltage for 10 Ω-cm material is 0.55

---

[5]Data obtained by H. W. Brandhorst, NASA Lewis Research Center, Cleveland, Ohio.

[6]Okimura, Hiroshi; Kawakami, Masachika; and Sakai, Yoshio: Photovoltaic Properties of CdS-p·Si Heterojunction Cells. Jap. J. Appl. Phys., vol. 6, no. 7, July 1967, p. 908.

volts. With the existence of this chain of devices it is then reasonably possible to apply junction theory used in the silicon solar cell case to the Cu_2S-CdS heterojunction.

Figure 14 details the simplest diode equation applied to silicon solar cells. (I = current, I_L = light generated current, I_O = reverse saturation current, V = voltage, A = factor to fit simple diode equation to observed cases, generally A = 1 to 2 for good cells but can be as high as 4.) It can be seen that as the A value increases from 1 to 3 the efficiency will fall. (V_m = voltage at maximum power, I_m = current at maximum power, $S_{(m=o)}$ = input power at air mass = 0 (outer space).)

Using the diode equation of figure 14 it is useful to calculate the maximum efficiency to be expected for the Cu_2S-CdS heterojunction as detailed in figure 15. The assumptions necessary to this calculation are straightforward and are designed to eliminate all losses. The only empirical information required is the value of the open circuit voltage (0.5 V). The calculation was performed for air mass zero sunlight at 25° C and I_O was determined from the equation by setting $I = 0$ and $V = 0.5$ (V_{oc}). It can be seen that the maximum theoretical efficiency is 14.7 percent.

However, this calculation represents a rather unachievable goal so it is more desirable to compute the probable maximum achievable efficiency. If reasonable assumptions are made as to the minimum losses to be expected, and reasonable A values are used as shown in figure 16, the maximum achievable efficiency is 10.6 percent.

A comparison between the present 5 percent Kapton covered cell with this future 10 percent cell is shown in figure 17. It is assumed here that the voltage stays approximately the same, increasing from 0.48 to 0.50 volts and the A factor of 1.7 is unchanged. By reducing the reflection loss from 10 to 5 percent, the grid loss from 15 to 5 percent and absorption in the cover from 20 to 0 percent an increase in output of 50 percent would be obtained. Suitable anti-reflective coatings exist which could accomplish the first goal. The grid coverage could be reduced if the conductivity of the Cu_2S layer were increased. The reduction of the cover absorption must await better materials, however. By increasing the absorp-

tion efficiency from 80 to 90 percent and the collection efficiency from 80 to 90 percent a further increase in output of 20 percent is obtained. Because both these factors and the grid loss as mentioned earlier are directly related to the Cu_2S layer it is obvious that significant improvement in cell output can be achieved by a study of the Cu_2S layer. If, for example, the diffusion length of minority carriers in this layer could be doubled it is probable that most of these improvements could be realized. The final losses in the cell come from the shunt and series resistance. The shunt resistance must be improved from its present value between 10 and 100 ohms to over 1000 ohms and the series resistance reduced below 0.05 ohms. For earth surface operation (m = 1), the short circuit current density of the 10 percent cell will be 28 ma/cm^2 as compared to the present value of 14.3 ma/cm^2.

FIGURE 13

VOLTAGE

V_{oc}

$$I = I_L - I_o \left[e^{\frac{qV}{AkT}} - 1 \right]$$

$$EFF. = \frac{V_m I_m}{S (m=o)}$$
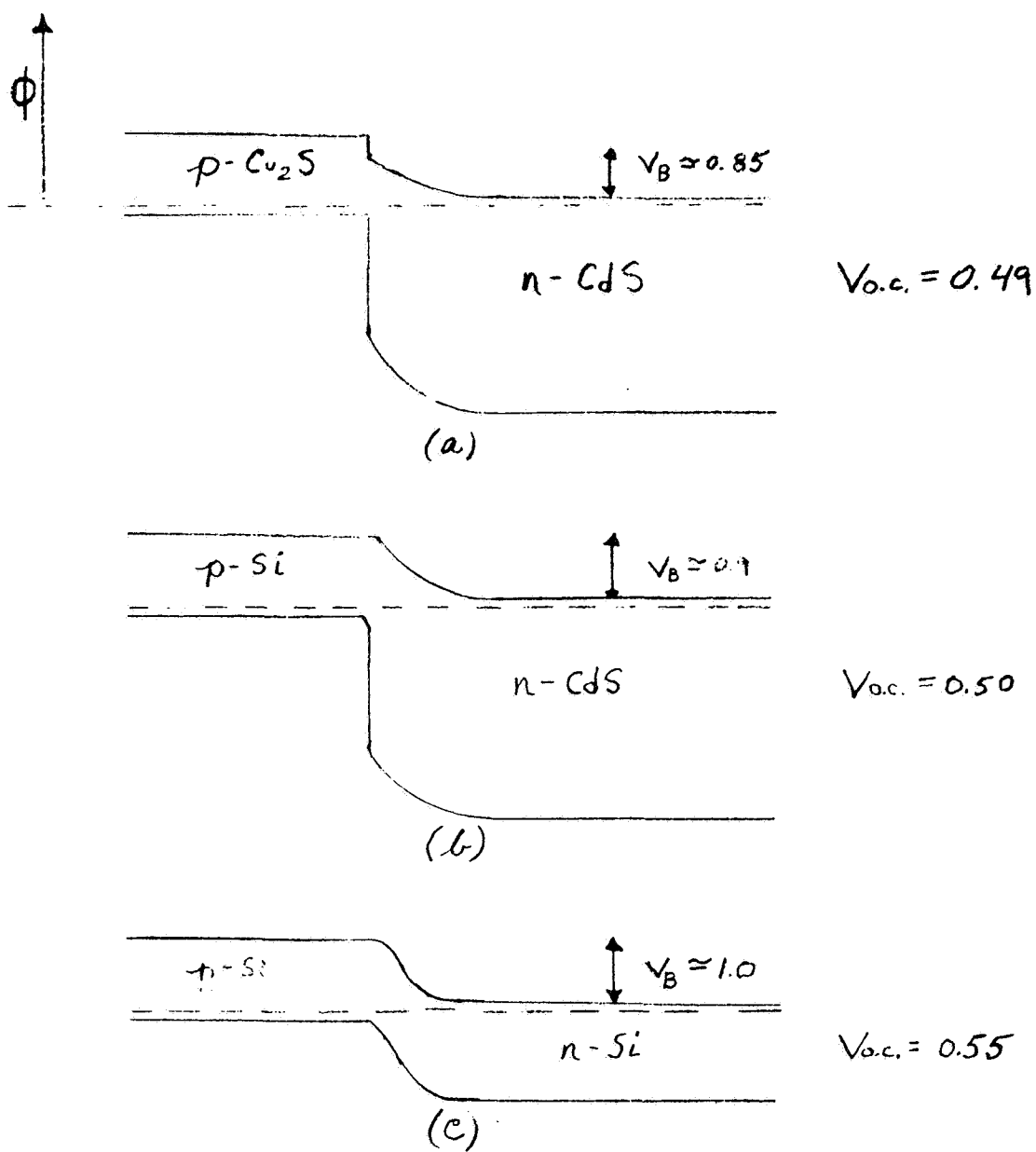
CURRENT
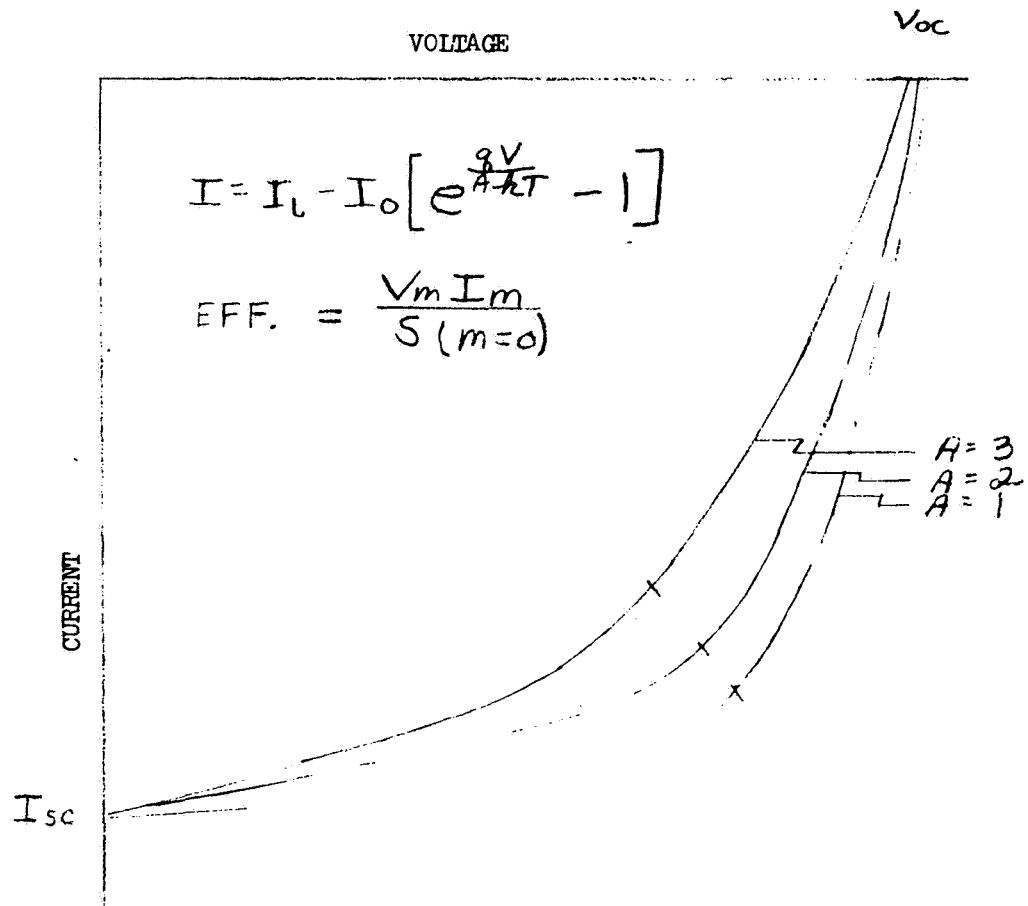
$A = 3$
$A = 2$
$A = 1$

I_{sc}

FIGURE 14

MAXIMUM THEORETICAL EFFICIENCY

14.7%

ASSUMPTIONS:

(1) REFLECTIONS AND GRID LOSSES = 0

(2) ALL PHOTONS $E > E_G$ (Cu_2S) ABSORBED

(3) 100% COLLECTION EFFICIENCY

(4) IDEAL DIODE, WITH A = 1

(5) NO ABSORPTION IN COVER

(6) m = 0, 25°C

(7) $V_{oc.}$ = 0.500

(8) R_s AND R_{sh} NEGLIGIBLE

FIGURE 15

MAXIMUM ACHIEVABLE EFFICIENCY

10.6%

ASSUMPTIONS:

(1) GRID LOSS = REFLECTION LOSS = 5%

(2) A-FACTOR = 1.70

(3) 95% ABSORPTION EFFICIENCY

(4) 95% COLLECTION EFFICIENCY

(5) COVER ABSORPTION = 0

(6) m = 0, 25°C

(7) $V_{o.c.}$ = 0.500

(8) R_s and R_{sh} NEGLIGIBLE

FIGURE 16

	PRESENT 5% KAPTON	FUTURE 10% CELL
V_{oc}	0.48	0.50
A-FACTOR	1.70	1.70
REFLECTION LOSS	10%	5%
GRID LOSS	15%	5%
COVER ABSORPTION	20%	0
ABSORPTION EFFICIENCY	80%	90%
COLLECTION EFFICIENCY	80%	90%
SHUNT RESISTANCE	10-100 Ω	>1000 Ω
SERIES RESISTANCE	0.05 Ω	NEGLIGIBLE
$I_{sc}(m = 1)$	14.3 ma/cm^2	28

FIGURE 17

SUMMARY OF STANFORD MECHANISM STUDIES

M. P. Godlewski, NASA-Lewis

This paper summarizes initial work performed under NASA Grant NGR-05-020-214 "Mechanism of the Photovoltaic Effect in II-VI Compounds" directed by Dr. Richard H. Bube at Stanford University. The diode structures used in this study are shown in figure 18. The CdS single crystals used in the work have a resistivity of about 0.8 ohm-cm with the C axis perpendicular to the junction. Some unoriented samples have also been run with essentially no difference. Little difference was observed among samples that were etched, ground, or left unchanged before dipping in the barrier forming solution. Two barrier forming solutions were tried, one a solution of CuCl in water at 90° C, and the other a solution of Cu_2S in NH_4OH. The CuCl bath appears to be superior.

The diodes were formed as mesa structures by masking and the Cu_2S has a thickness of about 50 microns. Four point probe measurements give a conductivity of about 10^{-3} ohm-cm for the Cu_2S. X-ray diffraction shows the Cu_2S to be polycrystalline but strongly oriented with its C axis parallel to the CdS C axis. An indium contact to the Cu_2S completes the structure.

Figure 19 shows the effect of heating one of the diodes at various times at 250° C. The open circuit voltage maximized after 2 minutes while the short circuit current continued to drop as the heating time increased.

Figure 20 shows typical dark I-V characteristics for these diodes. A good rectifying junction is obtained as shown in figure 20a. However, detailed analysis of the forward characteristic (figure 20b) shows an A value of 1.13 but an extremely high series resistance of 780 ohms. A barrier voltage estimated by extrapolating the forward characteristic back to zero current was 0.6 eV. (Editors' Note: This value is much lower than values of the barrier height (~ 0.85 eV) obtained at NASA-Lewis and Clevite. It is possible that the high series resistance of this device prevented an accurate assessment of the barrier height.)

Capacitance-voltage data were obtained for this diode (which had not been heat treated) and are plotted in figure 21. The ordinate of $C^{-1.25}$ was obtained by fitting the curve to the previously obtained barrier height of 0.6 V. Linearity of voltage versus $C^{-1.25}$ suggests a retrograde impurity

profile as reported by Anderson and O'Rourke, IBM J., $\underline{4}$, 264 (1960). Some transient effects were noted in the capacitance measurements and are shown in figure 22. The time scale represents the time in seconds of the application of a 1 volt reverse bias. Within the limits noted the capacitance rise fits an exponential with a time constant of 190 seconds. The total increase is about 2 percent.

The backwall spectral response for a non-heat treated cell is shown in figure 23. The response is quite similar to that observed for heat treated cells.

The diffusion lengths in the Cu_2S and the CdS layers were determined on beveled devices and an optical microprobe. Measurements indicate the diffusion length in the Cu_2S to be less than 0.1 μm and about 1 μm in the CdS.

POINT CONTACT

INDIUM

Cu_2S

P-N JUNCTION

CdS

$\rho_{Cu_2S} = 4.5 \times 10^{-4} \, \Omega\,cm$

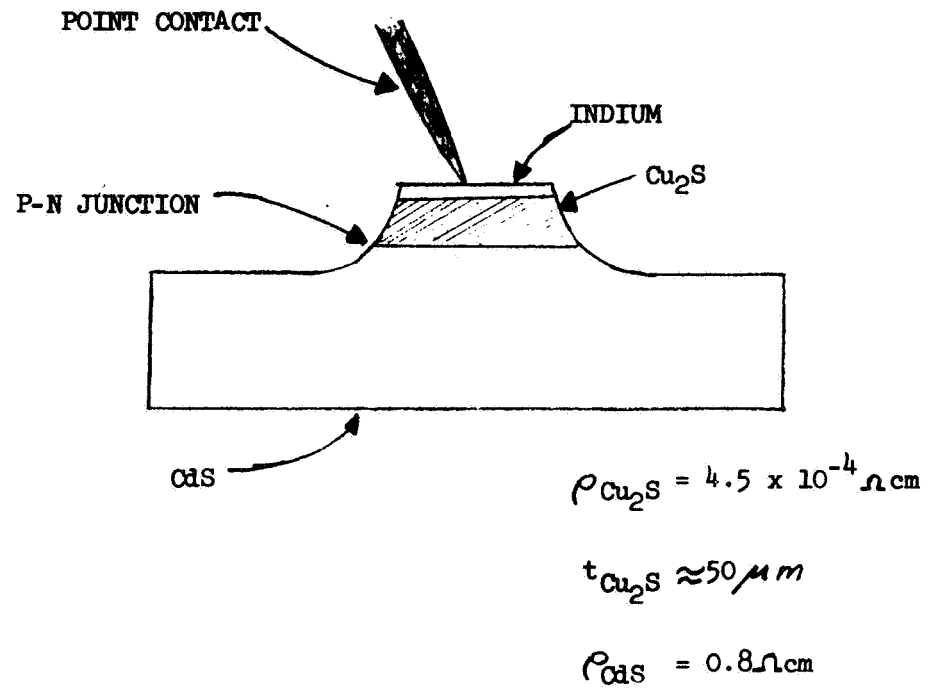$t_{Cu_2S} \approx 50 \, \mu m$

$\rho_{CdS} = 0.8 \, \Omega\,cm$

FIGURE 18. CONFIGURATION OF A Cu_2S-CdS MESA DIODE
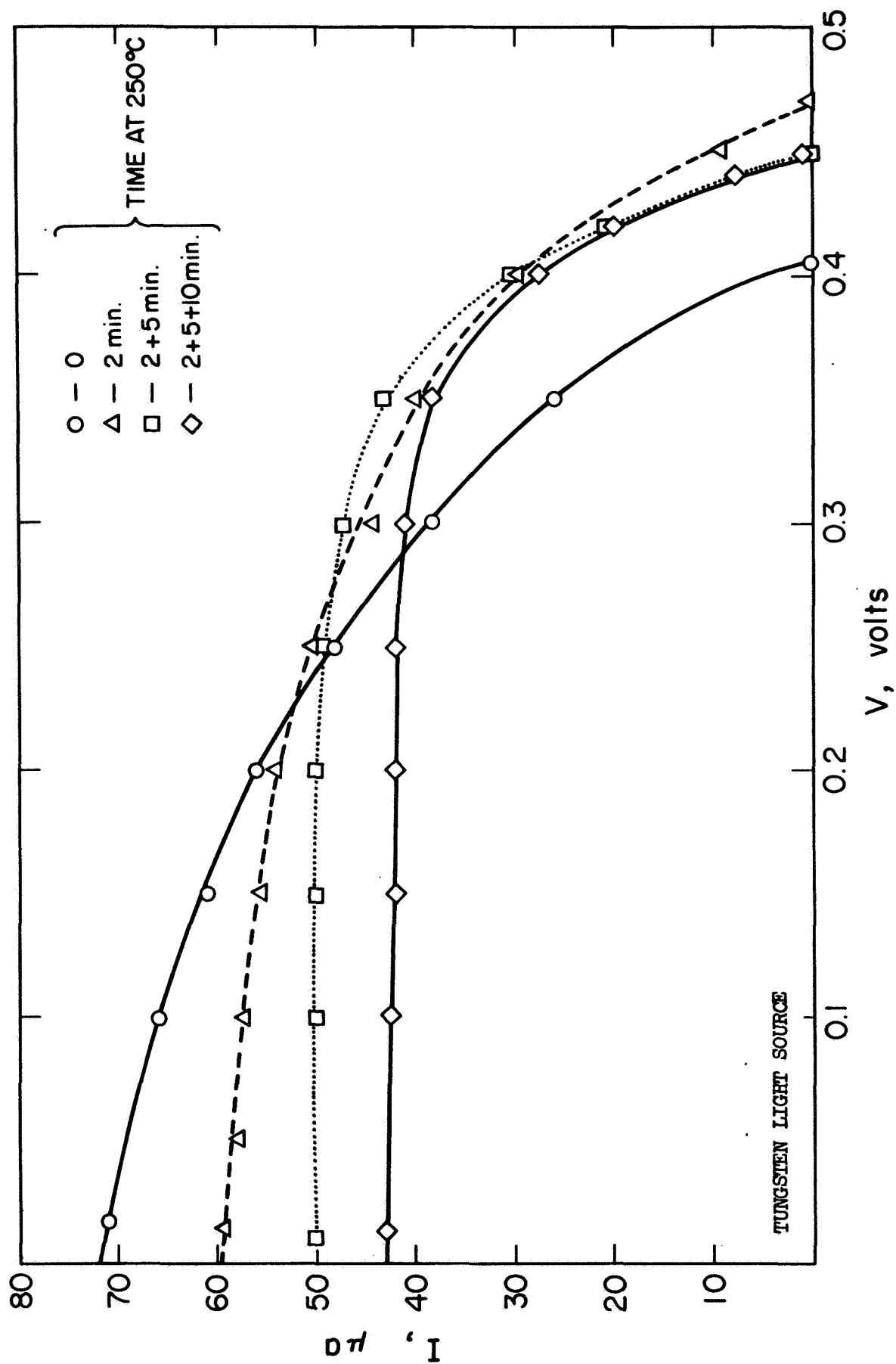WITH INDIUM CONTACT

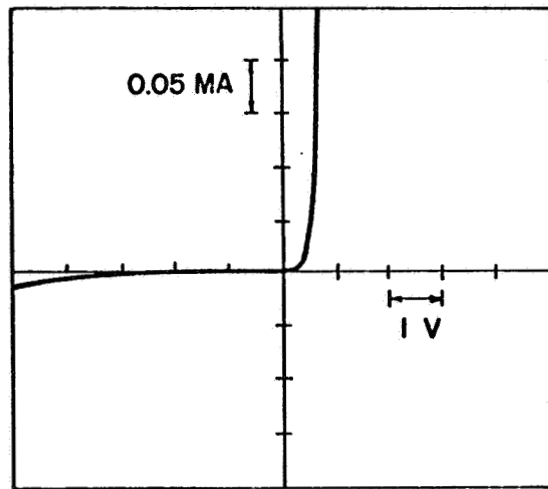FIGURE 19. CURRENT-VOLTAGE TRACES AS A FUNCTION OF TIME AT 250°C IN AIR FOR CdS
PHOTOVOLTAIC CELL WITH CLEAVED FACE DIPPED IN CuCl SOLUTION

(a)
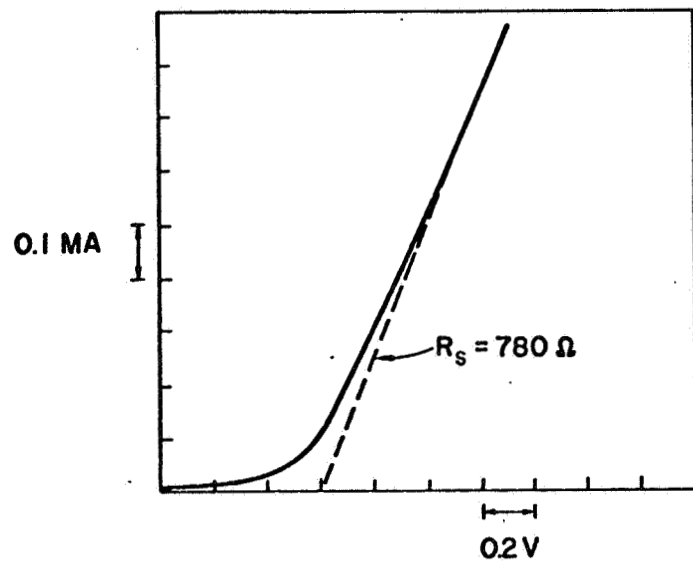
(b)

FIGURE 20. FORWARD CHARACTERISTIC OF MESA DIODE AT ROOM TEMPERATURE

FIGURE 21. C-V PLOT FOR MESA DEVICE (CORRECTED FOR SERIES RESISTANCE)

FIGURE 22. CHANGE OF CAPACITANCE WITH TIME AFTER APPLICATION OF 1 VOLT REVERSE BIAS FOR A CdS CELL DIPPED IN Cu_2S SOLUTION

FIGURE 23. SPECTRAL RESPONSE OF PHOTOCURRENT FOR EPITAXIAL Cu_2S-CdS, ILLUMINATION THROUGH CdS SIDE.

WAVELENGTH = $\lambda, m\mu$

6

EFFECT OF TEMPERATURE AND ATMOSPHERE IN HEAT TREATMENT
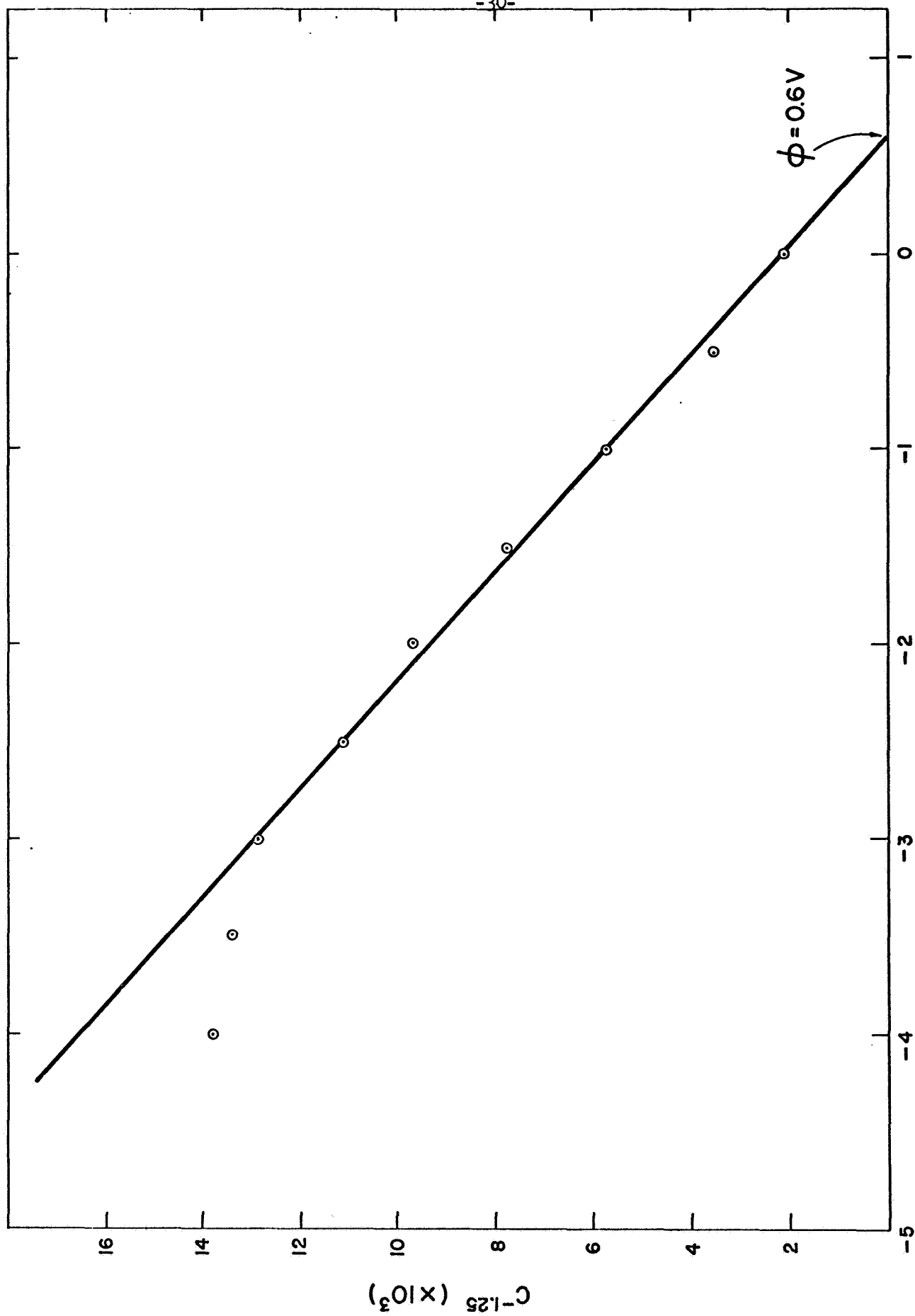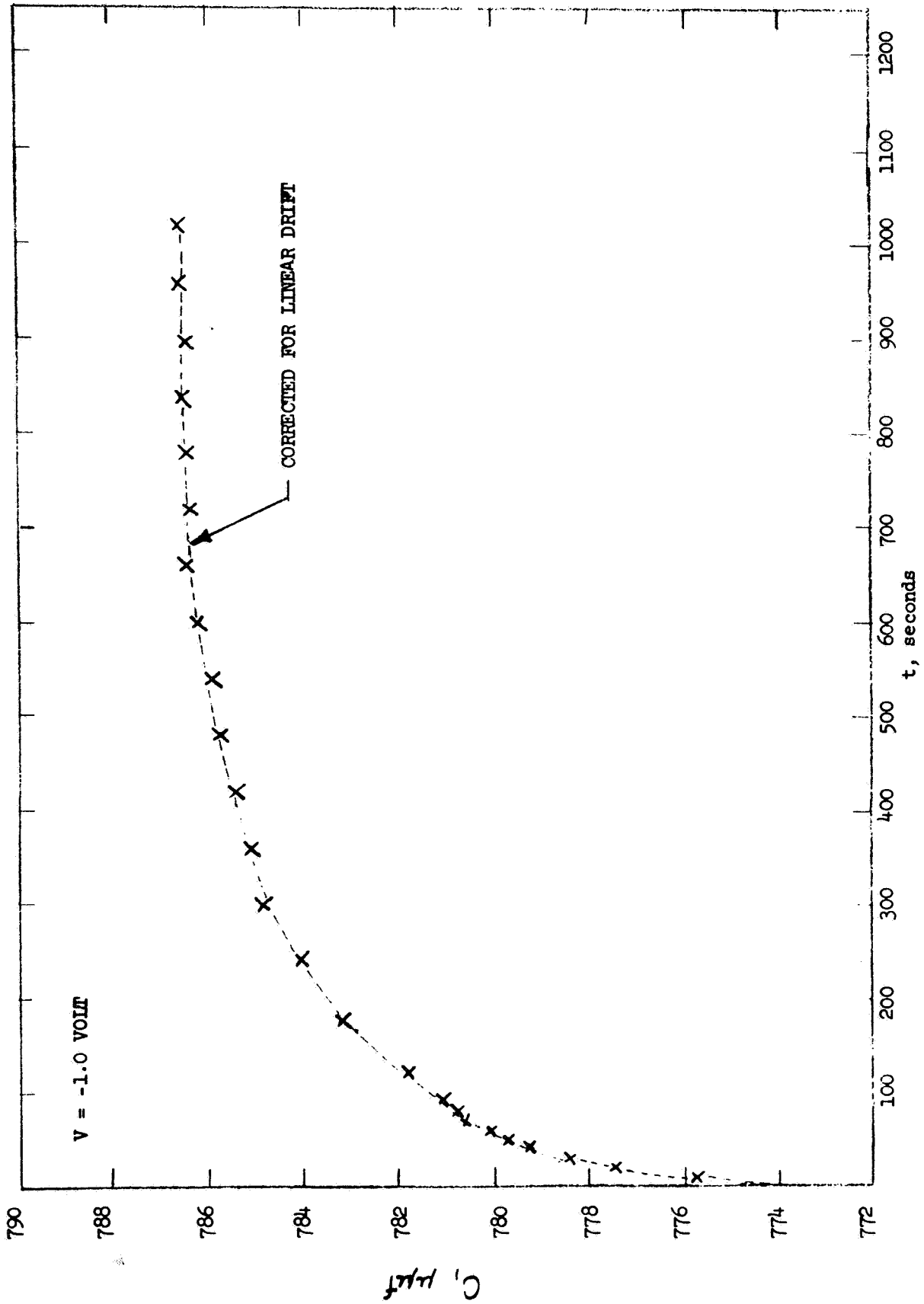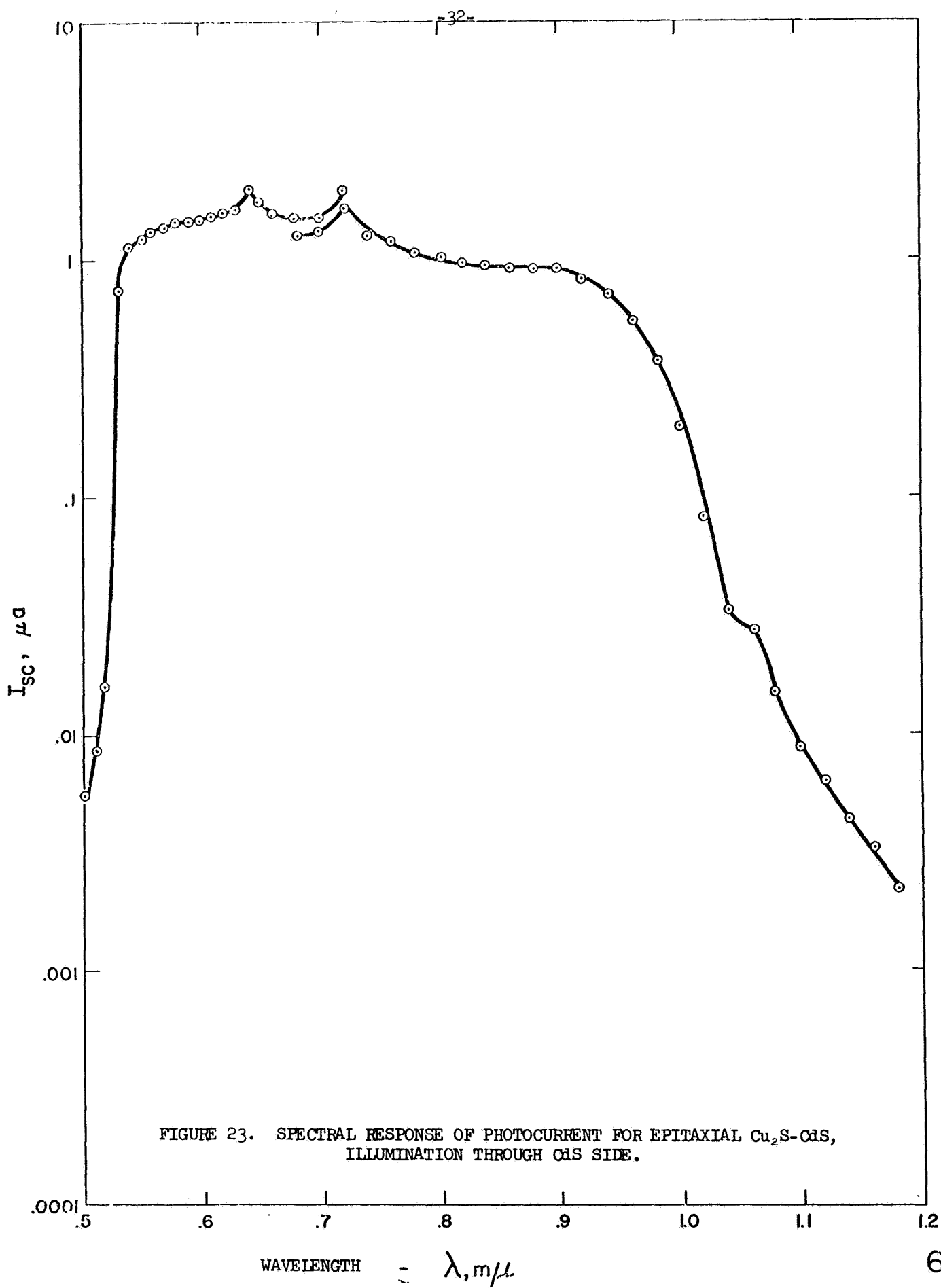
H. Nastelin, Clevite

A series of standard CdS films were heat treated after barrier formation at temperatures up to 550° C for two minutes in air, oxygen, or argon at a pressure of 1 atmosphere. The data are tabulated in Table II. Normal processing followed heat treatment. It can be seen that equivalent results were obtained between 100 and 300° C. A slight reduction is apparent at 350° C, and from 400 to 500° C the efficiencies dropped noticeably with the drop increasing with increasing temperature. Ultimately the cells shorted completely out. This is probably due to copper diffusing down grain boundaries and shorting the cell. From these results it also appears as if the cells are relatively unaffected by the atmosphere during heat treatment. However, the cells were exposed to air before the barrier dip and also before heat treatment. Therefore one series of experiments was run in which the environment was more carefully controlled. The results of these experiments can be summarized as follows:

1. Films processed through the barrier forming and heating process in an argon atmosphere had no output.

2. The same cells exhibited a photovoltaic junction and a measurable output after a later heating in air.

3. Dipped films exposed to air before heating in an argon atmosphere show output (Table II).

4. Dipped films exposed only to pure oxygen before heating to 250° C in argon also show outputs.

5. Heat treatment in pure oxygen resulted in outputs which were equivalent to cells processed in air.

6. Dipped films processed under argon hot rinsed in H_2O_2 at room temperature have outputs. However, when the dipped films were rinsed in hot (90° C) H_2O_2, dead cells resulted.

7. Dipped films processed under argon but exposed to $(NH_4)_2S$ vapors showed no outputs. The outputs were not altered by rebaking in air.

8. Dipped films processed under argon but exposed to iodine vapors also resulted in dead cells. The cells remained dead after baking in air.

It is quite apparent from this series of experiments that oxygen, even in minute amounts, is required for photovoltaic operation of the present cell. Steps 7 and 8 were designed to expose the cell to S_2 and I_2 molecules which presumably might act somewhat like O_2 in the lattice however it is quite clear that sulfur or iodine kill the cell completely.

As a further experiment, a 1 gram sample of powdered Cu_2S was heated at about 250° C in an air circulating oven and the weight change noted. The results are shown in Table III. There is a definite weight loss on heating which is recovered on sitting in air at room temperature. The heating action, then, appears to be reversible and may involve the desorption and adsorption of moisture and gases. There was no obvious change in the appearance of the Cu_2S at the end of the experiment.

The oxygen effect is not of immediate practical significance since all cells are exposed to oxygen during normal processing and hence show good output. The effect may, however, be very important in the explanation of the cell mechanism and may also be relevant to the long term stability of the cells.

TABLE II

Effect of Post-Barrier Heat Treatments on Cell Performance

Temperature °C	2 minutes in air			2 minutes in oxygen			2 minutes in Ar		
	V_{OC}	I_{SC}	EFF	V_{OC}	I_{SC}	EFF	V_{OC}	I_{SC}	EF.
	(volts)	(ma)	(%)	(volts)	(ma)	(%)	(volts)	(ma)	(%
100	.475	41.8	7.3	.485	36.7	6.8	.480	36.7	6.
200	.475	41.3	7.4	.480	37.8	6.9	.485	39.0	7.
300	.475	38.0	6.7	.485	37.8	6.9	.475	39.8	7.
350	.465	38.2	6.7	.455	33.1	5.2	.460	36.0	6.
400	.050	10.0	---	.210	19.8	1.0	.405	35.7	4.
450	----	----	---	.150	14.5	1.0	.370	31.8	2.
500	----	----	---	.020	3.0	---	.120	2.5	--

TABLE III

Changes in weight of a 1 gram sample of Cu_2S powder heated

in air at 250° C

t, min	△W, mg	T °C
0	0	25
1	-1.2	250
4	-2.3	250
9	-2.7	250
190	+0.1	25
280	+0.1	25

SPECTRAL RESPONSE

A. E. Spakowski, NASA-Lewis

In order to determine if any significant changes had taken place in cell response over the last three years, the spectral response of various cells made between January 1965 and March 1968 was measured under 25 mw/cm^2 white light bias. The data are tabulated in figure 24 in which the output at constant energy input is plotted against wavelength. The efficiencies (AMO, 25° C) of these Kapton covered cells varied from 2.6 to 3.4 percent. It can be seen that there are no significant differences between these cells.
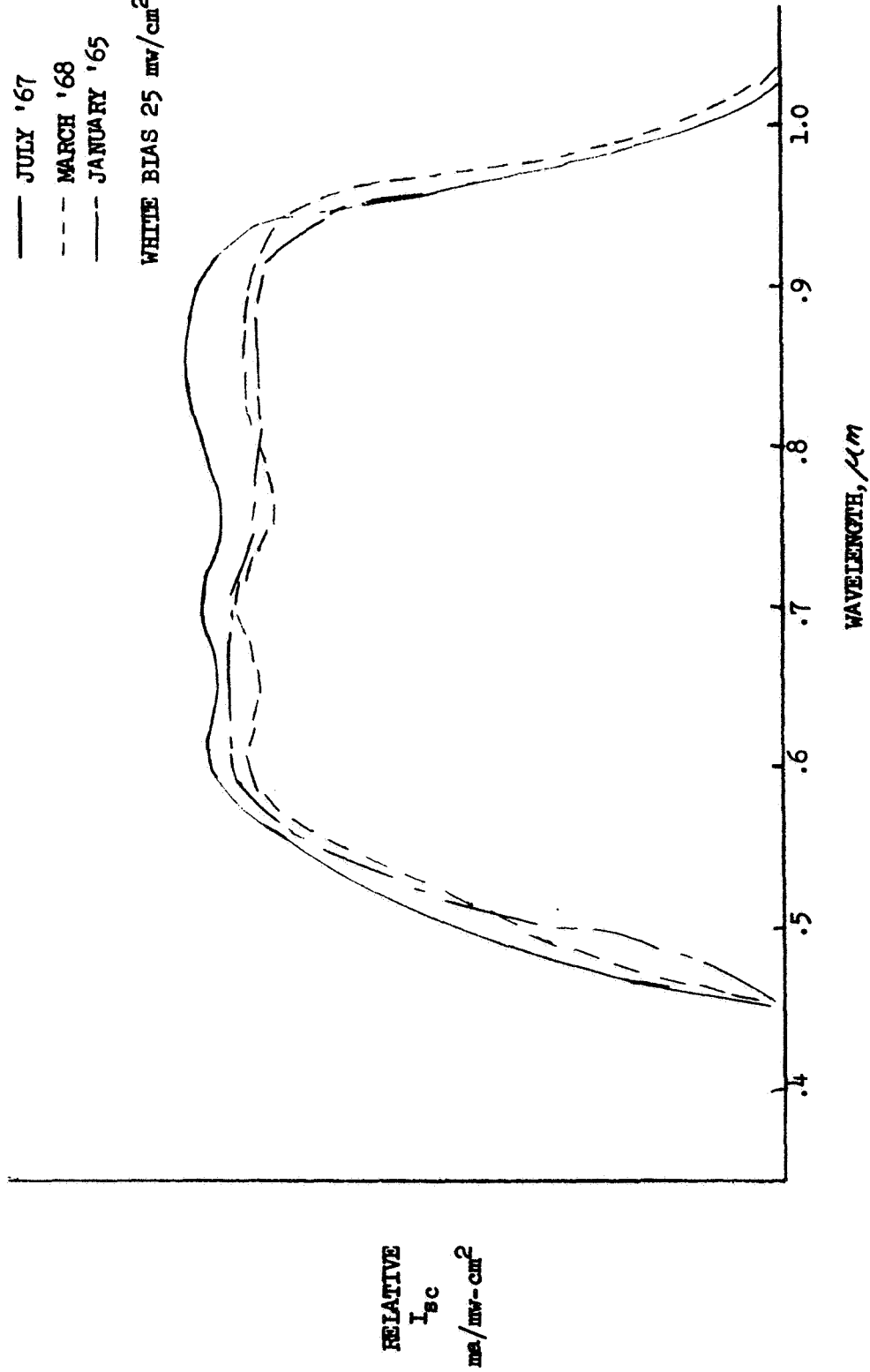
FIGURE 24. SPECTRAL RESPONSE OF CdS CELLS

EFFECT OF TEMPERATURE AND INTENSITY
C. H. Liebert, NASA-Lewis

In another series of experiments the performance of CdS thin film
cells (and also some Si cells) was measured at temperatures between 110° K
and 330° K and solar intensities (from a simulator) between 1 sun (136 mw/cm^2)
and 6.2 mw/cm^2. A plot of the variation of V_{oc} and I_{sc} with temperature
and at two intensities is shown in figure 25. At both intensities the short
circuit current increases slowly between 110 and 300° K and then tends to
level out or even decrease slightly. The open circuit voltage under both
intensities increases with decreasing temperature down to about 180° K and
then becomes relatively constant. The maximum value of V_{oc} obtained
under 1 sun illumination was about 0.65 V for this cell.

Figure 26 shows the efficiency of both a CdS thin film solar cell and
a silicon solar cell as a function of temperature and light intensity. For
the thin film cell the efficiency changes only slightly with temperature
from 3 percent at 340° K to 4.2 percent at about 200° K. It is also seen
that the efficiency of the thin film cell is slightly affected by light
intensity. On the other hand, the efficiency of the silicon solar cell
varies from 8 percent at 340° K under 1 sun illumination to nearly 20 per-
cent at 140° K. Also, in this case, the efficiency is affected by light
intensity showing a decrease from 19.6 percent to 14.3 percent (both at
140° K) as the light intensity changes from 136 mw/cm^2 to 6.2 mw/cm^2. Also
included in the figure is a plot of the probable efficiency of the silicon
solar cell as it travels from Earth to Jupiter.

Data on the various temperature coefficients of the CdS cell have been
collected from a number of different sources and is compiled in Table IV.
In all cases the measurements are at an intensity of 136 mw/cm^2 and cover
the temperature range between 0 and 60° C. It can be seen that the tem-
perature coefficient of the open circuit voltage varies from -1.5 to -1.8
$mv/°C$ and averages about -1.6 $mv/°C$. The short circuit current is quite
another matter, however, with both positive and negative coefficients being
observed. In many of the better cells the temperature coefficient is either
positive or very slightly negative. On the poorer cells, a large negative

temperature coefficient of short circuit current is observed. The temperature coefficient of the maximum power is also quite variable, ranging from -1.1 to -1.8 mw/°C. There does seem to be a rather wide variability in these various factors, however, and some effort should be devoted to narrowing the spread of values.

TABLE IV

TEMPERATURE COEFFICIENTS

CELL AREA = 54.75 cm²

TEMPERATURE = 0-60°C

INTENSITY = 136 mw/cm²

OCTOBER-NOVEMBER, 1967 CELLS

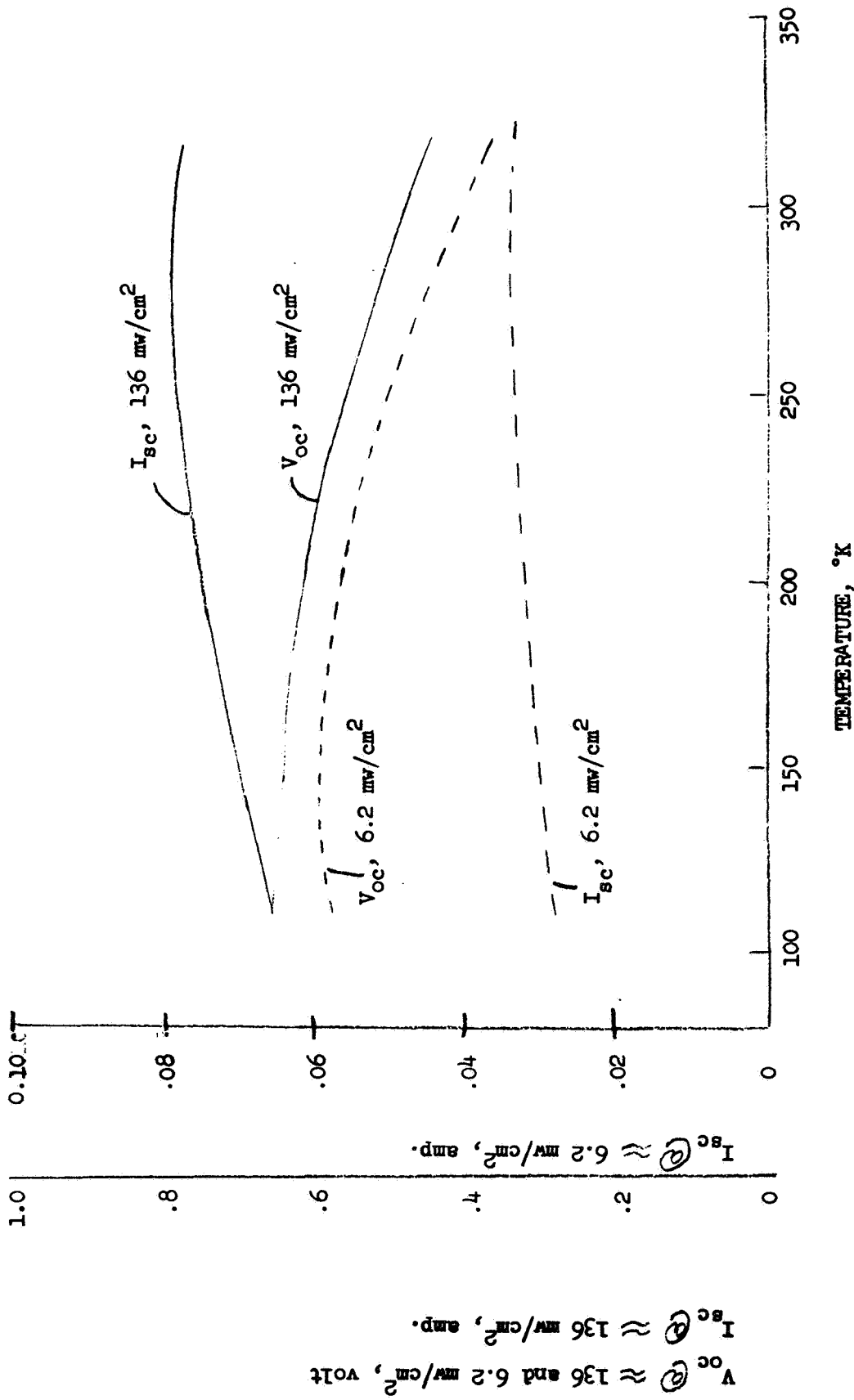|	LIEBERT-NASA 2 CELLS	RATAJCZAK-NASA 7 CELLS	BOEING 4 CELLS
V_{OC}, mv/°C	-1.6 to -1.7	-1.5 to -1.6	-1.7 to -1.8
I_{SC}, ma/°C	-0.5 to +0.2	------------	------------
P_m, mw/°C	-1.1 to -1.2	-1.5 to -1.6	-1.2 to -1.8

FIGURE 25. VARIATION OF V_{OC} AND I_{sc} WITH TEMPERATURE AND INTENSITY-- OCTOBER, NOVEMBER CELL
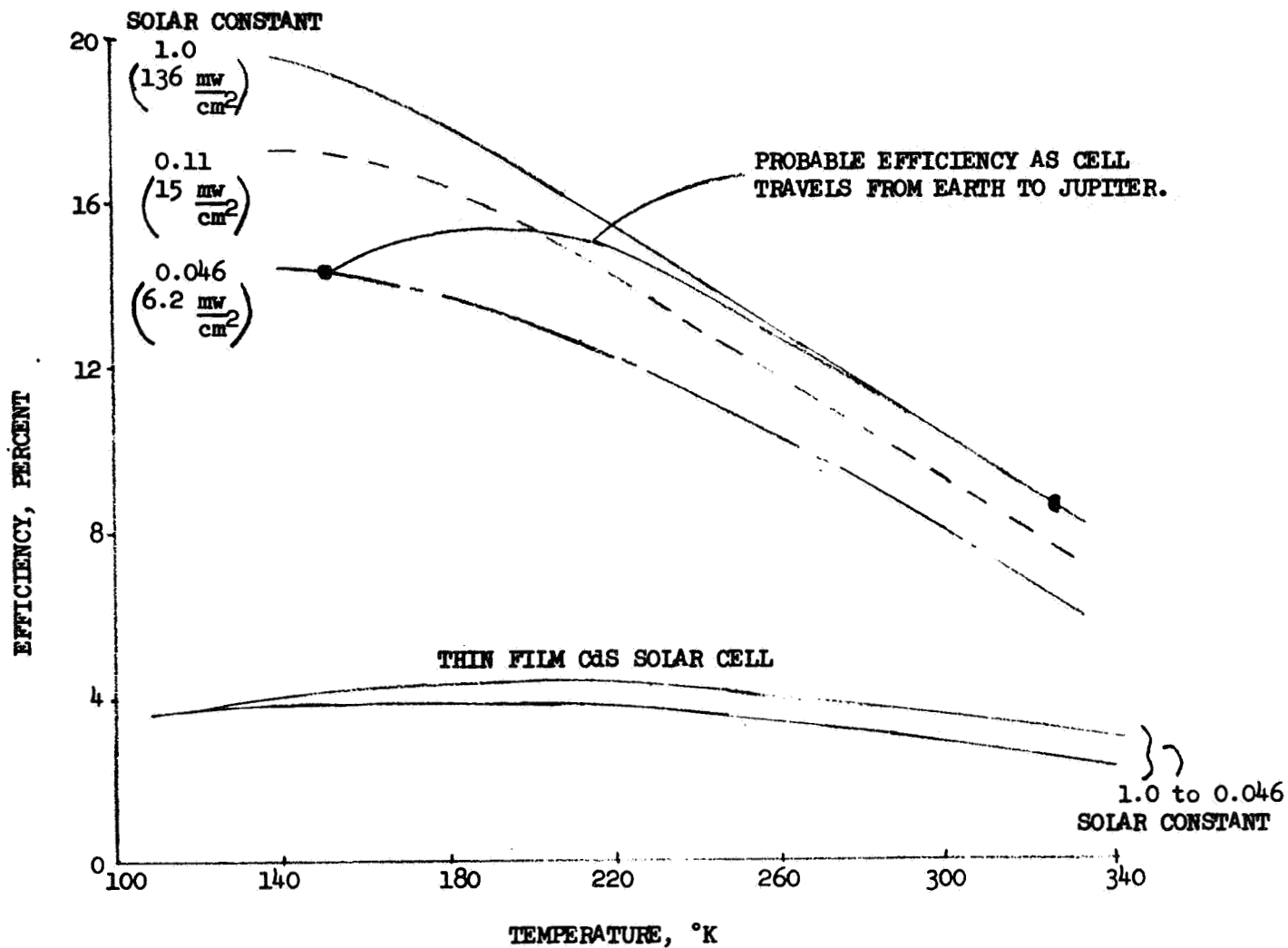
SILICON SOLAR CELL

FIGURE 26. EFFICIENCY OF SOLAR CELLS AGAINST
TEMPERATURE AND INTENSITY

TESTS CONDUCTED BY LINCOLN LABORATORIES

A. Stanley, Lincoln Labs.

A series of tests were set up at the Lincoln Laboratories to attempt thermal cycling film cells for long periods of time. A special bell jar system was fabricated that had a LN_2-filled copper shroud surrounding the four test cells on three sides. AMO light was provided by a xenon lamp. The temperatures reached by the four February 1968 (Clevite 3" x 3") cells are shown in Table V. In the following figures showing the degradation as a function of thermal cycles, a relation between the cell's temperature in the light and the onset of degradation will be noted. All cells were loaded at their V_{oc} to increase the likelihood of degradation.

The change of the I_{sc} is shown in figures 27 through 30 where the relative I_{sc} is plotted versus the number of thermal cycles. The characteristics are shown in figure 31. The slope of the first straight line portion of the degradation plots are shown as is the I/I_o at 250 cycles.

The change of the V_{oc} is shown in figures 32 through 35. There is an induction period before degradation begins and this point is related to the cell temperature, being the smallest for the cell with the highest temperature. The value of the relative V_{oc} at the end of 400 cycles is 0.88, 0.91, 0.87, and 0.74 for cells A, B, C, and D, respectively. It should be noted that several cells went through several days of erratic behavior. Cells B and C suffered catastrophic V_{oc} failure for some number of cycles. However, they did recover and then degraded in a normal manner. The characteristics of the V_{oc} are summarized in figure 36.

The change of the P_m is shown in figures 37 through 40. The rate of P_m degradation was related to the temperature of the cell during the light portion of the cycle as shown in figure 41. This relation is also true for the rate change as indicated at point A. All the cells then tended to level off.

The author speculated on a possible failure mechanism for these CdS film cells. In figure 42 is a typical series of I-V curves generated for cell C after 162 thermal cycles. The cell was cycled at open circuit conditions. It was taken to I_{sc} and the I-V curve traced to V_{oc} and then

back to I_{sc}. Each time an I-V curve was traced a large hysteresis was seen. It is postulated that this instability in the I-V curve reflects the beginning of the "pinhole effect." A fully developed "pinhole" yields a straight line I-V curve. This could be similar to the ionic diffusion theorized by Hill at Harshaw several years ago.

TABLE V

Cells	Dark	Light	$\triangle$ T
A	-113° C	47°C	160°
B	-112° C	53°C	165°
C	-132° C	57°C	189°
D	-136° C	66°C	202°

FIGURE 27. I_{sc} CELL A   -113 to 47°C

FIGURE 28. I_{sc} CELL B   -112 to 53°C
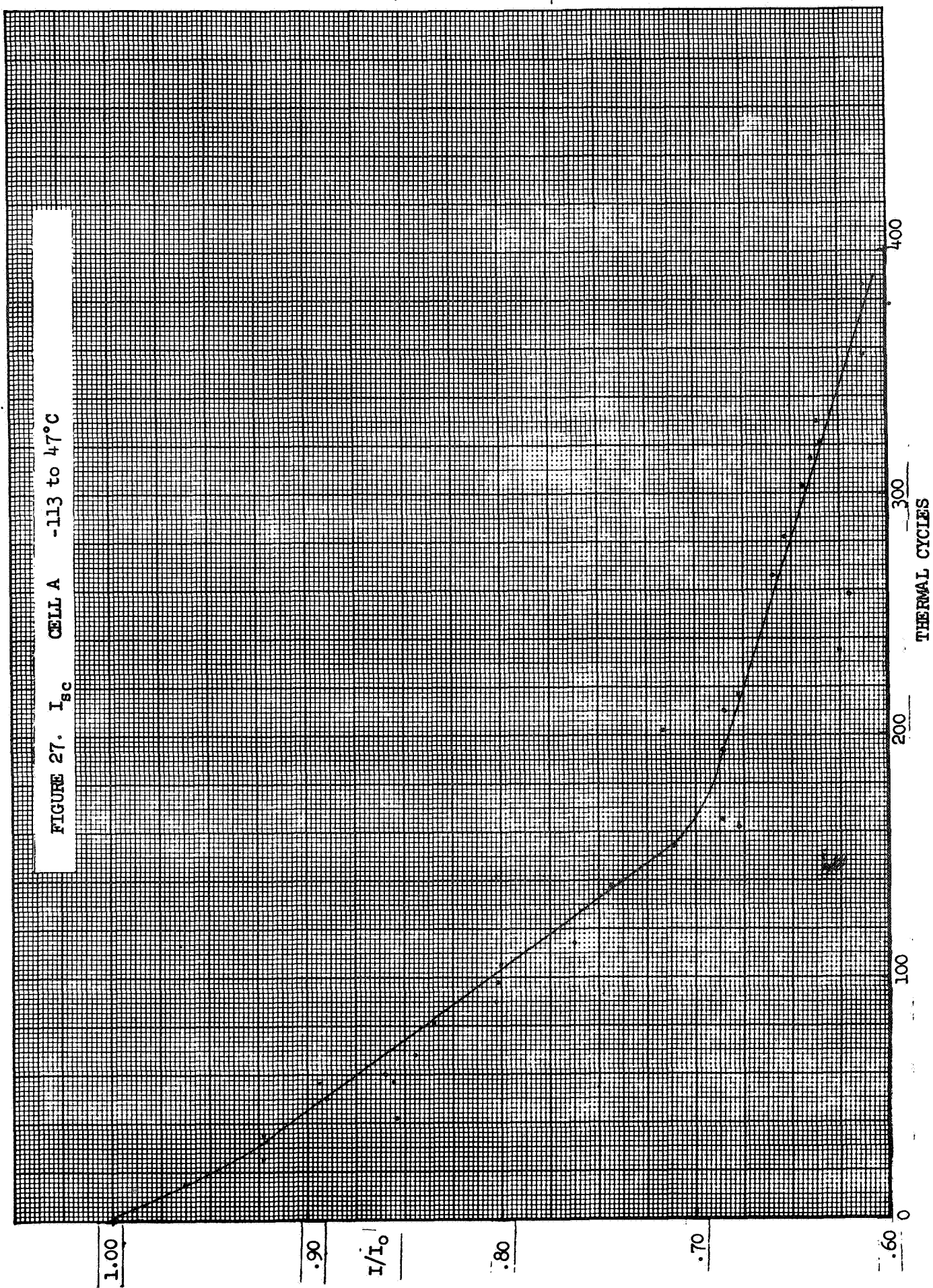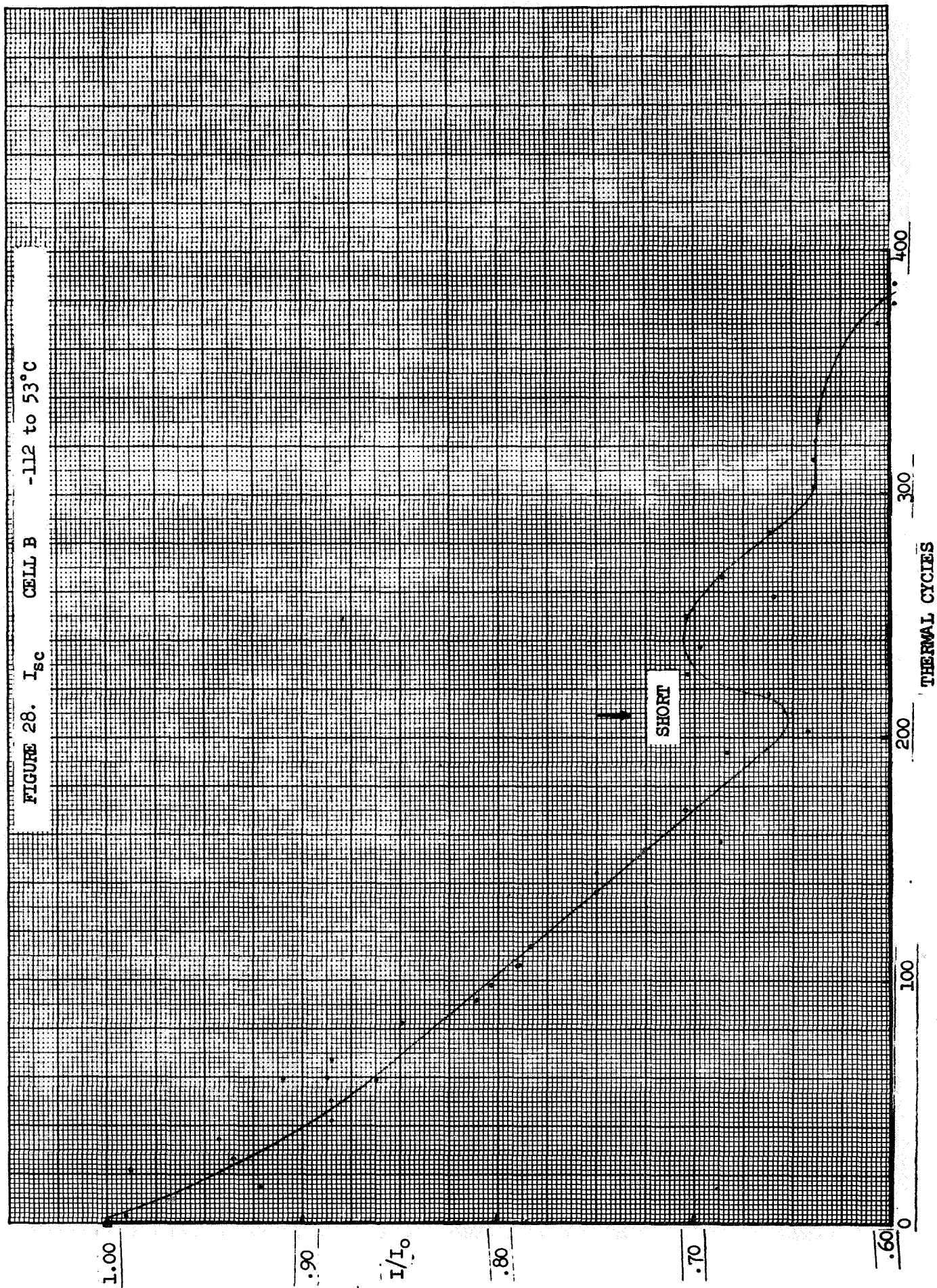
FIGURE 29. I_{sc} CELL C -132 to 57°C

FIGURE 30. I_{sc} CELL D

-136 to 66°C

THERMAL CYCLES

I/I_o
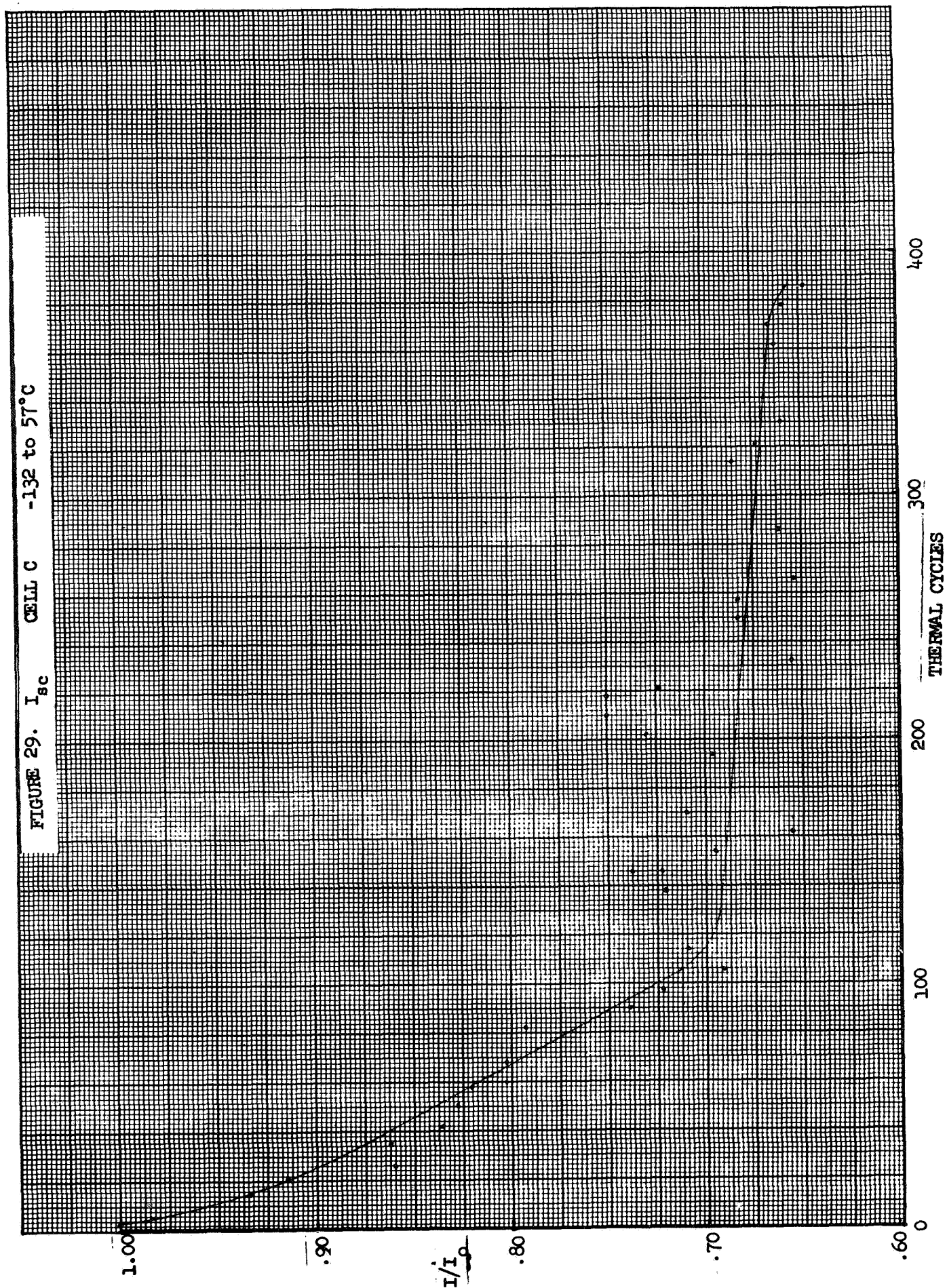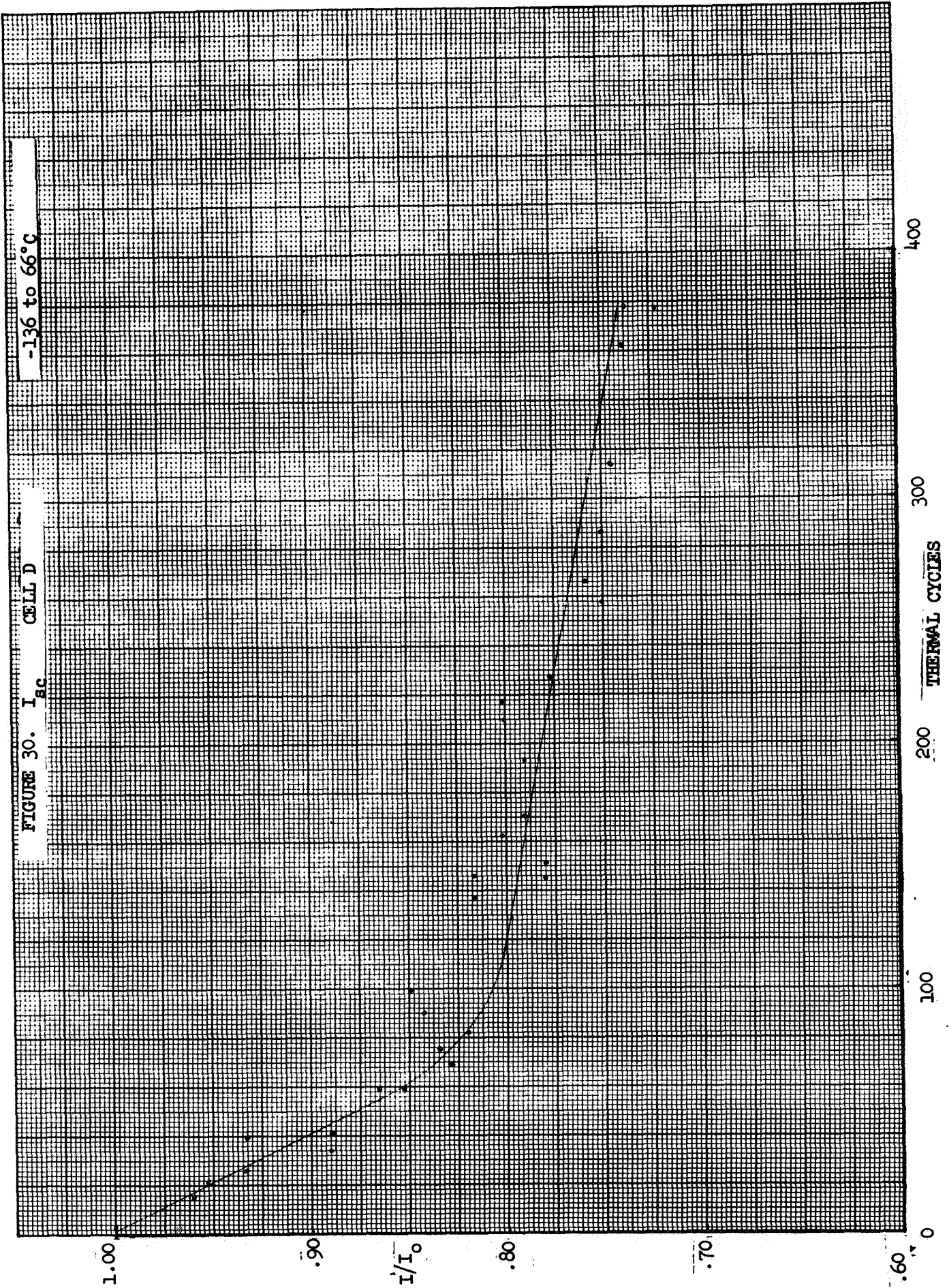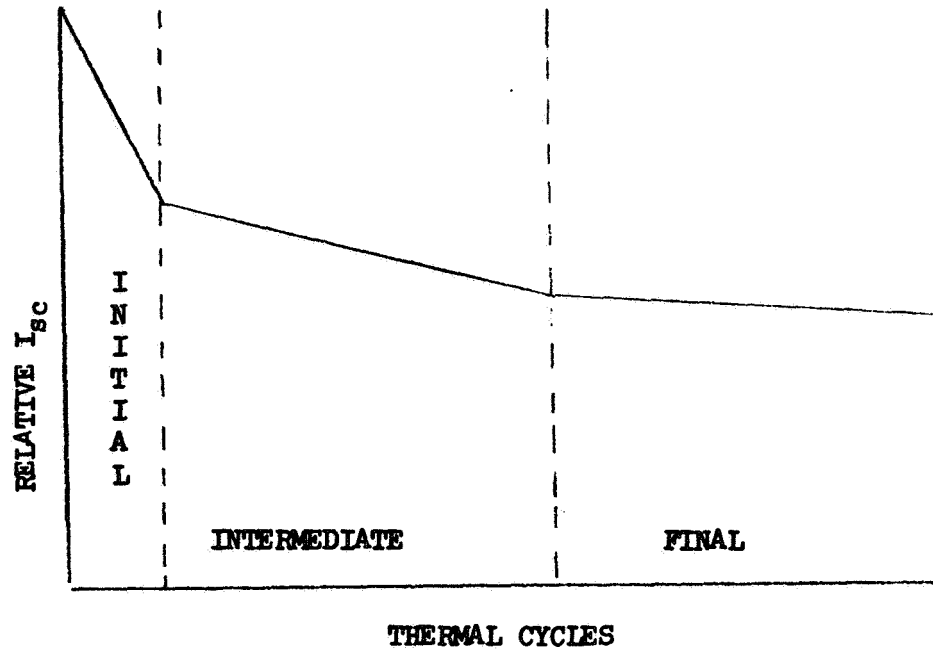
NOTES

1 - SLOPE OF INITIAL DEGRADATION IS STEEP

2 - END OF INTERMEDIATE DEGRADATION IS CELL DEPENDENT

CELL NO.	RELATIVE I_{sc}
A	0.7
B	0.65
C	0.7
D	0.8

3 - SLOPE OF FINAL DEGRADATION IS CELL TEMPERATURE DEPENDENT

4 - AFTER 250 THERMAL CYCLES (FINAL DEGRADATION MODE) THE
    RELATIVE I_{sc} IS CELL DEPENDENT.

CELL NO.	RELATIVE I_{sc}
A	0.65
B	0.7
C	0.68
D	0.75

FIGURE 31

FIGURE 32. V_{oc} CELL A   -113 to 47°C

FIGURE 33. V_{oc} CELL B   -112 to 53°C

FIGURE 34. V_{OC} CELL C   -132 to 57°C

FIGURE 35. V_{oc} CELL D   -136 to 66°C
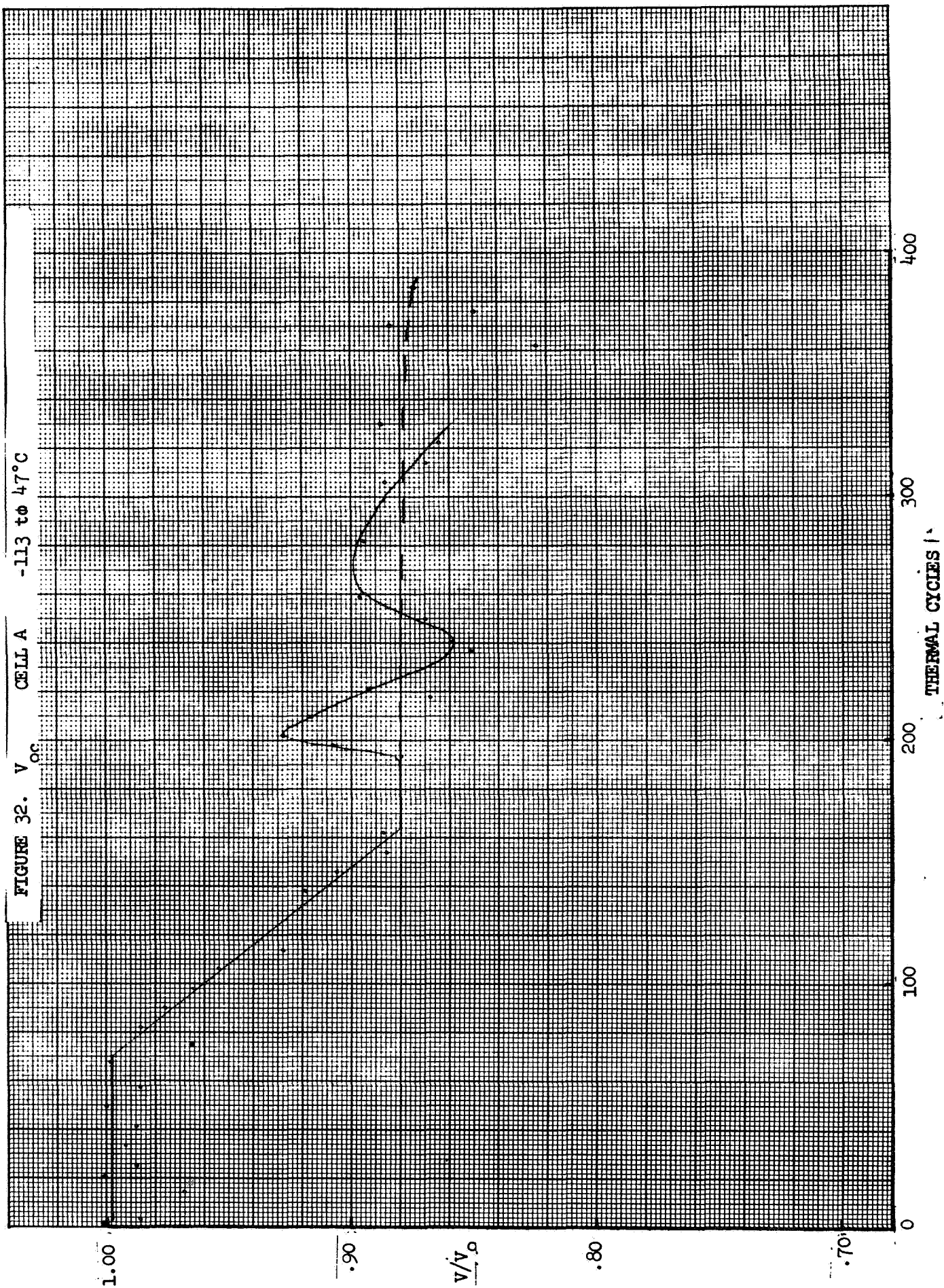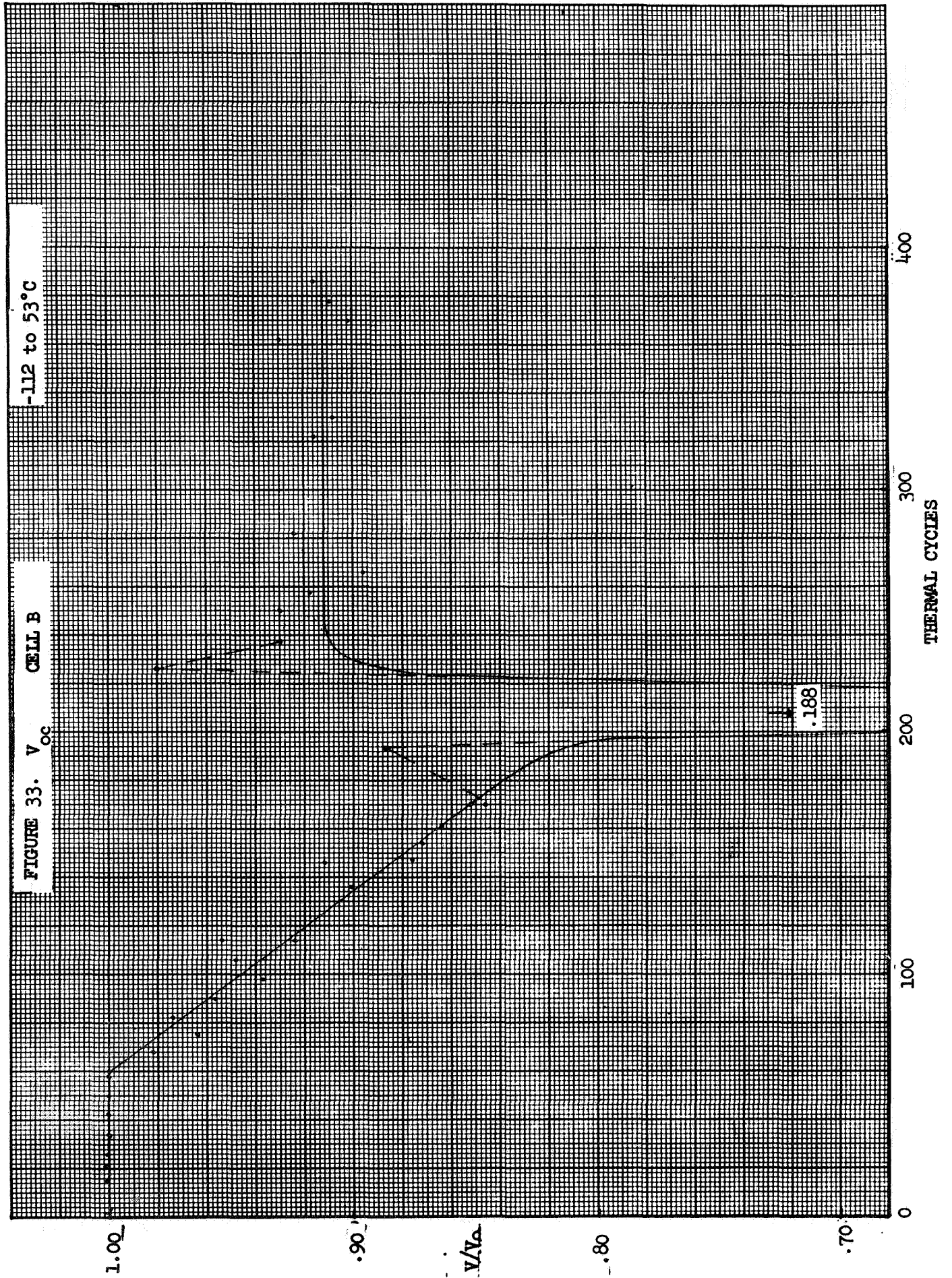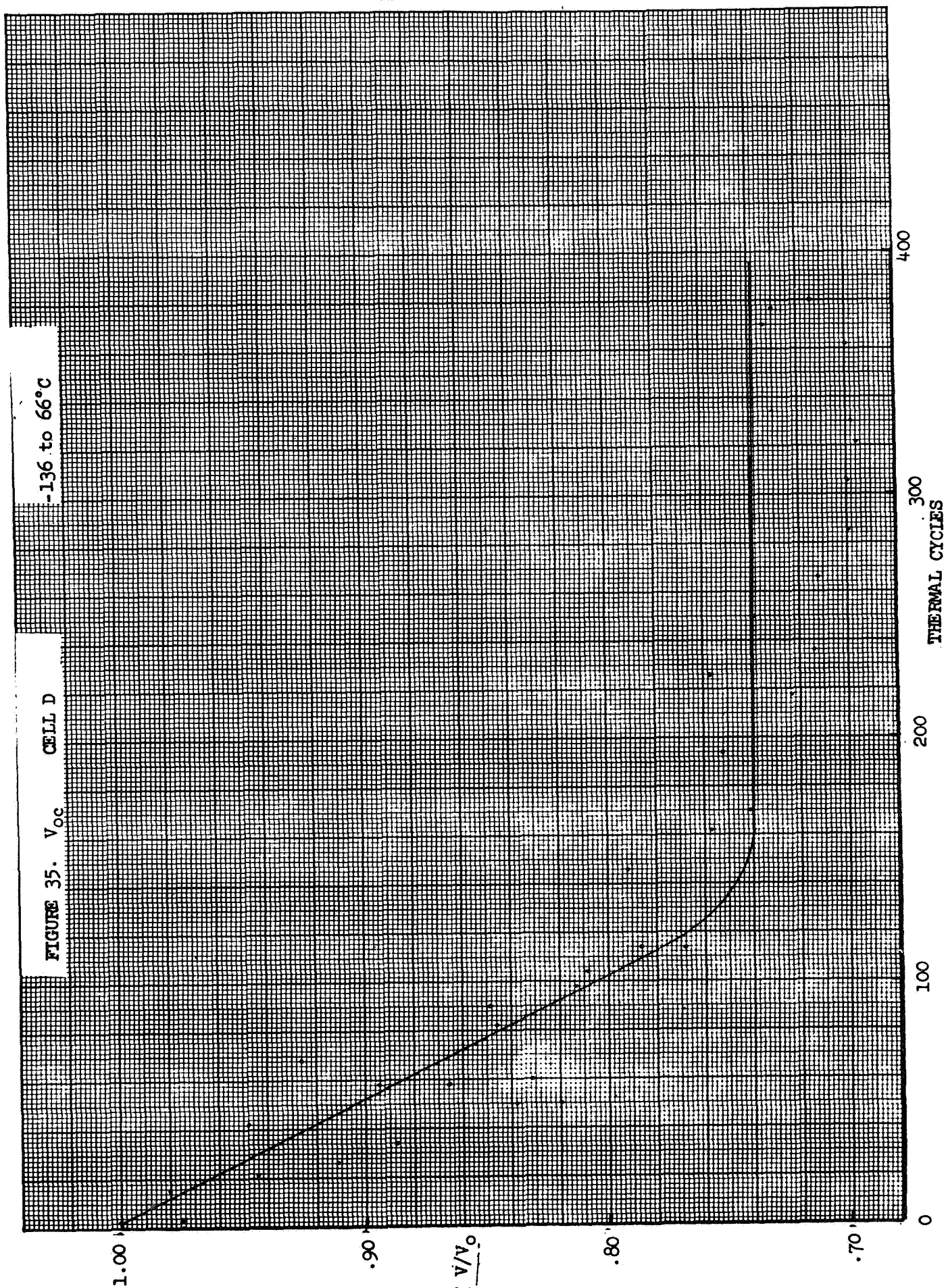
THERMAL CYCLES

NOTES

1 - INITIAL-INTERMEDIATE DEGRADATION DIVIDING LINE IS CELL
    TEMPERATURE DEPENDENT

CELL NO.	TEMPERATURE	THERMAL CYCLES
A	47°C	70
B	53°C	60
C	57°C	35
D	66°C	1

2 - SLOPE OF INTERMEDIATE DEGRADATION IS CELL TEMPERATURE
    DEPENDENT

CELL NO.	TEMPERATURE	SLOPE (% DEGRADATION/CYCLE)
A	47°C	0.126
B	53°C	0.133
C	47°C	0.155
D	66°C	0.220

FIGURE 36
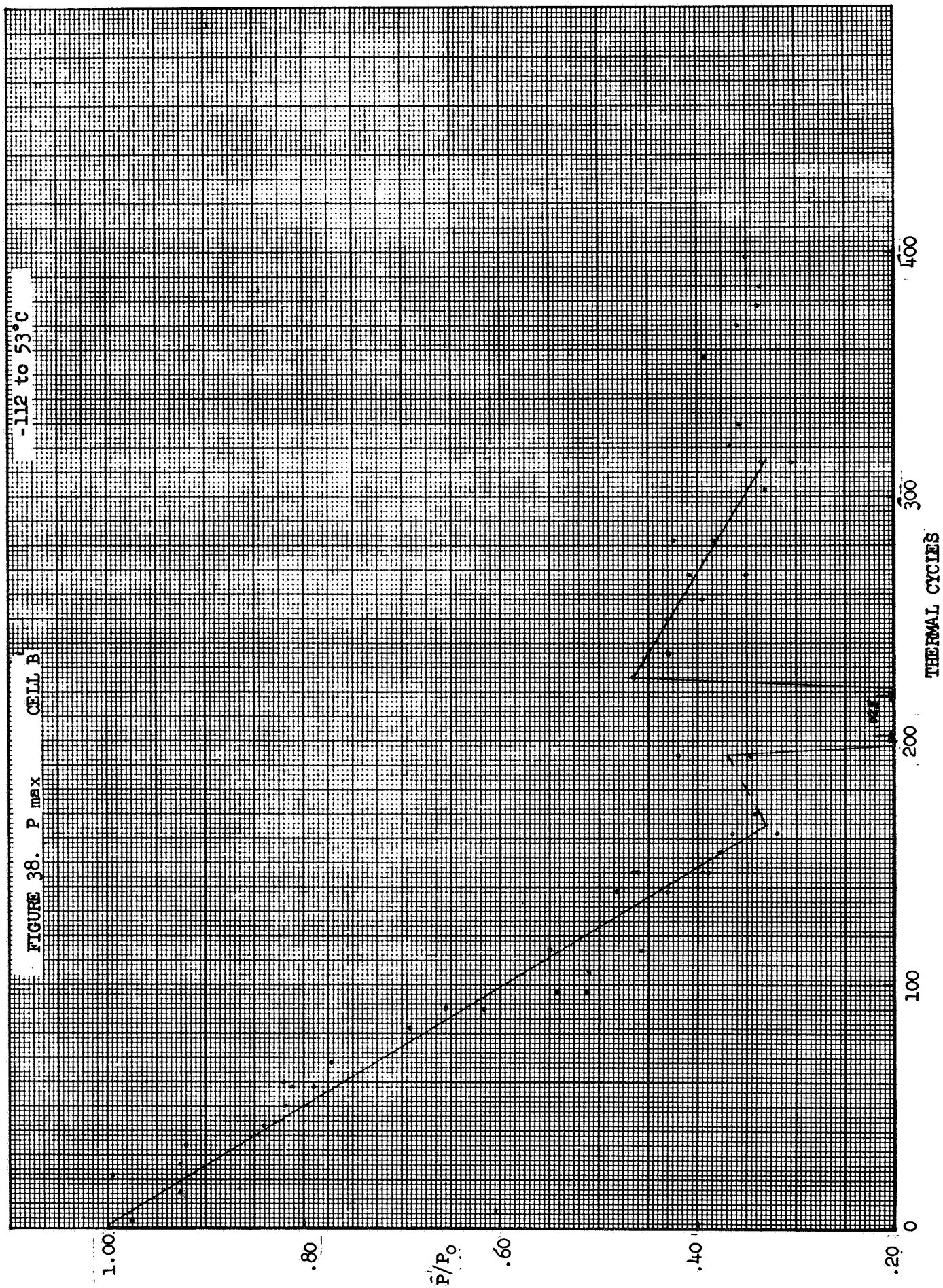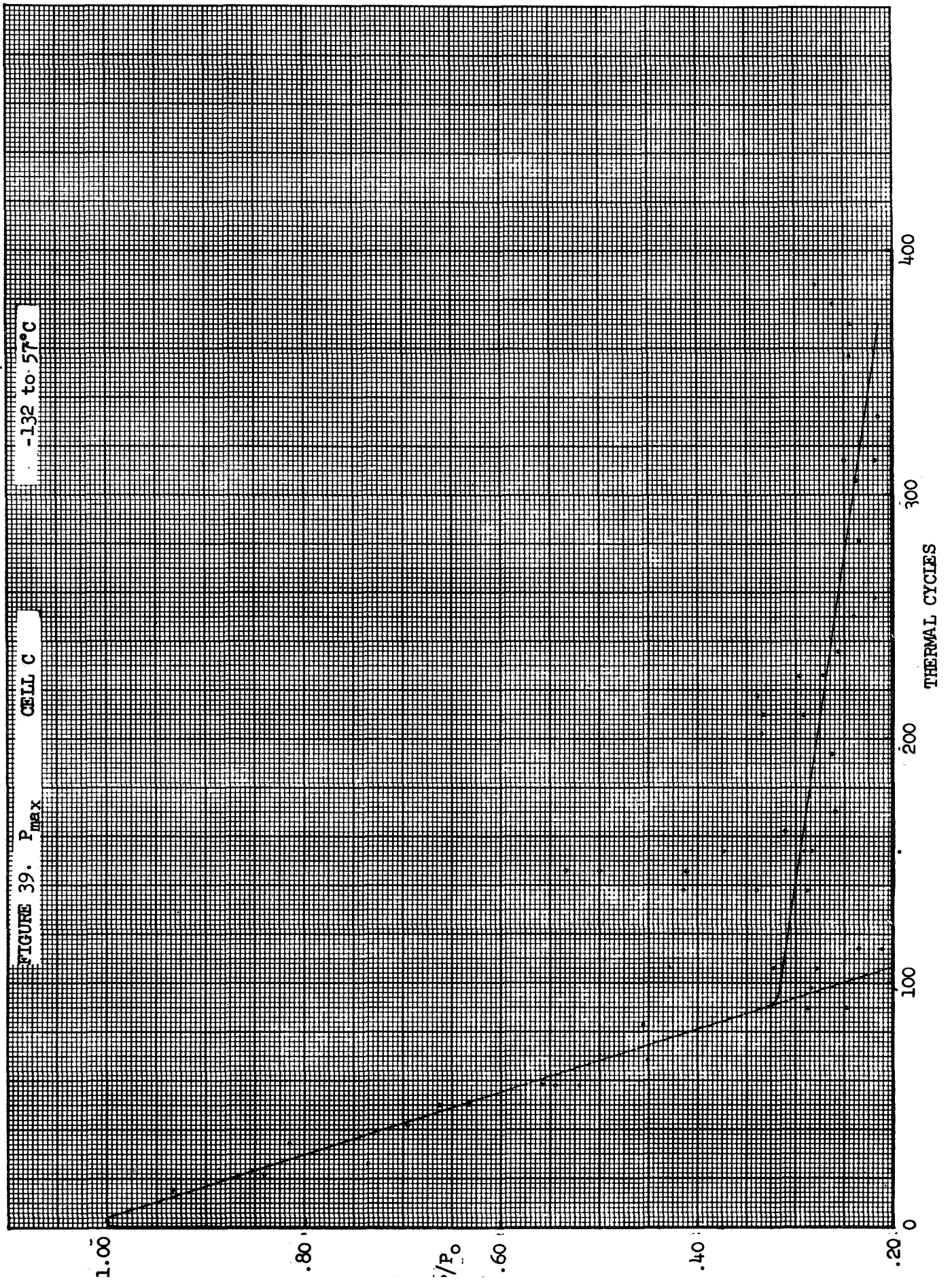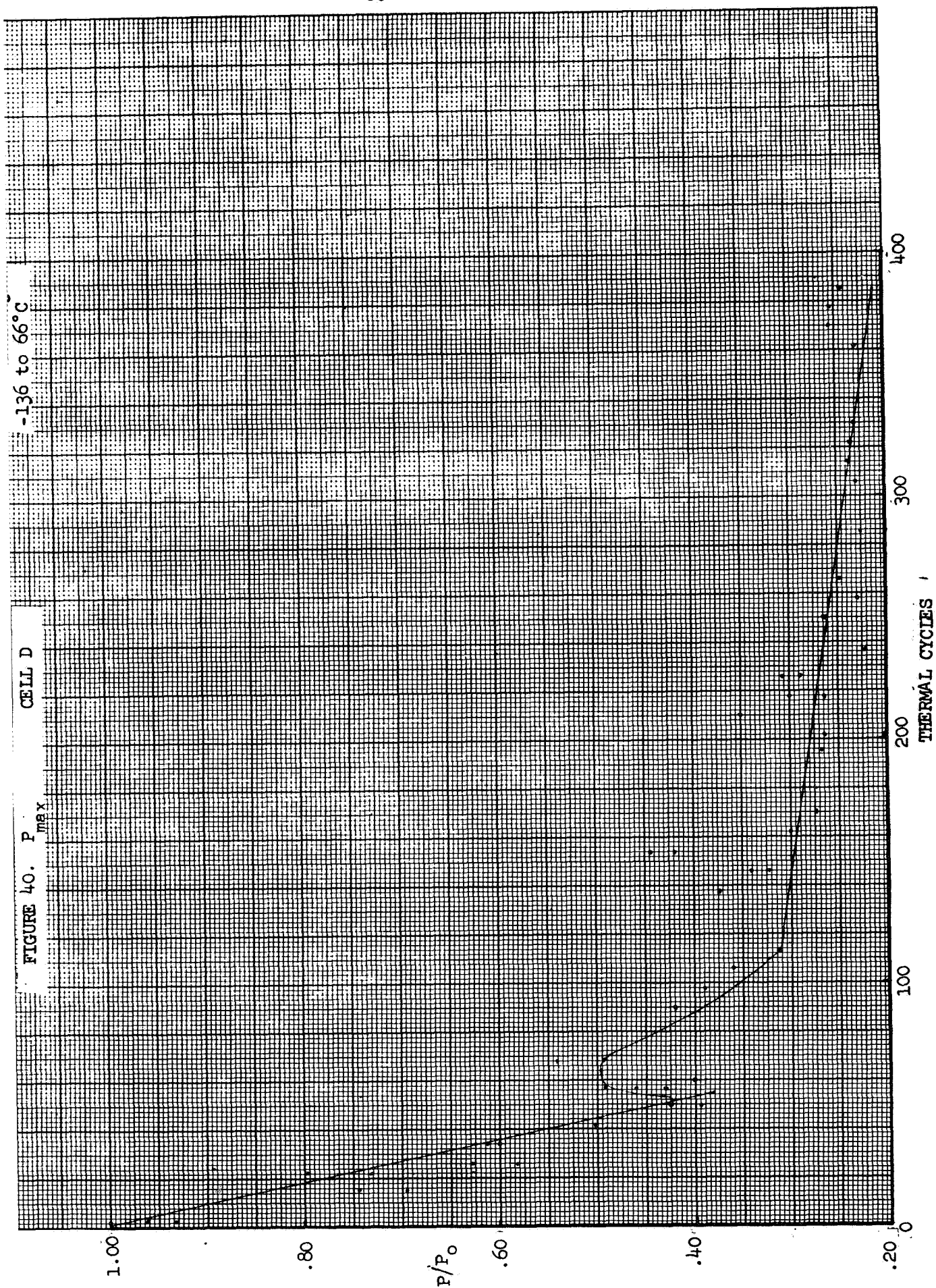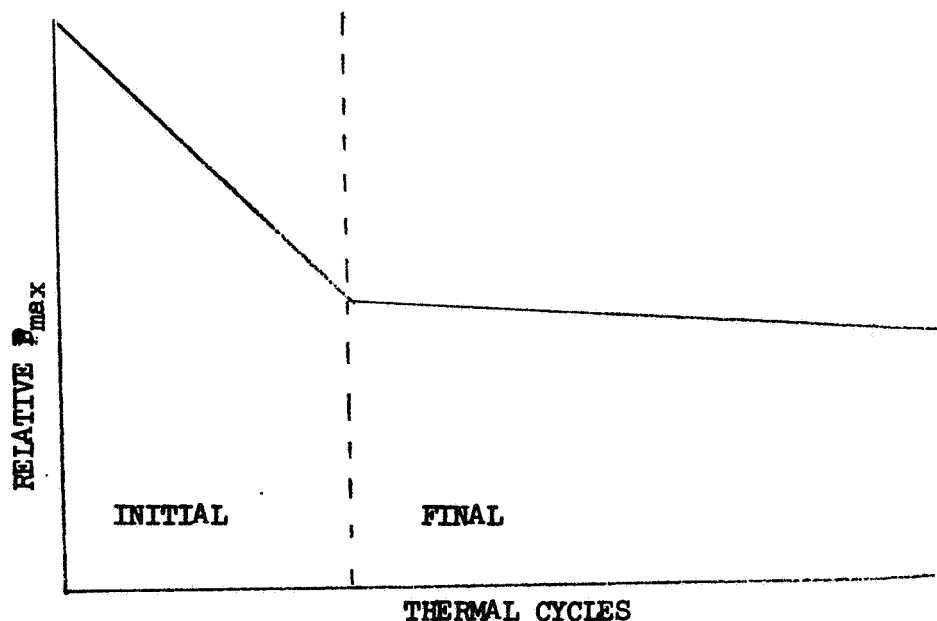
FIGURE 37. P_{max} CELL A   -113 to 47°C

FIGURE 38. P max   CELL B   -112 to 53°C

FIGURE 39. P_{max} CELL C   -132 to 57°C

FIGURE 40. P_{max} CELL D   -136 to 66°C

RELATIVE P_{max}

INITIAL   FINAL

THERMAL CYCLES

NOTES

1 - SLOPE OF INITIAL DEGRADATION IS CELL TEMPERATURE DEPENDENT

CELL NO.	TEMPERATURE	SLOPE (% DEGRADATION/CYCLE)
A	47°C	0.45
B	53°C	0.41
C	57°C	0.79
D	66°C	1.14

2 - INITIAL-FINAL DEGRADATION DIVIDING LINE IS CELL TEMPERATURE DEPENDENT

CELL NO.	TEMPERATURE	THERMAL CYCLES
A	47°C	155
B	53°C	165
C	57°C	90
D	66°C	70

3 - AFTER 400 THERMAL CYCLES (FINAL DEGRADATION MODE) RELATIVE P_{max} IS CELL DEPENDENT

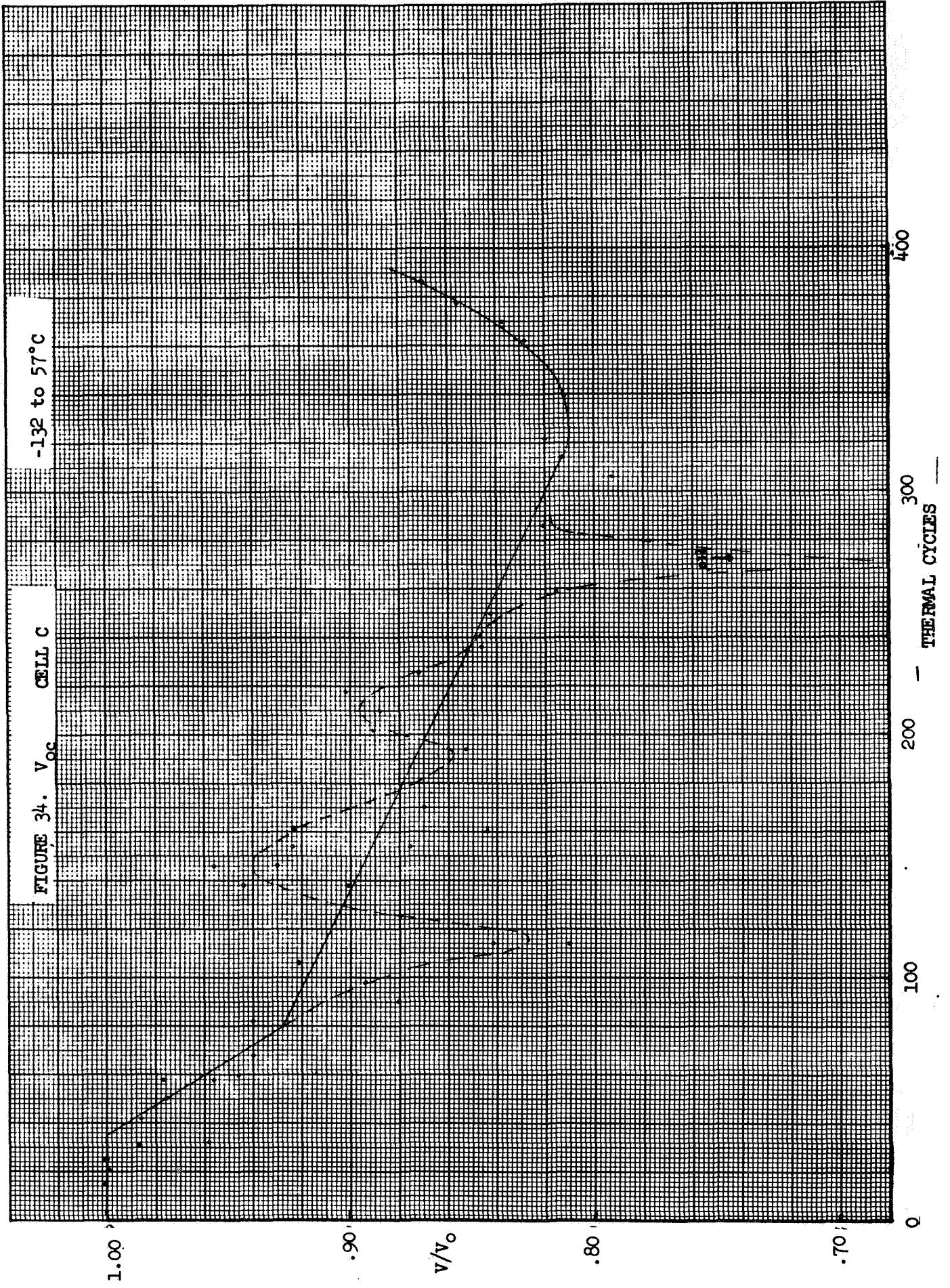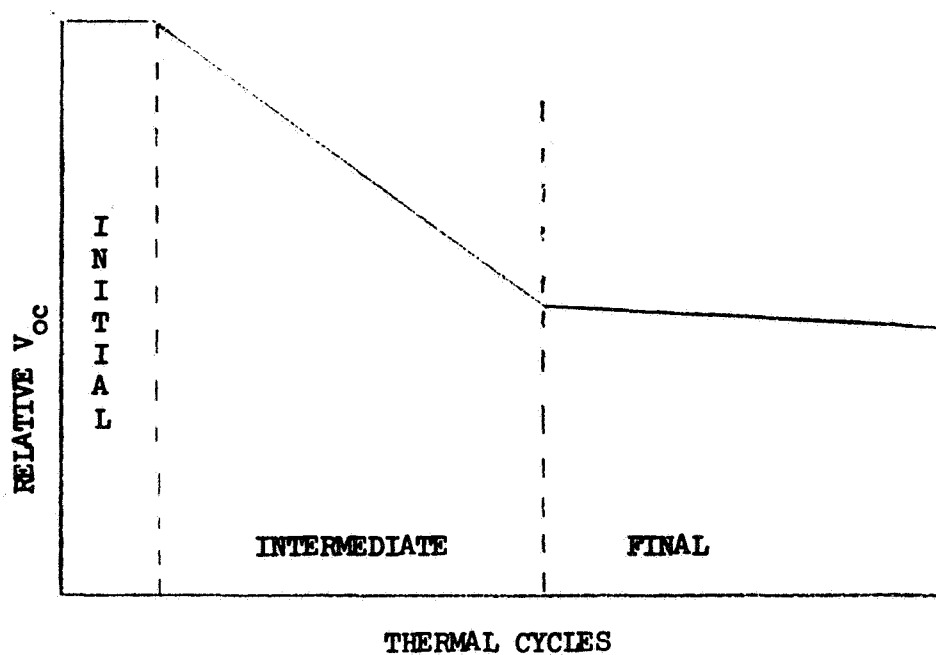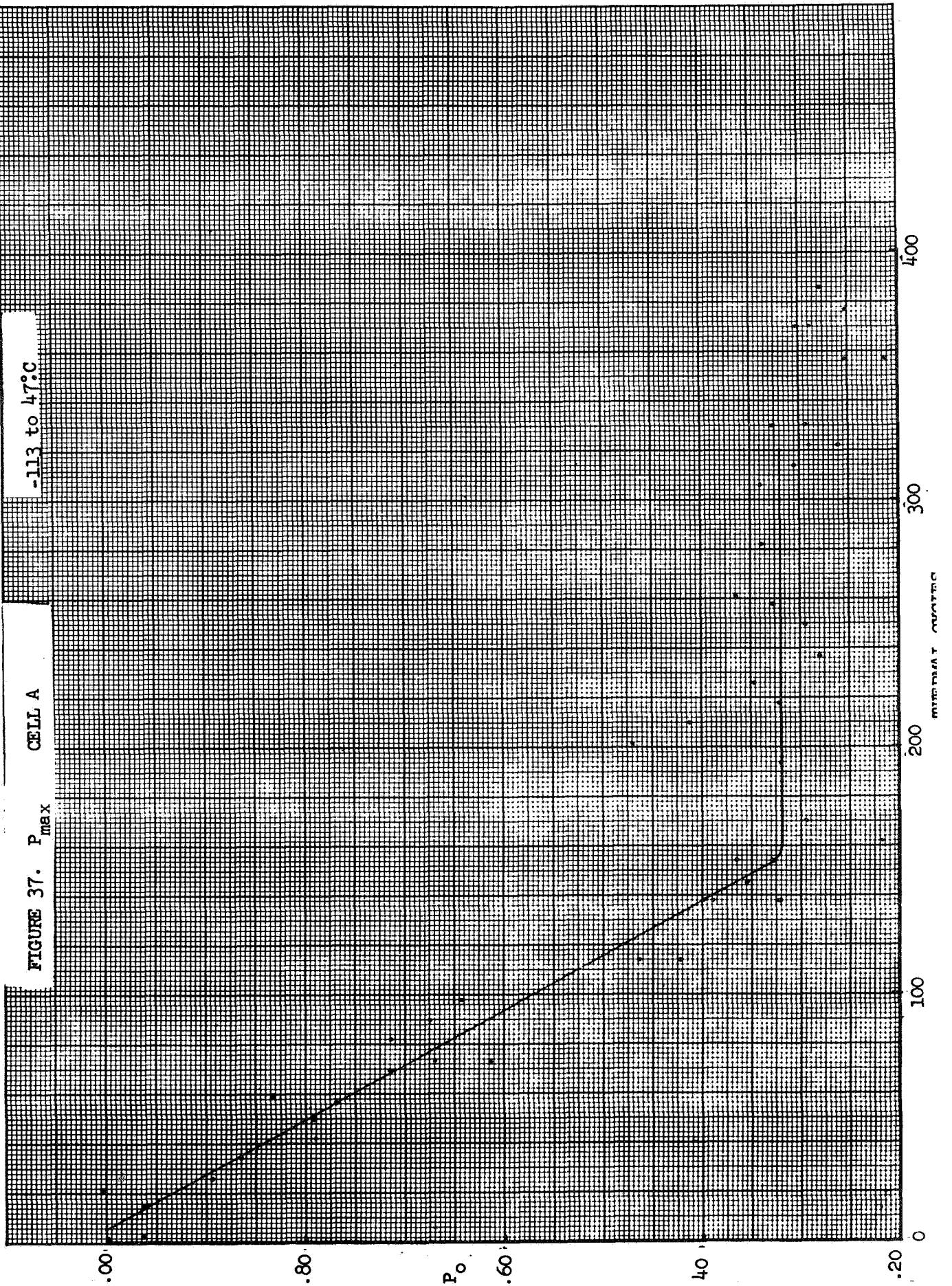| CELL NO.	RELATIVE P_{max}
A	0.32
B	0.35
C	0.25
D	0.25

FIGURE 41
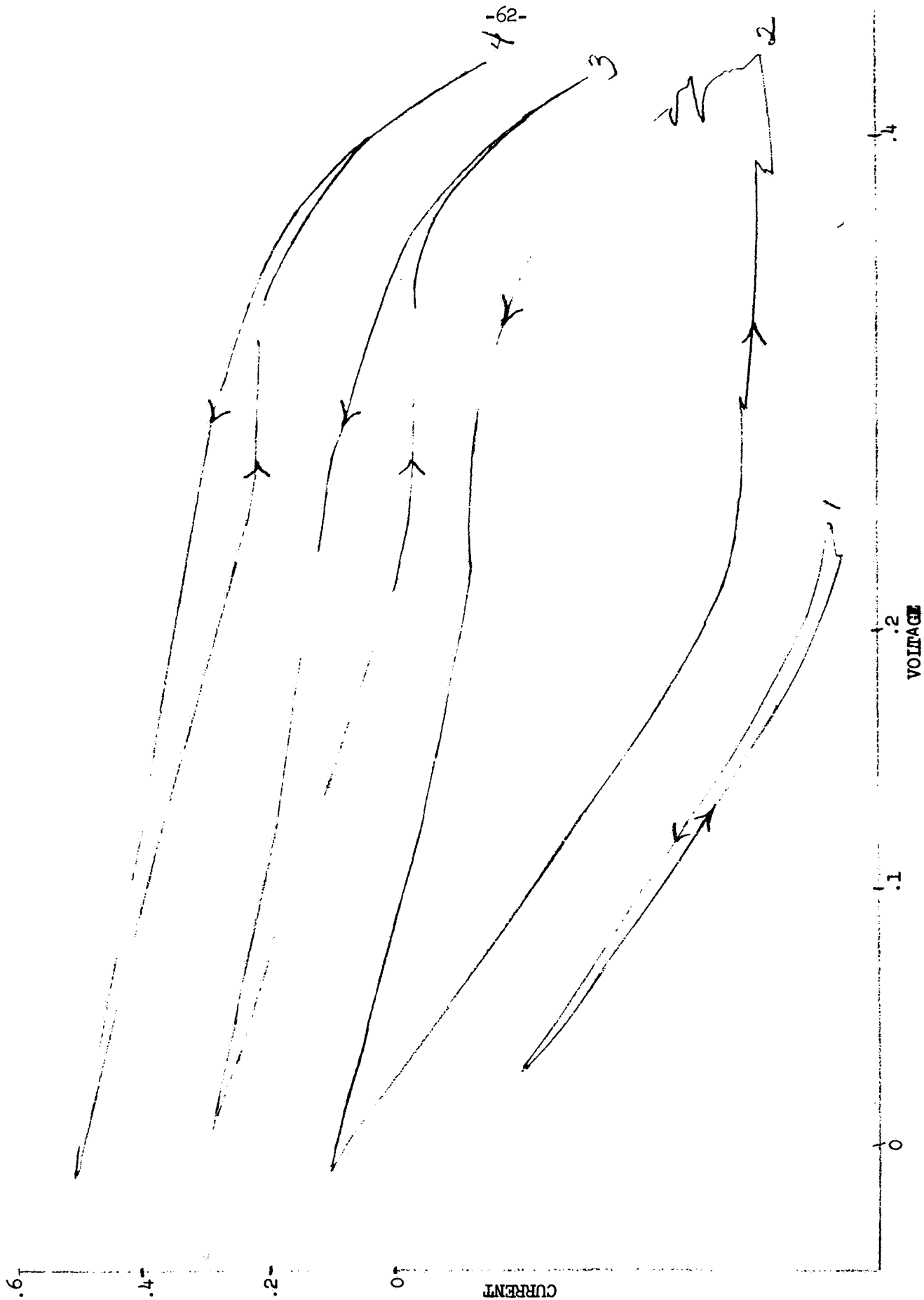
FIGURE 42. CELL C   0910 MAY 16, 1968   LIGHT 69.5   OLD BOX   CYCLE 162

LOAD EFFECTS

W. Dunn, Clevite

Clevite has run several tests in a vacuum oven at $60°$ C where the cells were loaded at P_m. In test #1 the grid overlapped the barrier. Within one week the P_m had dropped 30 percent, but completely recovered when returned to ambient conditions. In test #2, the P_m dropped 10 percent, but the efficiency increased from 4.3 to 4.5 percent when the cell was returned to ambient conditions.

In order to facilitate the interpretation of cell degradation and to assign probable causes for such degradation, a number of cells were tested with deliberately added amounts of series resistance (R_s) and shunt resistance (R_{sh}) and the I-V curves measured. The R_s is defined as the slope of the I-V curve at V_{oc}. The R_{sh} is the slope of the I-V curve at I_{sc}. The fill factor (FF) is defined as the P_m divided by the V_{oc} x I_{sc} and is an indication of the squareness of the knee of the I-V curve.

Figure 43 shows the change in the I-V curve as various series resistances are inserted between the cell and test circuit. The V_{oc} is not affected. The FF suffers from the smallest addition and gets progressively worse. The I_{sc} is not appreciably affected until the resistance exceeds about 0.2 ohms. The locus of the P_m curves into the voltage axis at half the V_{oc}.

Figure 44 shows the change in the I-V curve for various shunt resistances connected across the cell. The I_{sc} does not change for any values of R_{sh}, but the V_{oc} decreases as the shunting path increases. The locus of the P_m points finally intersects the current axis at half the I_{sc}.
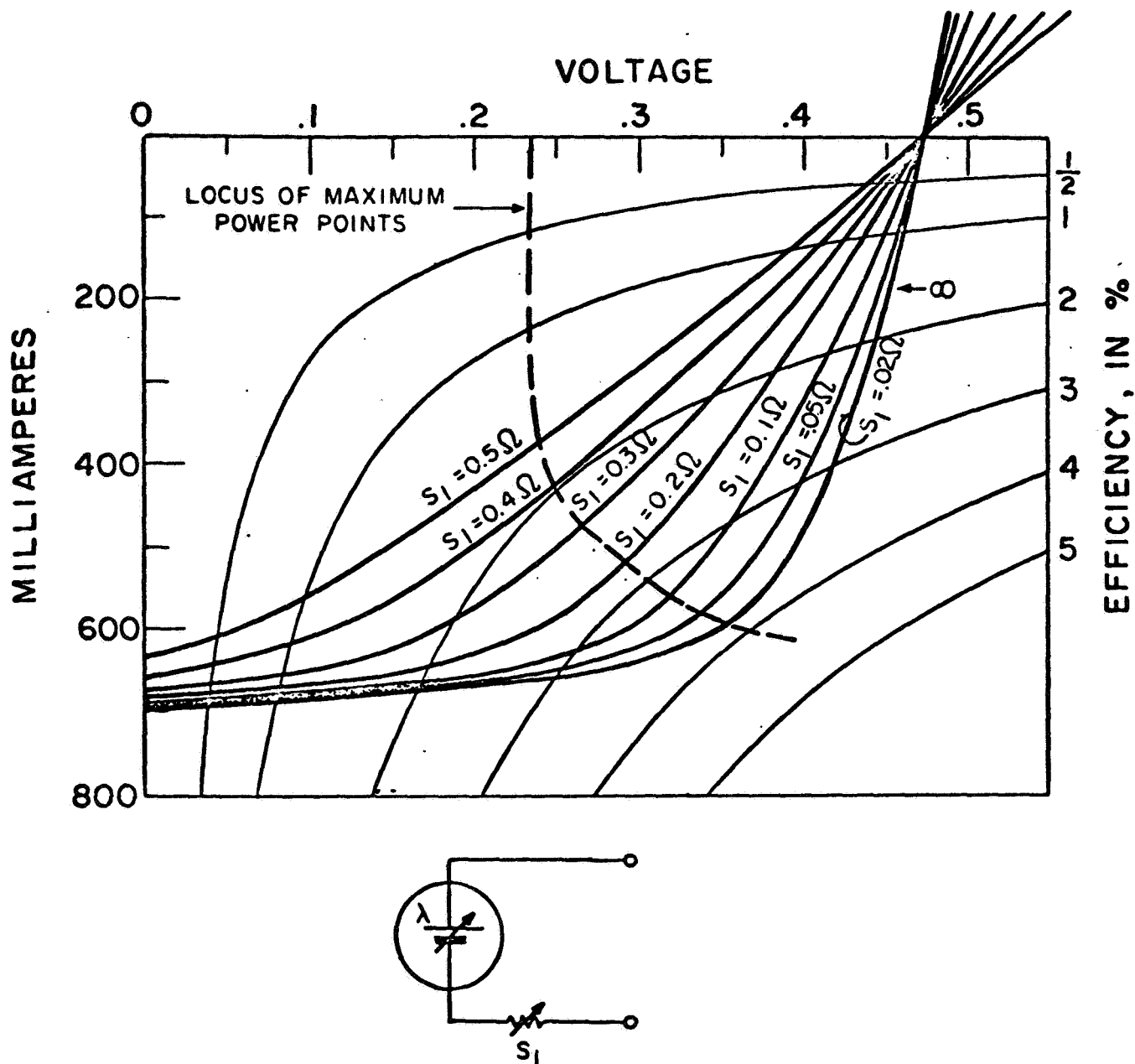
CELL No. A993C

FIGURE 43. - EFFECT OF EXTERNAL SERIES RESISTANCE.

CELL No. A993C

VOLTAGE
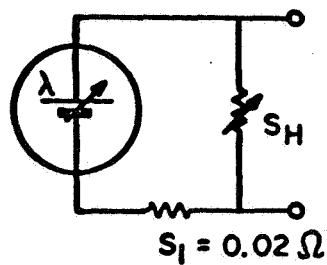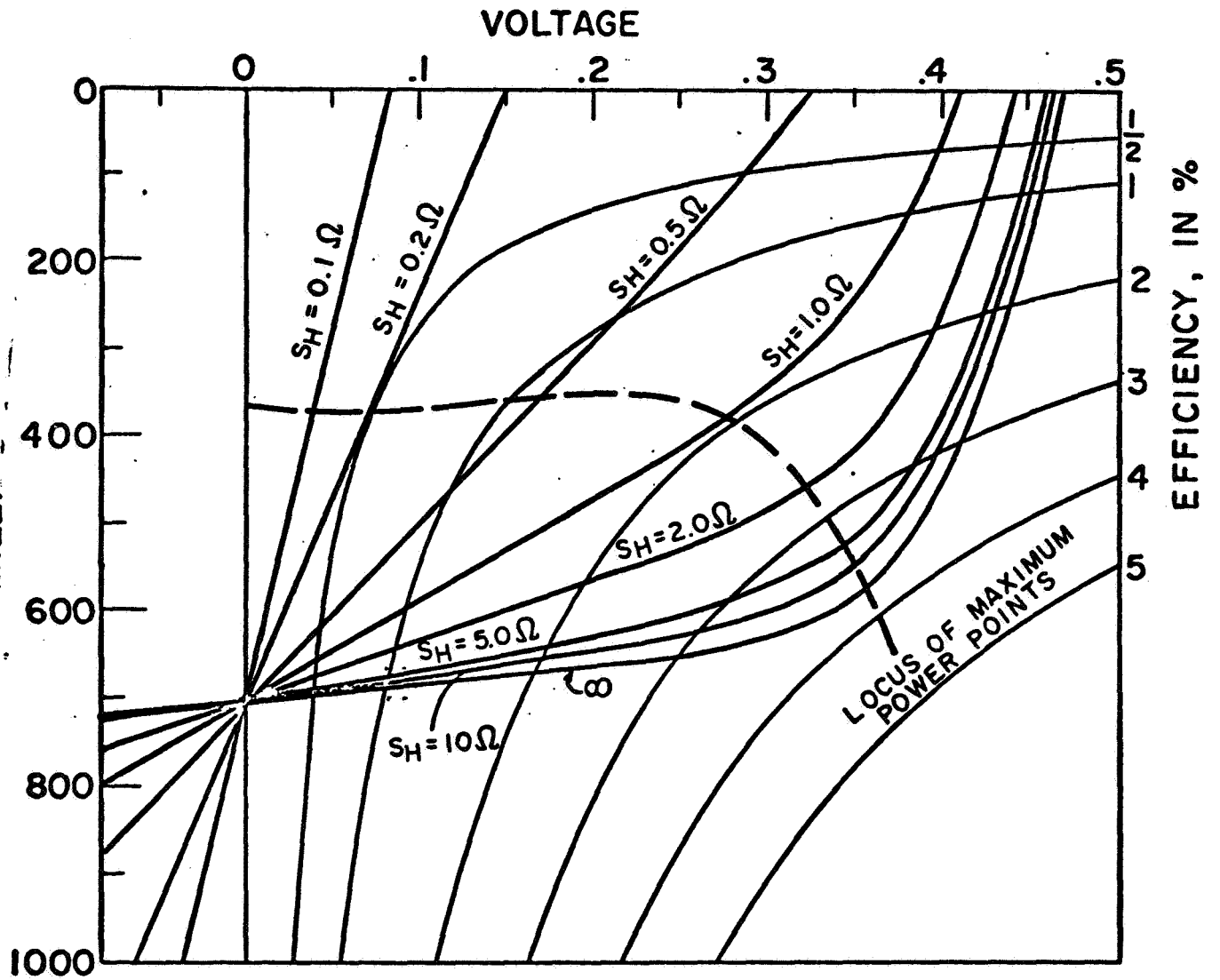
FIGURE 44. - EFFECT OF EXTERNAL SHUNT RESISTANCE.

LOAD EFFECTS

H. W. Brandhorst, Jr., NASA-Lewis

In resolving differences between various performance tests, thermal cycling data, and capacitance measurements, it became apparent that the cell characteristics were being affected by the electrical load. A series of tests were conducted at Lewis under a wide variety of conditions. Cells (1 x 2 cm) were mounted on temperature controlled blocks at 25° C to 60° C under light intensities from total darkness to AMO and I-V characteristics were traced on an oscilloscope. In general, the changes on the I-V curves were similar with only the amount of degradation changing with the particular conditions.

In figure 45 the degradation of a standard production 3" x 3" cell as a function of load is shown. The cell was mounted on a temperature control block at 60° C under one sun illumination. The solid line represents the original I-V curve. When the cell was held at open circuit conditions, the V_{oc} decayed in time and stabilized at the point shown (0.362 V). After the cell was held in the dark, either at 60° or 25° C, the V_{oc} recovered to its original value. Usually the recovery is much faster than the decay. If the cell is then illuminated and held at other constant voltage points, such as 0.3 and 0.2 volts, the current at each voltage gradually decreased to the values shown. Relaxing the cell by holding in the dark restored it to its original condition. Similar degradations were observed when the cell was held at constant current in the light; the voltage at each current decayed until it reached a constant value.

Similar degradation results have been obtained for cells held in the dark but under various forward current loads as shown in figure 46. The cell was held at 60° C. When 100 ma was drawn through the cell the voltage decayed from above 0.4 volt to the point shown (0.325 V). The cell recovered when the load was removed.

The next series of runs were made without any recovery period between load conditions. The sequence begins with 300 ma forward current and the voltage drops from close to 0.7 V to 0.355 V, step (1). When the current was immediately increased to 450 ma, step (2), the voltage necessary to

achieve this forward current was well over 0.7 V. In time the voltage dropped to 0.365 V. When the current was then decreased from 450 to 300 ma, step (3), the voltage required dropped from 0.365 V to a value near 0.2 V and then slowly increased to the stable value of 0.345 V. Finally the current was decreased to 200 ma, step (4), and the voltage dropped to 0.335 V.

In figure 47 the decay of the voltage is shown as a function of time. Here the cell was again held in the dark at 25° C and 300 ma reverse current was used. The voltage decayed as shown until the power was momentarily interrupted. Cell recovery began immediately. When power was restored the decay continued as before. Interruption of the light resulted in similar behavior of the cell.

In figure 48 the effect of measuring the I-V curve on the performance of the cell is shown. The original I-V curve is shown by the best curve labeled (2) and (3). This cell was degraded from a V_{oc} of 0.485 V to 0.440 V. When the I-V curve was measured a noticeable improvement was noted in the curve as the manual potentiometer was operated. At 0.250 V the load was increased and the curve retraced to open circuit conditions, and V_{oc} was found to have recovered to 0.460 V. When the I-V curve was then run to I_{sc} a noticeable recovery along the curve was noted. Subsequent runs showed the cell to be completely recovered. This recovery of degraded cells when I-V plots are made has been seen for many cells made during the past year.

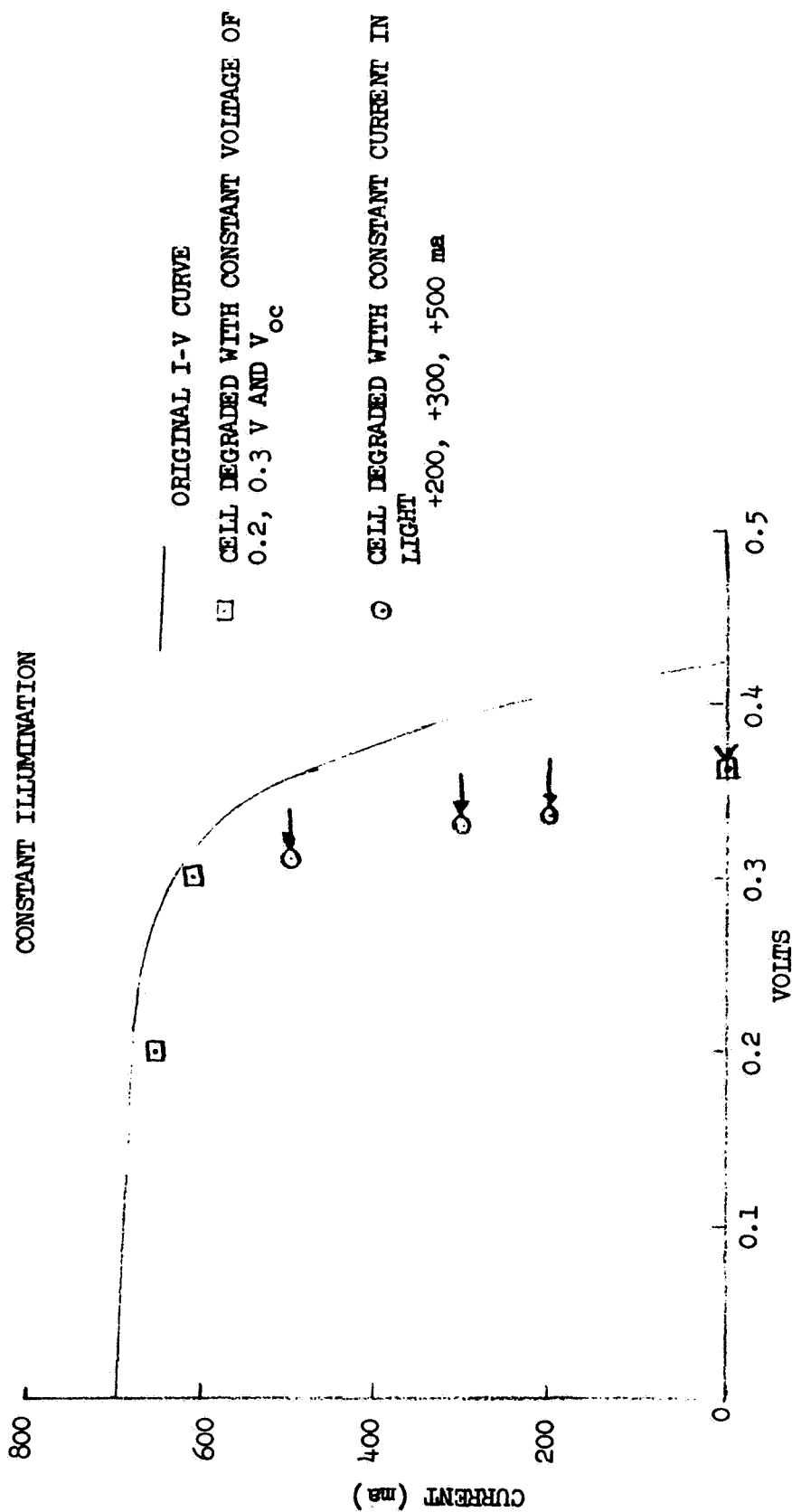We do not know what the explanation of this effect is.

FIGURE 45. CELL LOADED UNDER VARIOUS CONDITIONS
SHOWING DEGRADATION AS A FUNCTION OF LOAD
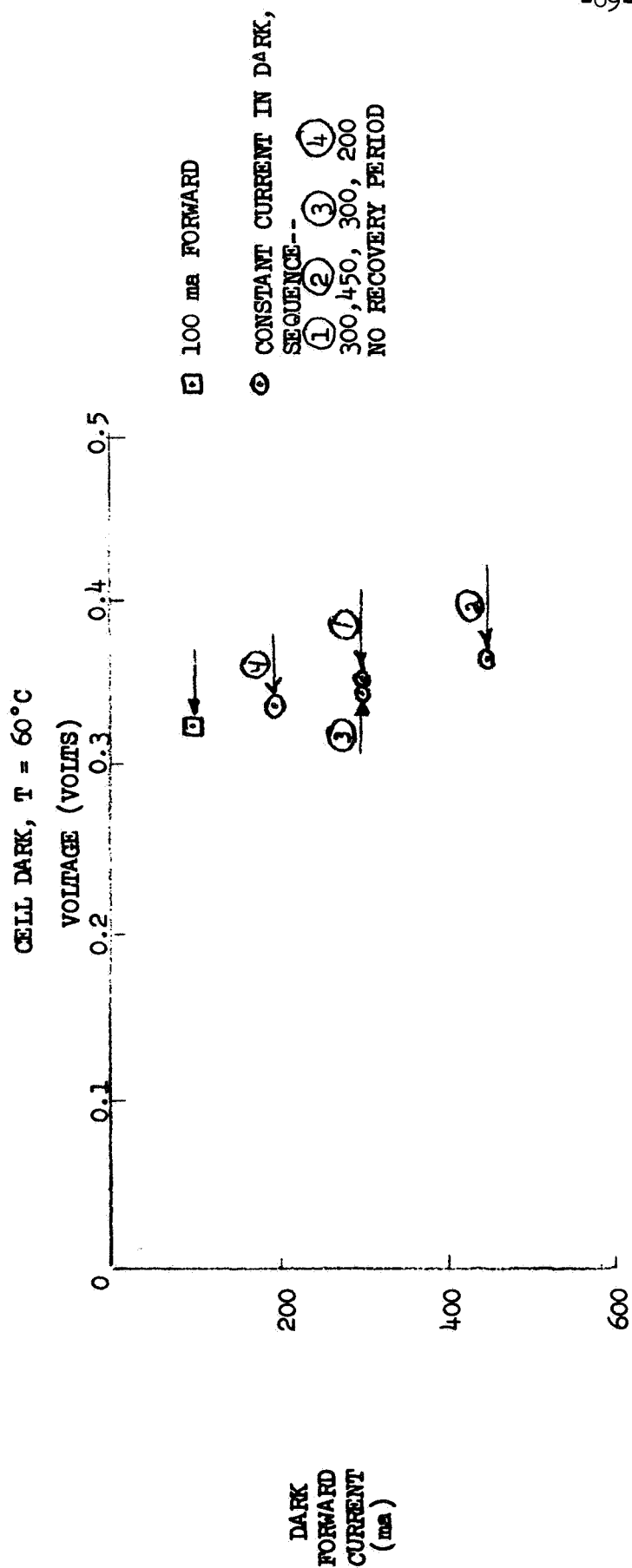
FIGURE 46. CELL DEGRADATION OBSERVED UNDER
VARIOUS FORWARD CURRENT LOADS
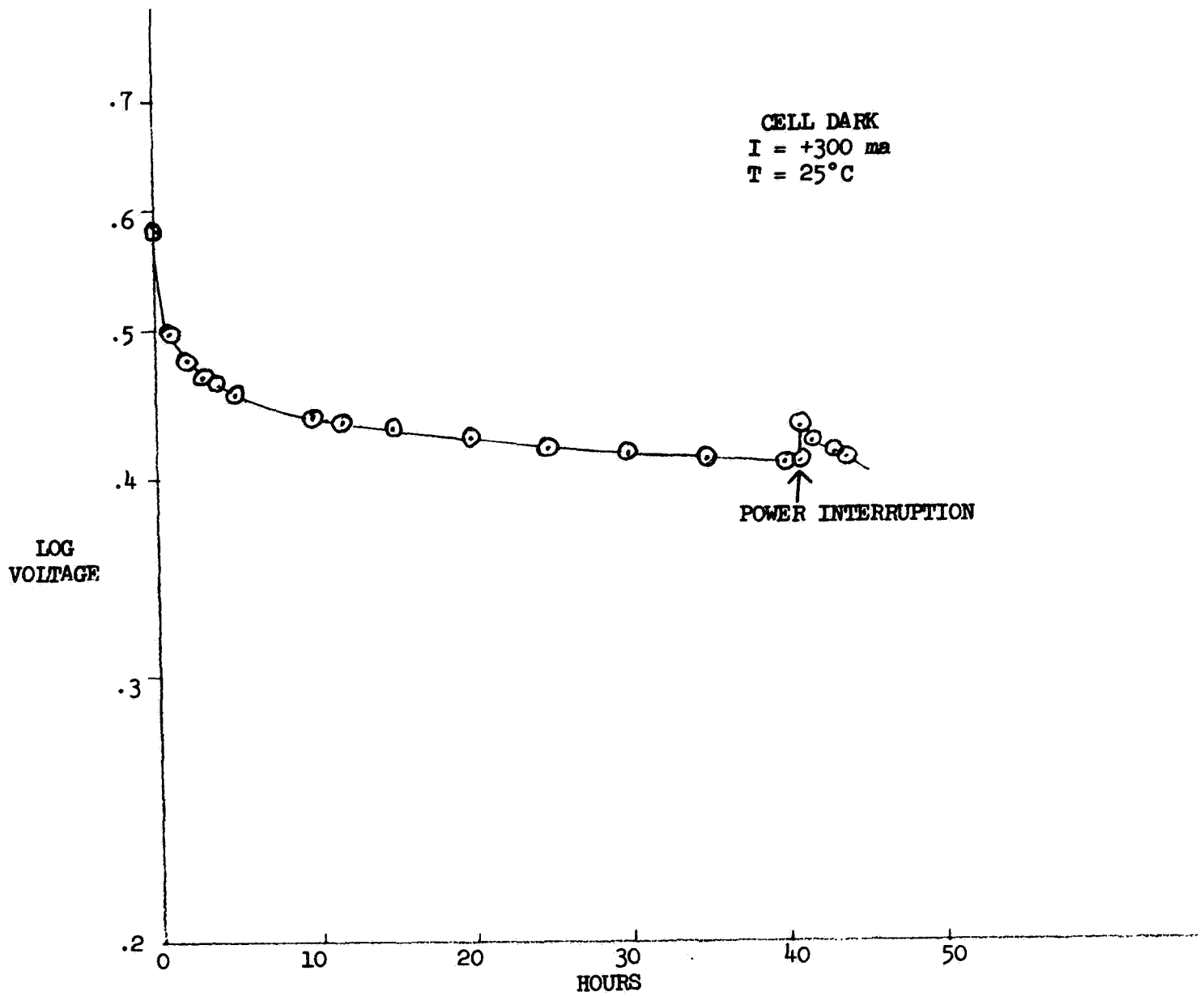
FIGURE 47. EFFECT OF MOMENTARY INTERRUPTION
ON DECAY OF VOLTAGE
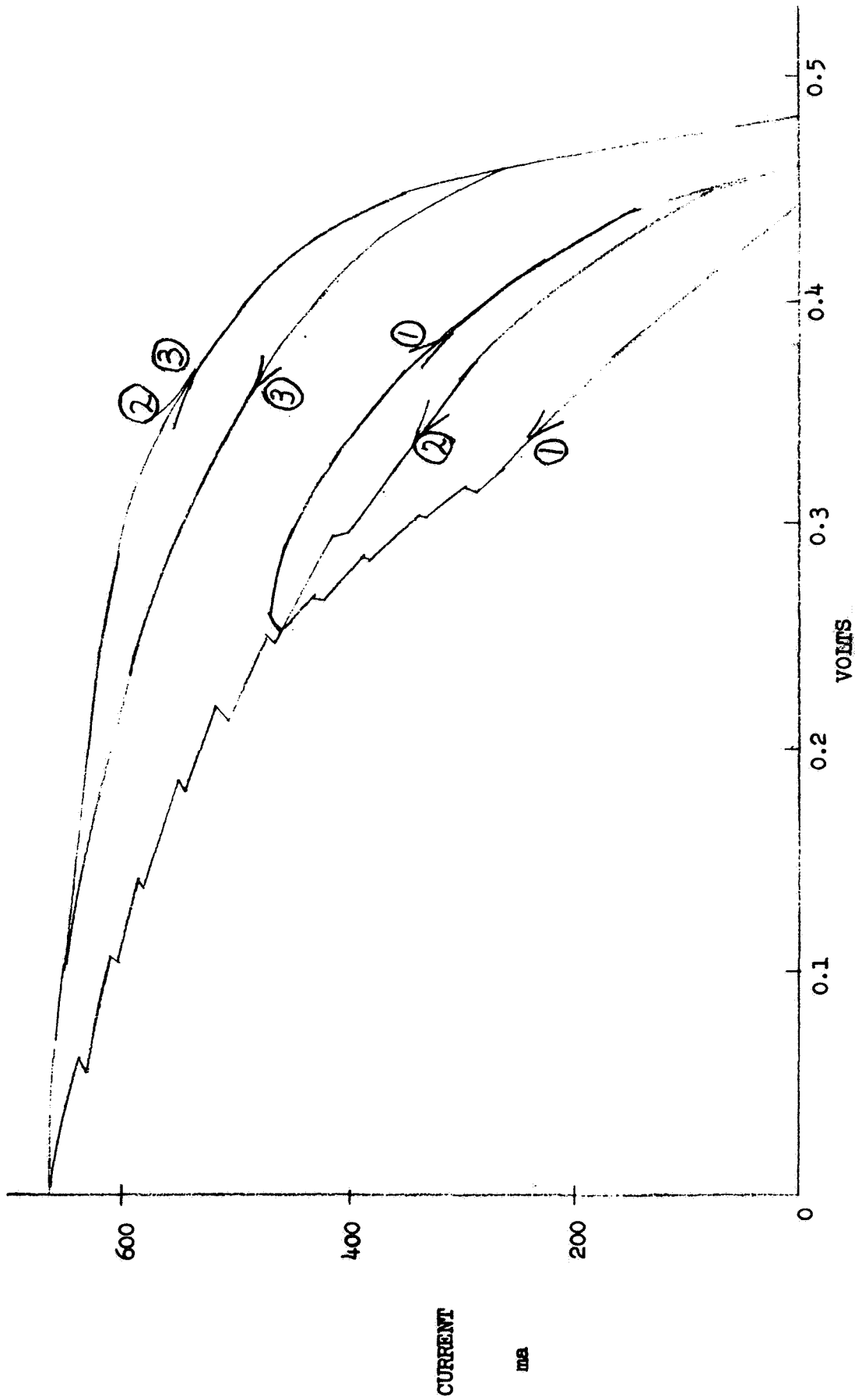
FIGURE 48. I-V CURVE OBTAINED ON DEGRADED CELL

IV. STABILITY TESTS

WET AND DRY STORAGE, THERMAL VACUUM STORAGE

W. Dunn, Clevite

During the NASA contract cells have been placed on both wet and dry shelf storage. From each month's production, four cells are placed on each test. The cells are stored at ambient temperature and pressure during the test, but in a desiccated container for the dry test and in an 80 percent relative humidity container for the wet test. The cells are removed periodically (usually every month) and their I-V curve measured on the standard performance set up at AMI and 25° C. The results from the dry storage tests are shown in Table VI. The cells made in the first half of 1967 were poor due to the bad batches of cover epoxy. The results from the wet storage are shown in Table VII. Here again the cells from the first half of 1967 did poorly, again attributed to the bad cover epoxy. Cells made after July 1967 have been more stable in both tests.

Storage tests have been carried out on each month's standard production cells at elevated temperatures. The cells are stored in a vacuum oven (10^{-4} torr) at 100° and 150° C and are removed periodically for performance measurements. The performance changes are therefore indicative of the permanent changes taking place in the cell. The degradation at 100° and 150° C are shown in Tables VIII and IX, respectively. The cells degrade about 10 percent in 8 months at 100° C. The change at both temperatures has been attributed to copper diffusion through the junction region. The question arose as to how this Cu diffusion could be slowed down. One solution put forth was to add In dopant to compensate the n-CdS during the evaporation process. Therefore, the subsequent diffusion of Cu into the i-layer will have less of an effect.

The results from 7 standard production cells thermally cycled at Boeing for 506 cycles are shown in Table X. These cells had degraded to between 75 and 88 percent of their initial P_m as measured in situ at 60° C. Of the two Cu substrate cells included in this test, the relative P_m of one degraded to 77 percent and the other catastrophically failed to 25 percent of its original P_m. After the tests were completed at

Boeing the cells were returned to Clevite where the performance was measured at 25° C. It is to be noted that the cells did not change much with the exception of the Cu substrate cells which recovered almost completely. Table XI lists complete data taken before and after the thermal cycling. These measurements were taken at AMI and 25° C on Clevite's standard performance set up.

TABLE VI - DRY SHELF STORAGE - LONG TERM TEST DATA

AM1, 25°C Efficiency after Indicated Months:

Cell No.	Date Mfrd.	0	1	2	3	4	5	6	7	8	9	10	11	12
D289D	5/66	4.9	-	-	4.9	4.8	4.8	4.9	4.8	4.9	5.0	4.7	4.9	5.0
D292D	5/66	4.7	-	-	4.9	4.6	4.6	4.9	4.9	4.8	5.0	4.8	4.9	5.0
D296B	5/66	4.5	-	-	4.4	4.3	4.2	4.3	4.3	4.4	4.4	4.4	4.4	4.4
D304A	5/66	4.8	-	-	4.5	4.5	4.5	4.5	4.5	4.5	4.5	4.4	4.5	4.2
D306D	6/66	4.9	-	-	4.9	4.8	4.8	4.9	4.9	5.0	5.1	5.1	5.1	4.8
D315A	6/66	5.2	-	-	5.2	5.0	5.0	5.2	5.3	5.2	5.2	5.1	5.3	5.3
D336D	6/66	4.2	-	4.1	4.0	4.0	4.1	4.0	4.2	4.4	4.1	4.3	4.3	4.3
D344C	6/66	5.2	-	4.9	4.8	4.7	4.7	4.7	4.8	4.9	4.7	4.9	4.8	4.8
D355C	8/66	5.7	-	5.3	5.2	5.3	5.4	5.4	5.5	5.4	5.4	5.8	5.3	5.3
D364F	8/66	4.7	-	4.2	4.1	4.1	4.1	4.0	4.2	4.2	4.2	4.2	4.3	4.3
D375C	8/66	4.4	4.3	4.4	4.1	4.4	4.6	4.4	4.4	4.4	4.4	4.4	4.4	4.2
D381A	8/66	5.1	5.1	5.2	5.1	5.1	5.2	5.1	5.1	5.1	5.1	4.8	4.8	4.7
D385B	9/66	5.0	5.2	5.1	5.1	5.2	5.0	5.1	5.1	5.1	5.1	5.1	4.9	5.0
D386E	9/66	5.1	5.2	5.1	5.2	5.2	5.2	5.2	5.2	5.1	5.2	5.2	5.0	5.0
D391B	9/66	4.7	5.0	5.2	5.0	5.1	5.1	5.0	5.1	5.1	5.0	5.0	4.9	5.0
D395C	9/66	4.2	4.2	4.1	4.2	4.2	4.3	4.2	4.3	4.3	4.2	4.2	4.1	4.3
D403B	10/66	4.6	4.7	4.8	4.9	4.8	4.7	4.8	4.8	4.7	4.6	4.6	4.6	4.7
D410B	10/66	4.9	4.8	4.8	4.9	4.9	4.9	4.9	4.9	4.7	4.7	4.6	4.6	4.7

TABLE VI - DRY SHELF STORAGE - LONG TERM TEST DATA, continued

Cell No.	Date Mfrd.	AM1, 25°C Efficiency after Indicated Months:										
		13	14	15	16	17	18	19	20	21	22	23
D289D	5/66	5.0	4.9	4.7	4.8	4.7	4.9	4.6	4.6	-	-	4.6
D292D	5/66	5.0	4.8	4.7	4.8	4.8	4.8	5.0	4.6	-	-	4.5
D296B	5/66	4.4	4.3	4.2	4.3	4.2	4.2	4.5	4.1	-	-	4.1
D304A	5/66	4.3	4.4	4.2	4.2	4.2	4.2	4.3				
D306D	6/66	5.0	5.0	4.8	5.0	4.9	4.9	5.0	4.8	-	-	4.6
D315A	6/66	5.2	5.3	5.0	5.2	5.0	5.1	5.2	4.9	-	-	4.7
D336D	6/66	4.2	4.2	4.0	4.3	4.2	4.1	4.2	4.1	-	-	4.2
D344C	6/66	4.6	4.3	4.0	4.3	4.0	4.3	4.3				
D355C	8/66	5.2	5.5	-	-	5.0	5.2	5.4	5.0	-	-	5.0
D364F	8/66	4.2	4.4	-	-	4.2	4.4	4.5	4.1	-	-	3.8
D375C	8/66	4.3	4.2	4.4	4.0	-	-	4.0				
D381A	8/66											
D385B	9/66	4.9	5.1	-	4.8	-	-	4.8				
D386E	9/66	5.1	5.2	-	5.0	-	-	4.8				
D391B	9/66	4.9	5.0	-	4.8	-	-	4.6				
D395C	9/66	4.2	4.3	-	4.0	-	-	4.0				
D403B	10/66	4.6	4.8	4.4	4.3							
D410B	10/66	4.7	4.7	4.5	4.5							

TABLE VI, continued – DRY SHELF STORAGE – SHORTER TERM TEST DATA

Cell No.	Date Mfrd.	AM1, 25°C Efficiency after indicated Months:												
		0	1	2	3	4	5	6	7	8	9	10	11	12
D507F	2/67	5.7	5.3	5.3	5.1	4.9	4.9	4.7	4.7					
D513E	2/67	5.1	5.0	5.1	5.0	4.8	4.8	4.8	4.6	-	-	4.6	4.6	4.5
D521F	3/67	4.6	4.4	4.6	4.6	4.4	4.5	4.3	4.3	-	-	4.0	4.3	4.4
D522E	3/67	4.8	4.7	4.8	4.7	4.5	4.6	4.5	4.4	-	-	4.5	4.4	4.4
D551E	4/67	4.5	5.0	4.7	4.7	4.6	4.6	4.8	-	4.5	4.5	4.5		
D563A	4/67	4.8	4.9	4.6	4.6	4.5	4.6	4.7	-	4.5	4.5	4.4		
D579B	4/67	5.1	4.9	4.6	4.7	4.5	4.6	4.8	-	4.5	4.4	4.4		
D583C	4/67	4.8	5.0	4.7	4.7	4.6	4.6	4.8	-	4.5	4.4	4.4		
N14B2	5/67	5.5	5.2	4.8	4.8	4.7	4.7	-	-	4.6	4.5	4.5		
N14B5	5/67	4.4	4.1	3.8	3.9	3.8	3.8	4.0						
N20B1	6/67	4.9	5.1	4.8	4.8	4.7	4.9	5.0	-	4.6	4.6	4.5		
N31BK4	6/67	4.1	4.2	4.0	4.1	4.0	4.0	4.2	-	3.7	3.8	3.8		
D597E	5/67	5.0	4.4	4.4	4.3	3.9	4.5	-						
D609B	6/67	4.6	4.1	4.1	3.9	4.0	4.2	-						
N35B3	6/67	5.0	4.9	5.0	4.9	4.9	5.2		4.5	4.6	4.6			
N44B3	6/67	4.4	4.4	4.4	4.3	4.4	4.4		3.7	3.7	4.0			
N64BK5	7/67	4.0	4.0	4.1	4.1	-	-	4.0	4.0	4.0	4.1	4.0		
N65BK5	7/67	4.2	4.0	4.2	-	-	4.0	4.0	4.0	4.0	4.0	4.0		
N71AK2	8/67	4.1	3.8	4.0	4.0	-	-	3.9	3.9	3.8	3.9	3.8		
N78AK5	8/67	4.7	3.6	4.2	4.5	-	4.2	4.2	4.2	4.9	4.2			
N80AK6	9/67	4.2	-	3.8	4.0	-	3.9	4.0	3.8	4.0	3.9			
N85BK3	10/67	4.4	-	3.9	4.2	-	3.9	3.9	3.8	3.9	3.9			
N86C5	10/67	5.9	4.7	5.4	5.9	-	5.5	5.4	5.4	5.1	5.2			
N99AK8	10/67	4.5	4.4	4.4	4.4	4.4								
N113CK7	1/68	3.9	3.7	4.0	3.8									
N128AK4	2/68	4.1	4.1	4.1	4.1									
N163BK1	3/68	4.0	4.0	4.0										

TABLE VII - WET SHELF STORAGE - LONG TERM TEST

Cell No.	Date Mfrd.	AM1, 25°C Efficiency after indicated Months:												
		0	1	2	3	4	5	6	7	8	9	10	11	12
D187B	2/66	5.5	-	-	-	-	-	5.5	5.2	5.3	5.3	5.3	5.3	5.4
D291A	4/66	4.6	-	4.5	4.6	4.2	4.1	4.2	4.3	4.2	4.2	4.0	4.1	4.1
D294A	4/66	4.3	-	3.4	3.2	3.2	3.2	3.2	3.1	3.2	3.2	3.9	2.8	2.8
D297C	5/66	4.6	-	4.4	4.3	4.0	4.2	4.2	4.2	4.3	4.4	4.2	4.3	4.3
D301A	5/66	4.6	-	4.3	4.3	4.0	4.0	4.2	4.2	4.2	4.2	4.1	4.1	4.1
D313C	5/66	4.4	4.1	-	4.1	3.8	4.0	3.8	3.9	4.1	3.9	3.8	3.8	3.8
D348C	6/66	4.8	-	4.8	4.2	4.3	4.4	4.4	4.5	4.4	4.2	4.5	4.6	4.4
D350F	6/66	4.8	-	4.8	4.5	3.8	3.9	4.0	4.2	4.4	3.7	4.3	4.2	4.2
D350C	7/66	4.3	4.3	4.4	4.2	4.3	4.4	4.5	4.5	4.2	4.4	4.4	4.2	4.4
D357E	7/66	4.4	4.3	4.5	4.4	4.3	4.4	4.4	4.3	4.3	4.3	4.3	4.1	4.3
D372A	8/66	4.5	4.3	4.3	4.3	4.3	4.2	4.2	3.9	4.0	4.2	4.2	4.0	4.3
D378B	8/66	4.8	4.6	4.6	4.5	4.5	4.4	4.4	4.3	4.3	4.5	4.5	4.0	4.4
D385F	9/66	5.1	5.2	5.0	5.0	5.1	4.8	4.7	4.8	4.7	4.3	4.6	4.3	4.4
D401B	9/66	5.2	5.2	5.0	5.0	5.0	4.8	4.7	4.7	4.8	4.7	5.0	4.6	4.8
D405A	10/66	4.8	4.5	4.6	4.5	4.5	4.4	4.4	4.4	4.3	4.5	4.3	4.4	4.4
D411F	10/66	4.6	4.4	4.4	4.4	4.3	4.3	4.3	4.3	4.2	4.4	4.0	4.3	4.3
D454A	12/66	5.2	4.6	4.6	4.5	4.4	4.4	4.3	4.2	4.0	4.0	3.9	3.9	4.1

TABLE VII - WET SHELF STORAGE - LONG TERM TEST, continued

Cell No.	Date Mfrd.	AM1, 25°C Efficiency after indicated months:												
		13	14	15	16	17	18	19	20	21	22	23	24	25
D187B	2/66	5.3	5.3	5.3	5.3	5.2	5.1	5.0	-	-	-	-	-	4.8
D291A	4/66	4.1	4.0	4.1	3.9									
D294A	4/66	2.7												
D297C	5/66	4.3	4.2	4.4	4.2	4.3	4.0	-	-	-	-	-	-	4.0
D301A	5/66	4.1	3.9	4.0	3.7									
D313C	5/66	3.7	3.9	3.7	3.7									
D348C	6/66	4.4	4.6	4.4	4.4	4.6	4.5	4.1	-	4.0				
D350F	6/66	4.2	4.4	4.2	4.3	4.3	4.4	3.8	-	3.7				
D350C	7/66	4.1	4.2	4.2	4.2	3.8	-	3.7						
D357E	7/66	4.0	4.1	4.0	4.1	3.9	-	3.8						
D372A	8/66	4.0	4.0	4.0	4.1	3.8	-	3.6						
D378B	8/66	4.0	4.1											
D385F														
D401B	9/66	4.8	4.7	4.1	-	4.0								
D405A	10/66	4.4	4.1	-	4.1									
D411F	10/66	4.3	4.0	-	3.9									
D454A	12/66	-	3.6											

TABLE VII, continued-   WET SHELF STORAGE - SHORTER TERM TEST DATA

Cell No.	Date Mfrd.	AM1, 25°C Efficiency after Indicated Months:																	
		0	1	2	3	4	5	6	7	8	9	10	11	12	13	14	15	16	17
D436E	1/67	5.3	4.7	4.6	4.6	4.5	4.3	4.3	4.3	4.2	4.4	-	4.1	4.0	4.0	4.0	-	-	4.0
D450C	1/67	5.3	4.2	4.1	4.3	4.3	4.0	4.0	4.1	3.8	3.8								
D454E	1/67	5.3	4.1	-	-	-	3.7	3.7	3.5	3.6	3.7								
D480B	2/67	5.1	4.6	4.5	4.7	4.4	4.3	4.3	4.3	4.1	4.4	-	4.0	4.0	4.0	4.0	3.9		
D495A	2/67	5.4	4.8	4.7	4.7	4.5	4.5	4.5	4.5	4.5	4.7	-	4.3						
D487C	2/67	5.5	5.1	5.0	5.1	4.8	4.8	4.8	4.8	4.7	5.0	-	4.5	4.5	4.5	4.5	4.5		
D476A	2/67	5.0	4.8	4.7	4.8	4.6	4.5	4.5	4.5	4.1	4.7	-	4.3	4.3	4.2	4.2	4.2		
D506B	3/67	5.7	-	5.9	4.9	4.8	4.7	4.8	4.9	-	4.5	4.5	4.4	4.5	4.3				
D509E	3/67	5.5	-	4.8	4.4	4.4	4.3	4.3	4.4	-	4.0	3.9	3.8	3.7	3.6				
D516A	3/67	5.3	-	4.6	4.4	4.4	4.3	4.2	4.5	-	4.1	4.1	4.0	4.1	4.0				
D526C	3/67	4.4	-	3.9	3.8	3.8	3.8	3.8	4.0	-	3.7	3.6	3.6	3.7	3.6				
D554A	4/67	5.7	5.4	5.0	-	4.9	5.0	5.2	-	4.6	4.5	4.5	4.5	4.3					
D562E	4/67	4.7	4.2	3.9	3.9	3.8	3.7	3.8	-	-	-	-							
N17B3	4/67	4.8	4.6	4.2	4.3	4.1	4.0	4.1	-	3.6	3.5	3.5	3.4	3.2					
D602D	4/67	4.6	3.2	4.0	3.9	4.0	4.1	-	-	-	-	-							
N14B8	5/67	5.0	5.1	4.7	4.7	4.7	4.6	5.0	-	4.5	4.5	4.5	4.5	4.4					
N580E	5/67	5.0	4.3	4.0	4.1	3.9	4.0	4.1	-	3.7	3.6	3.6	3.6	3.6					
N585C	5/67	5.1	5.1	4.7	4.7	4.5	4.5	4.7	-	4.2	4.1	4.0	4.0	3.8					
D615C	6/67	5.3	4.9	5.0	4.8	4.8	5.1	-	4.5	4.4	4.3	4.2	4.1						
N38B7	6/67	4.6	4.1	4.2	4.1	3.9	4.0	-	3.8	3.6	3.6	3.6	3.6						
N51B8	6/67	5.3	4.4	4.8	4.6	4.6	4.8	-	4.2	4.2	4.1	4.0	4.0						
N52B4	6/67	4.9	4.7	4.5	4.6	-	4.5	3.9	3.7	3.7	3.5	3.6							
N59BK7	6/67	3.4	3.2	3.6	3.5	-	3.7	3.7	3.7	-	3.6								
H107B5	8/67	5.3	5.4	-	-	5.4	-	5.5	5.5	-	5.4	5.1	5.4	5.2					
N98BK5	10/67	5.0	5.0	-	-	-	4.9	4.6	4.6	4.5									
N112AK5	1/68	4.2	4.2	4.4	4.3	4.3	4.3	4.2											
N127BK8	2/68	4.4	4.1	4.5	4.5	4.3													
N165BK9	3/68	3.6	4.2	-	-	4.0	4.0												
N185BK4	4/68	4.0	-	4.0	-	4.0													
N187AK5	4/68	4.2	-	4.1	-	4.1													

TABLE VIII - 100°C VACUUM STORAGE

AM1, 25°C Efficiency after Indicated Months:

Cell No.	Date Mfrd.	0	1	2	3	4	5	6	7	8	9	10	11	12	13	14	15	16	17
D349A	6/66	4.0	4.8	4.6	4.5	3.8	3.3	2.9	2.6	2.3	2.1	1.5	1.0	0.7	0.7				
D357B	7/66	4.3	4.0	3.4	2.8	1.2	0.9	0.3	0.3	0.4	0.3	0.2	0.1	0.1	0.2				
D357C	7/66	4.8	3.8	1.7	-	0.3	0.2	0.2											
D363E	7/66	3.3	3.0	3.0	2.9	2.0	1.8	1.0	0.9	1.0	1.0	0.5	0.2	0.2	0.2				
D369E	8/66	4.9	4.6	4.6	4.4	4.5	4.3	4.1	3.8	3.5	2.5	2.1	1.7	1.0					
D373C	8/66	4.1	3.9	3.9	3.6	3.8	3.7	3.6	3.5	3.4	3.1	3.0	2.6	2.4					
D377A	8/66	5.0	4.7	4.7	4.2	4.1	3.6	3.2	2.6	1.6	0.5	0.4	0.5	0.4					
D379E	8/66	5.1	5.2	5.2	5.0	5.1	5.0	4.9	4.7	4.7	4.6	4.3	4.3	4.0	3.8	3.7	-	3.0	2.6
D385E	9/66	4.7	4.5	4.3	4.2	4.2	4.0	3.8	3.7	3.8	3.4	3.3	3.2						
D388F	9/66	4.6	5.0	4.8	4.9	4.9	4.6	4.5	4.4	4.4	4.2	4.2	4.0	3.8	3.9	-	-	3.5	3.3
D392A	9/66	5.0	5.3	5.0	5.1	5.0	4.8	4.7	4.5	4.5	4.5	4.4	4.3	4.1	4.1	-	-	3.6	3.4
D401F	9/66	4.5	4.7	4.6	4.7	4.8	4.5	4.5	4.5	4.5	4.0	3.6	3.5	3.7	4.0	-	-	3.6	3.6
D403D	10/66	6.0	5.7	5.5	4.2	3.4	1.9	1.3	1.3	short									
D405C	10/66	5.6	5.6	5.5	4.6	4.9	4.4	4.2	4.2	3.4	3.6	3.2	3.5	3.3	-	-	3.2	2.7	
D407D	10/66	4.9	3.1	3.0	2.5	2.8	2.7	4.0	4.0	3.7	4.0	3.7							
D411D	10/66	5.0	4.4	4.2	3.4	3.3	2.3	1.7	1.7	0.9									
D438D	1/67	5.6	5.8	5.6	5.7	5.5	4.8	4.3	-	3.9	3.6	3.9	3.3						
D462E	1/67	6.1	5.8	5.7	5.7	5.8	5.3	5.7	-	5.1	4.9	5.2	4.8						
D504E	2/67	5.6	5.7	5.5	5.5	5.3	5.1	4.5	4.6	-	4.2	4.0	4.5	3.9					
D514E	2/67	5.3	4.8	4.6	4.6	4.5	4.4	4.0	4.3	-	3.9	3.4	3.1	3.3					

TABLE VIII, continued -100°C VACUUM STORAGE

Cell No.	Date Mfrd.	AM1, 25°C Efficiency after Indicated Months:									
		0	1	2	3	4	5	6	7	8	9
D455D	1/67	5.9	5.0	4.5	4.3	3.9	3.1	2.0			
D462A	1/67	5.9	5.0	4.9	3.4	3.8	4.6	3.3			
D463C	1/67	5.3	3.6	2.8	4.5	1.5	0.9	0.5			
D481C	2/67	5.2	4.9	4.6	2.9	4.3	3.7	3.7	3.4	3.6	
D484B	2/67	6.1	5.3	4.5	4.7	1.7	0.9	0.4			
D485E	2/67	5.3	5.0	4.7	4.7	4.7	4.2	4.2	4.0		
D518F	2/67	4.7	4.7	4.4	4.3	3.6	3.1	2.4	2.0		
D526B	3/67	4.3	4.2	4.1	4.0	3.8	3.5	3.0			
D532D	3/67	4.3	2.0	2.9	1.7	1.5					
D554E	3/67	5.4	5.4	5.1	5.1	5.2	-				
D568E	3/67	4.5	4.9	4.5	4.4	4.5		4.6	4.4	4.5	4.1
D574D	4/67	5.6	3.5	4.3	4.4	4.5		4.3			
D579F	4/67	5.0	4.7	4.6	4.5	4.6	-	4.5	4.2	4.1	4.1
D580B	4/67	5.3	5.1	4.9	4.9	4.9	-				
D588DK	4/67	3.8	3.7	3.4	3.1	2.1					
H108A4	8/67	5.0	5.3	-	5.3	5.3	-	5.0	4.7	5.0	4.7
H108A5	8/67	5.0	5.3	-	5.2	-	5.0	5.0	4.8	5.0	4.6
H108B2	8/67	4.9	5.0	-	5.0	5.0	-	4.7	4.6	4.7	4.5
H108B5	8/67	5.1	5.3	-	5.0	5.3	-	5.0	5.0	5.0	4.8
N85BK7	10/67	4.2	4.5	-	-	-	4.1	4.0	4.2	3.8	
N90BK2	10/67	5.0	5.1	-	-	-	4.8	4.0	4.0	3.4	
N112AK5	1/68	4.2	4.2	4.4	4.3	4.3	4.3	4.2			
N116AK8	1/68	4.5	4.5	4.6	4.6	4.6	4.6	4.4			
N128BK5	2/68	4.8	4.8	4.7	4.6	4.5					
N127BK2	2/68	4.4	4.5	4.4	4.5	4.2					
N163BK8	3/68	4.1	4.2	-	-	4.0					
N165BK9	3/68	4.3	4.2	-	-	4.0					
N185BK4	4/68	4.0	-	4.0	-	4.0					
N187AK5	4/68	4.2	-	4.1	-	4.1					

TABLE IX - 150°C VACUUM STORAGE

Cell No.	Date Mfrd.	AM1, 25°C Efficiency after indicated Weeks:						Remarks
		0	1	2	3	4	5	
D527A	3/67	4.0	3.6	3.6	3.3	2.0		Standard
D527B	3/67	4.0	3.6	3.7	3.4	3.2	3.0	Standard
N81AK3	9/67	4.1	3.9	3.5	2.8	3.2	3.2	Standard
N84C3	9/67	5.0	4.4	3.7	3.1	2.8	2.8	Standard
N85A2	9/67	5.5	4.7	4.5	4.3	4.1	3.7	Standard
N87C2	10/67	5.3	4.6	3.5	3.7			Standard
N87C3	10/67	5.7	4.0	2.7				Annealed Cu Grid · Au Plated
N87C8	10/67	5.8	3.9	3.5				Solid Gold Grid
A981C	8/67	4.7	5.0	4.9	4.8	4.5		Al Interlayer
A981D	8/67	4.3	4.6	4.2	4.0	3.5	2.4	Al Interlayer
A997A	8/67	4.6	4.6	4.6	3.7			Al Interlayer
A981A	8/67	4.9	5.0	5.1	4.9	4.2	3.3	Al Interlayer
A997D	8/67	4.7	4.0	3.9	3.7			Al Interlayer
B439F	8/67	4.0	3.8	3.9	3.8	3.5	3.5	Moly Substrate
A970D	8/67	5.9	5.7	5.1	3.7	2.1		Copper Substrate (zinc plated)

Clevite Corp.
WFDunn 6/10/68

TABLE IX, continued - 150°C VACUUM STORAGE

Cell No.	Date Mfrd.	AM1, 25°C Efficiency after Indicated Weeks:													Remarks
		0	1	2	3	4	5	6	7	8	9	10	11	12	
N97BK1	12/67	4.1	-	-	2.0	-	1.9	1.8	1.7	1.4					
N103CK3	12/67	3.1	-	-	3.3	-	3.1	3.0	3.0	2.8	2.4	1.8	2.0	1.8	
N108AK9	12/67	4.0	-	-	3.5	-	3.2	2.5	1.9	1.4					
N120CK7	12/67	4.1	4.0	3.9	3.8	3.7	-	3.4	3.2	-	2.5	1.9			
N120CK8	12/57	4.2	4.1	4.0	4.0	4.0	-	3.2	2.7	-	1.0				
N123BK7	12/67	4.5	3.9	2.3	1.5										
N123BK8	12/67	4.2	2.4	1.0	.5										
N123CK1	1/68	3.4	3.3	3.2	2.5	-	1.0								
N124CK1	1/68	3.4	3.5	3.3	3.0	-	2.4	2.0							
N125AK1	1/68	3.6	3.6	3.0	2.5	-	1.1								
N125AK7	1/68	3.3	3.4	3.4	2.5	-	1.0								
N128AK6	2/68	4.2	3.3	2.3	2.5										
N128AK5	2/68	4.8	3.6	2.3	3.0										
N127BK5	2/68	4.5	3.3	1.0	2.5										
N127AK8	2/68	4.2	4.0	3.8	-	2.7	2.5	-	1.0						
N162BK3	3/68	4.4	3.4	-	1.0										
N163BK6	3/68	4.3	3.1	-	1.0										
N164BK6	3/68	4.2	3.2	-	1.0										
N167BK1	3/68	4.4	3.3	-	2.3	1.0									
N166A4	3/68	4.3	-	3.5	-	3.4	-	1.0							Moly
N166B3	3/68	4.2	-	2.0	1.0		-								Moly
N155BK6	3/68	3.5	3.6	3.6	-	3.5	-	2.0							Grid overlay
19	4/68	3.0	-	2.0	-										Cond. epoxy grid
N172CK5	4/68	4.4	-	1.0	-										
N186BK5	4/68	4.1	-	1.0	-										
N186CK2	4/68	4.0	-	2.1	-										
N187BK3	4/68	4.0	-	4.0	-	3.6									

<u>TABLE X.</u> – DEGRADATION OF BOEING THERMAL CYCLED
CELLS OF OCTOBER 1967 PRODUCTION

Cell No.		Maximum Power as Percent of Original	
		End of Test (506 cycles)	Post Test at Clevite
1	A970B*	77	98.3
2	A969D*	25	96.5
3	NH188AK2	75	92.3
5	N89CK7	78	71.0
6	N90AK5	83	82.5
7	N90BK4	82	90.7
9	N90AK9	85	77.0

*Copper Substrate, Mylar Cover

Clevite Corp.
WFDunn 6-10-68

TABLE XI.

CLEVITE TEST DATA ON CELLS USED FOR BOEING THERMAL CYCLING OF OCTOBER 1967 PRODUCTION - 506 CYCLES

TESTED AM1, 25°C

Boeing No.	Clevite No.	OCV (volts)	SCC (amps)	Vmp (volts)	Imp (amps)	M.P. (watts)	Fill (%)	Eff. (%)
		A - BEFORE THERMAL CYCLING						
1	A970B*	.485	.925	.390	.800	.312	70	5.7
2	A969D*	.487	.925	.380	.823	.317	71	5.8
3	NH188AK2	.478	.700	.368	.625	.230	69	4.2
5	N89CK7	.498	.700	.388	.618	.240	69	4.4
6	N90AK5	.485	.848	.380	.746	.283	69	5.2
7	N90BK4	.480	.780	.380	.684	.260	70	4.7
9	N90AK9	.481	.740	.378	.660	.250	70	4.6

*Copper Substrate , Mylar Cover

Boeing No.	Clevite No.	OCV (volts)	SCC (amps)	Vmp (volts)	Imp (amps)	M.P. (watts)	Fill (%)	Eff. (%)
		B - AFTER THERMAL CYCLING						
1	A970B*	.495	.870	.392	.790	.310	72	5.6
2	A969D*	.500	.870	.390	.780	.304	70	5.6
3	NH188AK2	.478	.685	.354	.605	.214	66	3.9
5	N89CK7	.475	.662	.360	.515	.185	59	3.4
6	N90AK5	.470	.800	.356	.700	.249	66	4.6
7	N90BK4	.460	.745	.350	.665	.232	68	4.3
9	N90AK9	.465	.710	.352	.620	.218	66	4.0

*Copper Substrate , Mylar Cover

Clevite Corp.
WFDunn 6-10-68

BALLOON FLIGHTS AND ARRAYS

F. A. Shirland, Clevite

NCAR (National Center for Atmospheric Research) has been testing thin-film solar cell panels for use on their constant altitude weather balloons. The primary objective in using thin-film solar cell panels is to develop a system that can be safely ingested by jet aircraft. The latest flight launched in December 1967 used a CdS panel as its sole source of power. The panel was composed of 33 quarter-size cells connected in series across a 100Ω load. The balloon operated between 30,000 and 40,000 feet altitude reaching $+30°$ C in the light and $-50°$ C during the dark portion of the cycle. The V_{oc}, V_{load}, and the angle of illumination of the panel were measured. After six months of continuous operation the panel has shown no degradation. NCAR is planning to equip all weather balloons with CdS panels based on their digestibility and cost. The French have already switched all of their weather balloons to CdS.

JPL BALLOON CALIBRATION FLIGHTS[1]

H. Nastelin, Clevite

Three CdS solar cell modules were fabricated for the Air Force Propulsion Laboratory (AFAPL) to be flown on a JPL balloon flight experiment. Each module consisted of two 1 x 2 cm cells loaded with a 1Ω resistor and mounted on a Cu plate. The Cu substrate cells used the Mylar-epoxy package with conductive epoxy for grid attachment. The modules were delivered to APL in May 1966 and then to JPL for the August 1966 flight. The cells were flown at an altitude of 80,000 feet around the solar noon. After the flight the cells were returned to APL where they were again tested at 100 mw/cm^2 in natural sunlight. The JPL measurements during the flight are very close to the 140 mw/cm^2 carbon arc measurements taken at AFAPL. The AFAPL measurements in sunlight taken before and after the tests indicate that the cells degraded 6.45 percent in I_{sc} during the five-month period from May 19 to October 21, 1966.

In May 1967 three balloon flight modules were fabricated and delivered to AFAPL. Again two 1 x 2 cm cells were loaded with 1Ω resistors and mounted on copper plates. These cells were made with metallized plastic substrates, used conductive epoxy cement to hold the grids, and clear epoxy to attach the Mylar cover plastic. Only the I_{sc} was measured. No data is available from the flight.

In early 1968 three more balloon flight modules were prepared for still another calibration flight. Cell construction, mounting, and measurement were the same as in 1967 except the cells were covered with Kapton plastic. No data is available.

---

[1] AF 33(615)-3253, Project 7885, Clevite Final Report, November 1967.

MEASUREMENT ACCURACY AND REPRODUCIBILITY
A. E. Spakowski, NASA-Lewis

An attempt was made to determine the size of the errors associated with the measurement of the performance parameters V_{oc}, I_{sc}, and P_m. Four laboratories (Lewis Space Power Systems Division, Chemistry & Energy Conversion Division, Clevite, and Boeing) were included in the study. The first three laboratories had identical light sources made up of tungsten-iodine lamps, $CuSO_4$ water filter, and a temperature controlled cell holder. Boeing used a Spectrolab X-25 solar simulator as their light source. The intensity was set at AMO using a Lewis calibrated Kapton-covered CdS cell. A temperature of 25° C was used. Twenty 3" x 3" cells were randomly selected from the lot fabricated at Clevite in October 1967 and these cells were sequentially measured at each laboratory. The performance of the cells was obtained from the I-V curves taken in the following manner. The I-V curves were run for all 20 cells in rapid sequence and then run again for all the cells. Two blocks of data were thus generated. From these curves the V_{oc}, I_{sc}, and P_m were obtained. All the data was returned to Lewis where it was handled by an analysis of variance.

The results are presented in Table XII. The grand mean represents the average of two runs from each of four laboratories for 19 cells. One I-V curve was inadvertently missed at one laboratory which necessitated dropping the cell from the analysis and using only 19 cells. The standard deviation contains all the variables and uncertainties associated with the measurement of the current and voltage of a solar cell. The error due to the fact that the 20 cells did not have identical performance characteristics has been taken into consideration. The standard deviations in percent of the parameters are 2.6, 0.7, and 1.2 percent for the P_m, I_{sc}, and V_{oc}, respectively.

In Table XIII the reproducibility of the P_m is given for the participating laboratories. The standard deviations are defined as for the previous table. Here one sees that the precision in each laboratory is much better than that for all the data combined. The larger deviation for the

-88-

for the Boeing data is due primarily to the larger fluctuations of their xenon light source as compared to the tungsten-iodine sources used by the other labs. This we interpret to mean that the individual labs can hold constant the many variables associated with the measuring of I-V curves. However, the value of these variables must vary from lab to lab due to the lack of suitable standards and equipment specifications. More work needs to be done in standardizing the set up.

TABLE XII. - INTERLAB PERFORMANCE MEASUREMENTS

	Grand mean	Standard deviation
P_m, mw	238.6	6.2
I_{SC}, ma	786.8	5.2
V_{OC}, mv	490.7	5.9

TABLE XIII.- MAXIMUM POWER REPRODUCIBILITY FOR LABORATORIES

	Mean P_m, mw	Standard deviation, mw
Lewis SPSD	237.6	2.8
Lewis C&ECD	233.9	2.3
Clevite	243.0	1.9
Boeing	239.9	5.3
Grand mean	238.6	6.2

THERMAL CYCLING TESTS AT LEWIS AND BOEING

A. E. Spakowski, NASA-Lewis

The thermal cycling tests are one of the most important tests for solar cells that are to be used in near earth orbits or on spinning satellites. Results will be given for thermal cycling tests conducted on Clevite cells fabricated in the latter half of 1967 and early 1968. Tests were conducted both at Lewis and at the Boeing Company.

In figure 49 the results from the tests on late 1967 solar cells are shown with the relative P_m as a function of the number of thermal cycles. The conditions in the Lewis tests were: 2×10^{-7} torr, 60 min. light/30 min. dark, $+41°$ C to $-70°$ C, AMI xenon light. The conditions in the Boeing test were: 10^{-6} torr or lower, 60 min. light/30 min. dark, $+60°$ C to $-70°$ C, AMO xenon light. The average AMO, $60°$ C efficiencies of the September, October, and November cells were 2.7, 2.7, and 2.9 percent, respectively. The four September cells cycled at Lewis degraded after 210 cycles in P_m to an average of 70 percent with the best cell at a P/P_o of 89 percent and the poorest at 59 percent. The cells labeled here as September cells were received from Clevite for testing at Boeing. Since they tested poorly, later cells (Oct. and Nov.) were sent to Boeing. The average P/P_o for the cells cycled at Boeing after 506 thermal cycles was 82 percent with the best cell at 88 percent and the poorest at 75 percent. In both sets of tests the V_{oc} remained at 100 percent while the I_{sc} and FF (fill factor) dropped about 10 percent indicating an increase in the R_s of the cells.

The recovery of the Oct-Nov cells at Boeing is shown in Table XIV. The seven cells are averaged.

There was no apparent recovery of the cells when the tank was back-filled with N_2 or air, or when the temperature and pressure were returned to ambient conditions. On the temperature-controlled plate, however, the V_{oc} and I_{sc} were recovered completely and about half of the P_m loss was recovered.

In figure 50 the results from tests conducted on March 1968 cells are shown. The conditions of the tests are the same as in the previous

tests with the exception that at Lewis AMO xenon light was used and the temperature of the cells cycled between +55° C and -110° C. The results at Boeing after 554 cycles show the P/P_o degraded to an average of 90 percent with the best cell at 97 percent and the poorest at 84 percent. The arrows on the figure designate the cycle at whixh a cell was removed from the average because its P/P_o had degraded below 80 percent. In one case the drop below 80 percent was sudden. In the Boeing tests 1 cell dropped to 47 percent at cycle 369 and later recovered to 78 percent at cycle 432. The average P/P_o for the 8 remaining cells at Lewis after 587 cycles was 93 percent with the best cell fully recovered and the poorest at 82 percent.

A comparison of the tests' results are shown in figure 51. This is a log-log plot of the actual degradation as a function of the number of thermal cycles. It is clearly seen that the March 1968 cells are more stable than the late 1967 cells. (The Boeing results for the March 1968 cells will fall below the Lewis curve.)

The increased stability is a result of many factors, two of which can be identified. There has been a general improvement in the quality control in every process step at Clevite. Probably the most significant influence on the test results has been the tighter performance specifications adapted for the March cells. The cells must now be measured at 25° C and at 60° C. The cell characteristics (I_{sc}, V_{oc}, etc.) can vary only a prescribed small amount to meet the new specifications. Thus we can surmise that the poorer cells have been culled from the lot.

TABLE XIV

RECOVERY OF OCT-NOV CdS CELLS AT BOEING

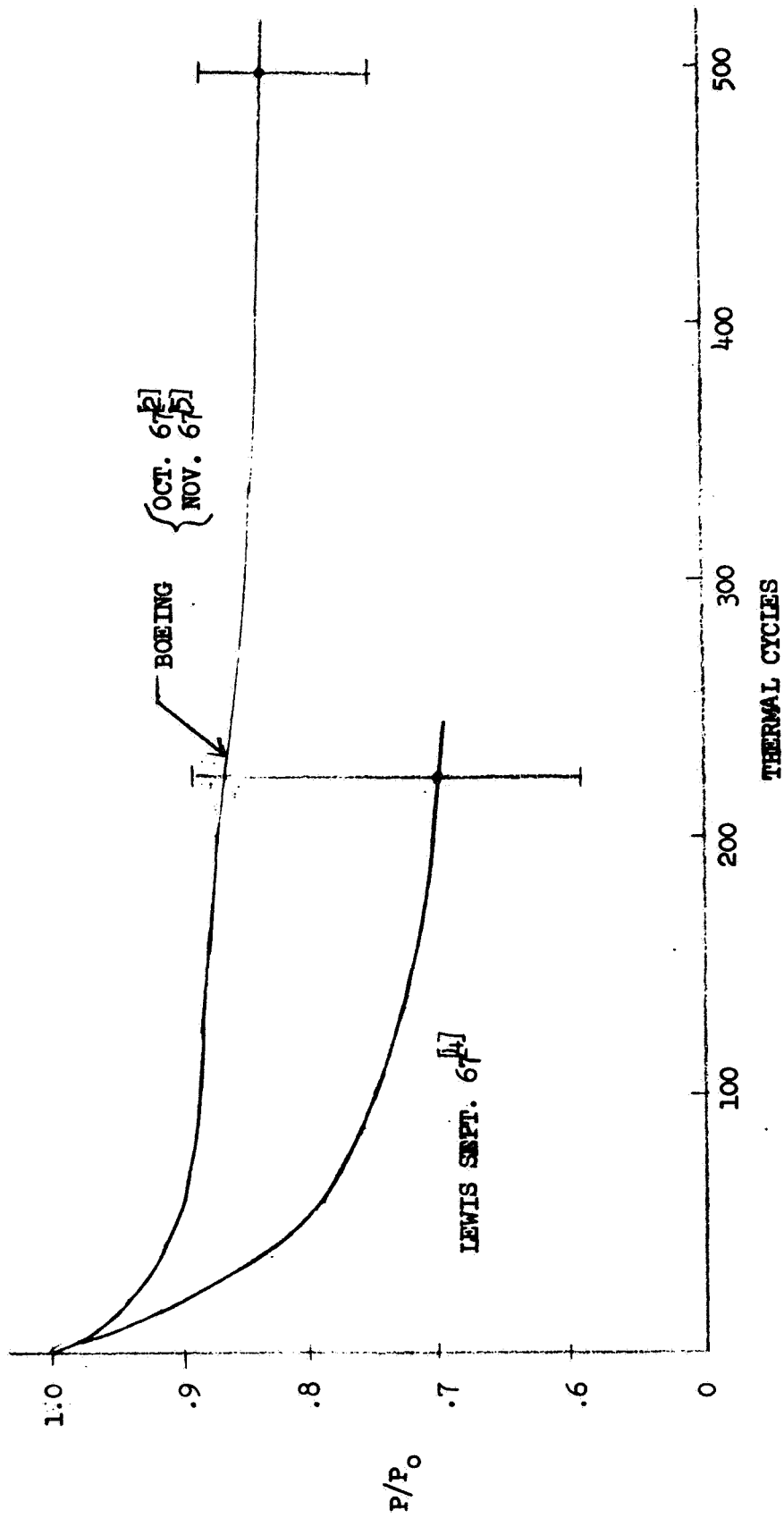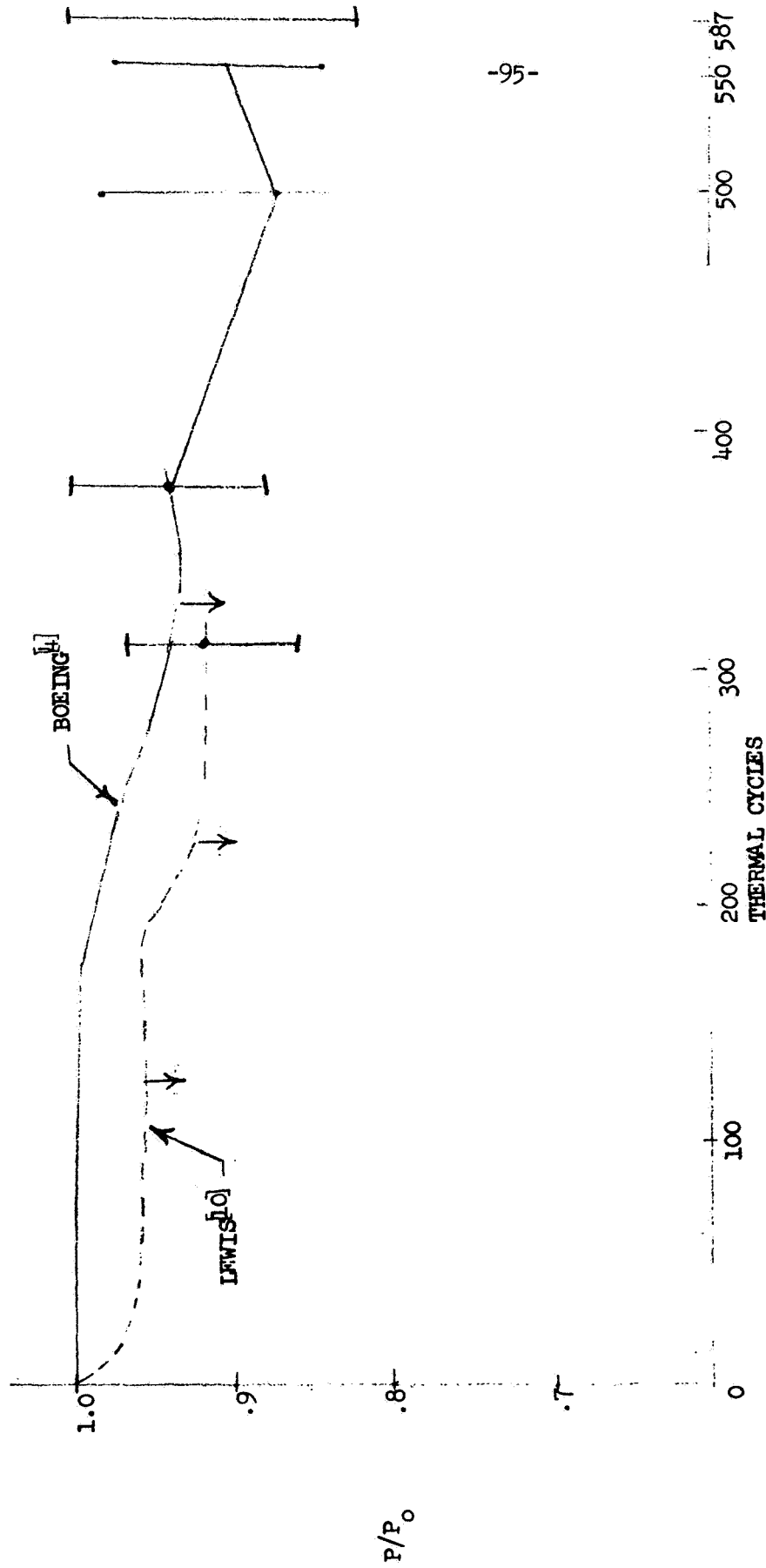|	V_{OC} v/v_o, %	I_{sc} I/I_o, %	P_m P/P_o, %
Cycle 506	100.3	92.5	82.5
25 hours in N_2, ambient T, P	99.5	94.1	83.3
39 hours in air, ambient T, P	98.6	93.6	82.5
47 hours in air on temperature-controlled plate	101.7	100.4	92.7

All measurements at AMO and 60° C

FIGURE 49. THERMAL CYCLING OF 1967 CdS CELLS

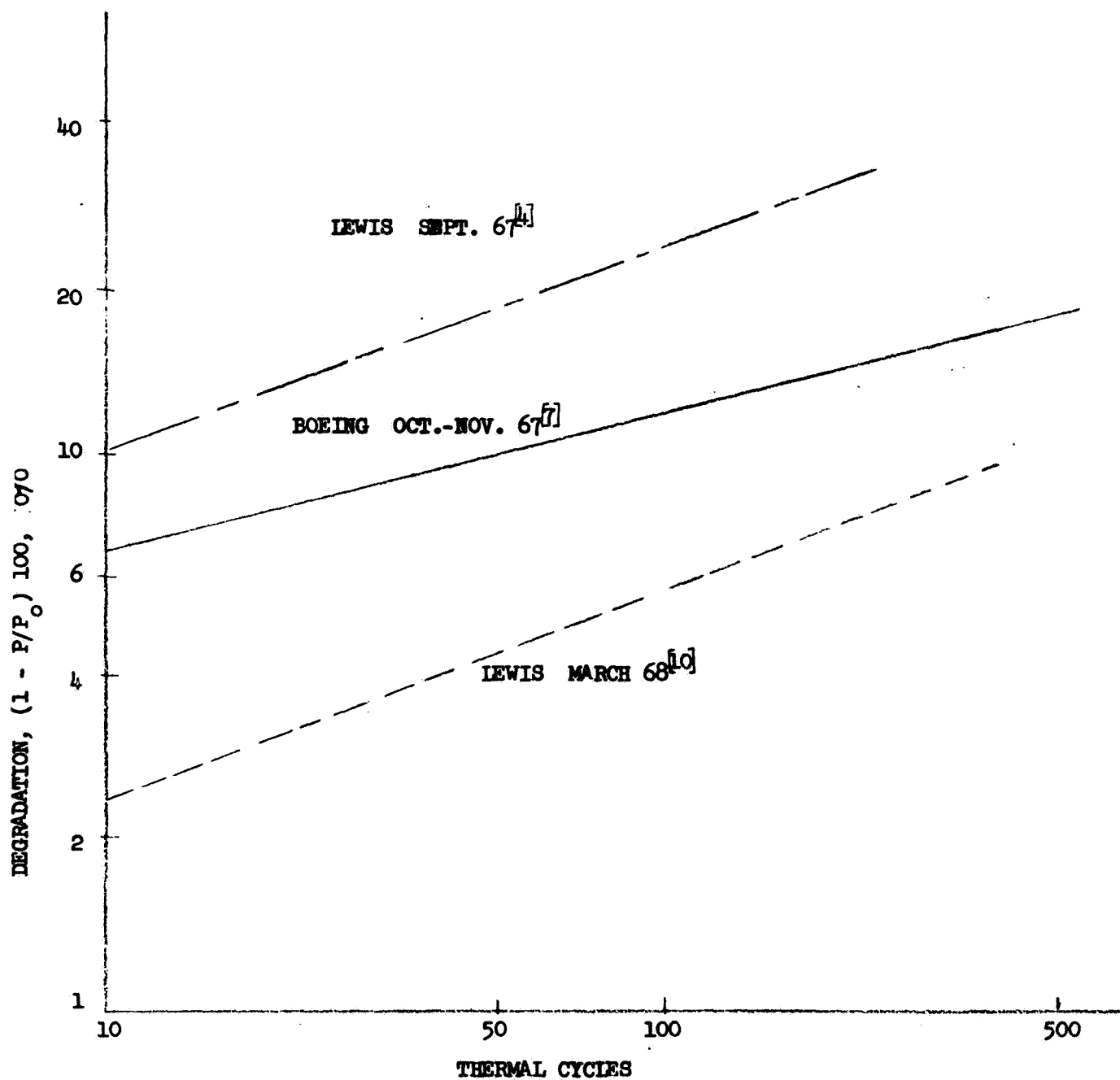FIGURE 50. THERMAL CYCLING OF MARCH 1968 CELLS

FIGURE 51. STABILITY OF CdS CELLS

SPACE POWER SYSTEMS DIVISION STABILITY TESTS

A. F. Ratajczak, NASA-Lewis

The thermal shock cycling of CdS cells was planned to evaluate quickly and inexpensively the effects of thermal stress. Kapton, Cu, and Mo substrate cells were cycled by heating them between two heater plates and then dipping the cells into liquid nitrogen. A cell temperature of 65° C was maintained during the heat portion of the cycle. A cycle consisted of five minutes of heat followed by five minutes of cold.

All of the October and November 1967 Kapton substrate cells delaminated. The cells split in about the center of the CdS. The two halves are shown in figures 52 and 53 with the light that illuminates the specimen coming from the left. The substrate side and the upper side of the CdS cell after splitting were characterized by ridges and valleys, respectively, and corresponded to the current collecting grid pattern of the cells. There was no change in the V_{oc} of these cells. However, there was a change in the P_m and I_{sc} which could be accounted for by the loss in active cell area due to delamination.

The one Clevite Cu cell (Dec. 1967) and the one Harshaw Mo cell (May 1967) did not delaminate. There was no degradation in the photovoltaic characteristics of the Cu substrate cell after 1352 thermal cycles but some degradation in the Mo cell. However, it could not be concluded that this degradation was due to thermal cycling since this vintage Mo cell degrades on shelf storage.

To determine the effect of cell area on cell degradation, a group of whole, half, and quarter cells were subjected to constant illumination and to thermal cycling in a 10^{-8} torr vacuum chamber. The cells were Clevite cells fabricated in September 1967. In the first test the cells were exposed to continuous AMO light (carbon arc solar simulator) for 250 hours and the performance measured periodically as I-V curves. At the end of this time the P_m of the whole, half, and quarter cells had degraded 30, 20, and 1 percent, respectively. Subsequently, it was found that the cells were not all loaded at P_m but that the whole cells were loaded between P_m and V_{oc}, the quarter cells near I_{sc}, and the half cells between them.

Much evidence has been obtained to indicate that the degree of degradation is related to the load point as in this test.

The results from the second test were not so clear. A new set of whole, half, and quarter cells were thermally cycled for five minutes at +74° C and then for five minutes at -110° C. Performance I-V curves were taken in situ using the carbon arc simulator. After 400 cycles the P_m for the whole, half, and quarter cells had degraded 9, 6.5, and 8 percent, respectively. Again in this test the cells were loaded with the whole cell between V_{oc} and P_m, the quarter cell on the short circuit current side of P_m, and the half cell between the two. The loads were selected before their significance was fully appreciated.

The third test was set up with all cells deliberately loaded at the P_m. Four whole, 4 half, and 4 quarter cells were thermal cycled in vacuum for 60 minutes of light followed by 30 minutes of darkness. The temperature ranged from +65° C to -120° C. The results, based on measured I-V curves before and after the 383 cycles, are shown in Table XV. It was concluded that the area did not affect the stability of the cells, but that the loading during the tests was the main influencing factor.

TABLE XV

CHANGE OF P_m AT 60° C

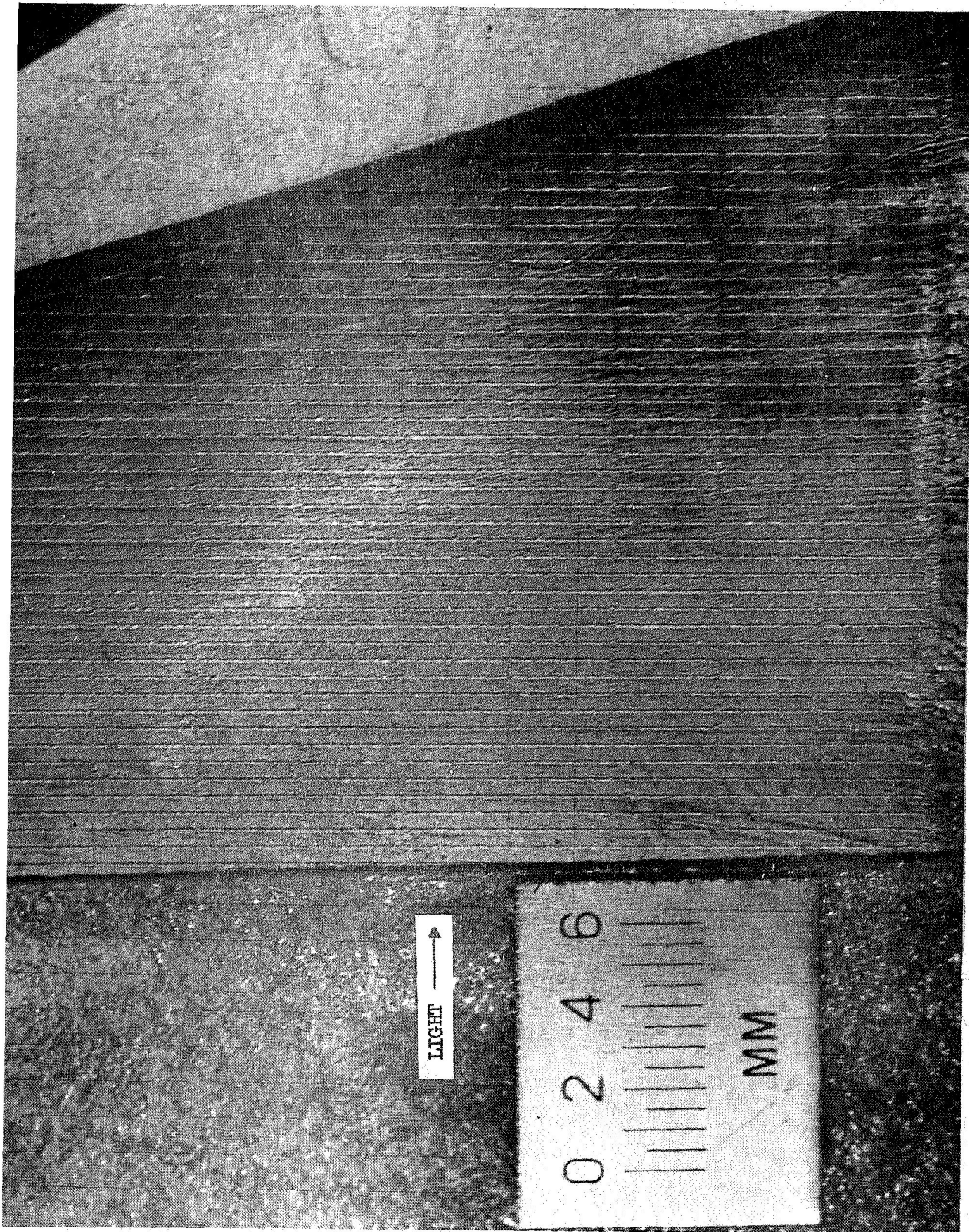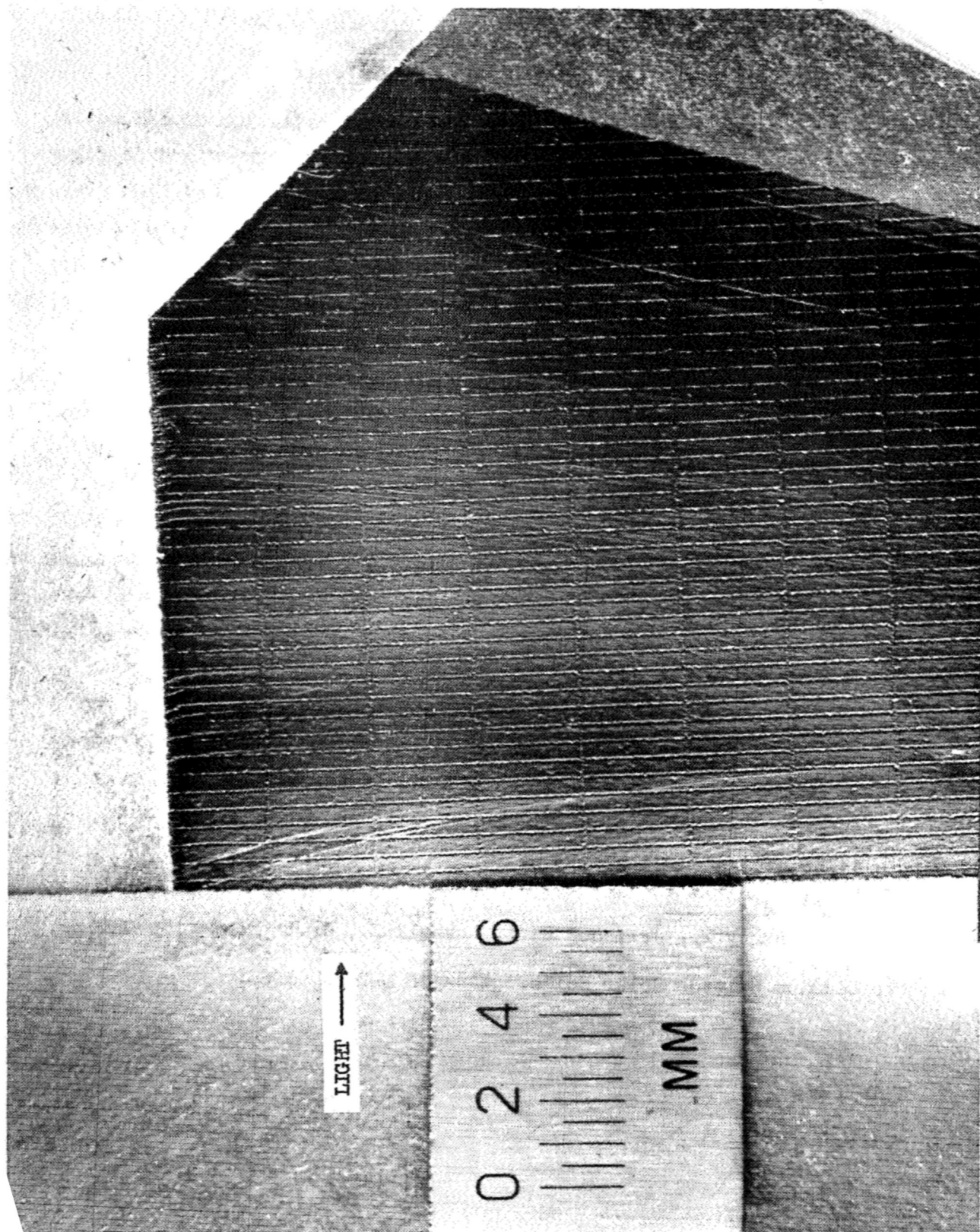|	Whole	Half	Quarter
$(1 - P/P_o)$ 100	1.3	15.8	14.1
	10.6	12.8	10.1
	7.3	8.5	7.5
	14.3	12.9	11.4

FIGURE 52. SUBSTRATE SIDE OF C3S SHOWING RIDGES

FIGURE 53. TOP HALF OF CELL SHOWING VALLEYS

RADIATION EFFECTS

H. W. Brandhorst, Jr., NASA-Lewis

A study of the effects of electron and proton radiation on CdS cells was made at Lewis several years ago.[1] The results are summarized in figure 54 for the P_m. Five 1 x 2 cm cells covered with Kapton and with an average efficiency of 4.2 percent (AMI, 25° C) were used. For the range of electrons (0.6, 1.0, 2.5 MeV) and protons (2, 5, 7, 10 MeV) used, no effect of energy on cell degradation was measured. The equivalent time in the van Allen belt would be roughly equal to 10 years for fluences of 10^{15} protons and 10^{17} electrons of these energies. The studies were extended by irradiating three May 1967 cells with 1 MeV electrons to a dose of 1.35 x 10^{16} electrons/cm^2. The 1 x 2 cm cells were encapsulated in an experimental polyimide plastic (X101) and had an average initial efficiency of 4.5 percent (AMI 25° C). The point (X) at 94.5 percent in figure 54 represents the average of the three cells. The X101 plastic cover is slightly darkened by the radiation. It is reasonable to suggest that if the cells were encapsulated in Kapton, the loss in P_m would have been about 3.5 percent. The dose level in this test corresponded to approximately one year in a worst case orbit.

The prospect of communication satellites in synchronous orbits for extended periods of time has focused attention on the effect of low energy protons. COMSAT is investigating the effects of 250 keV to 5 MeV protons at doses to 10^{15} protons/cm^2 on CdS solar cells and plastic materials. Data will be published.

---

[1]Brandhorst, Henry W., Jr.; and Hart, Russell E., Jr.: Radiation Damage
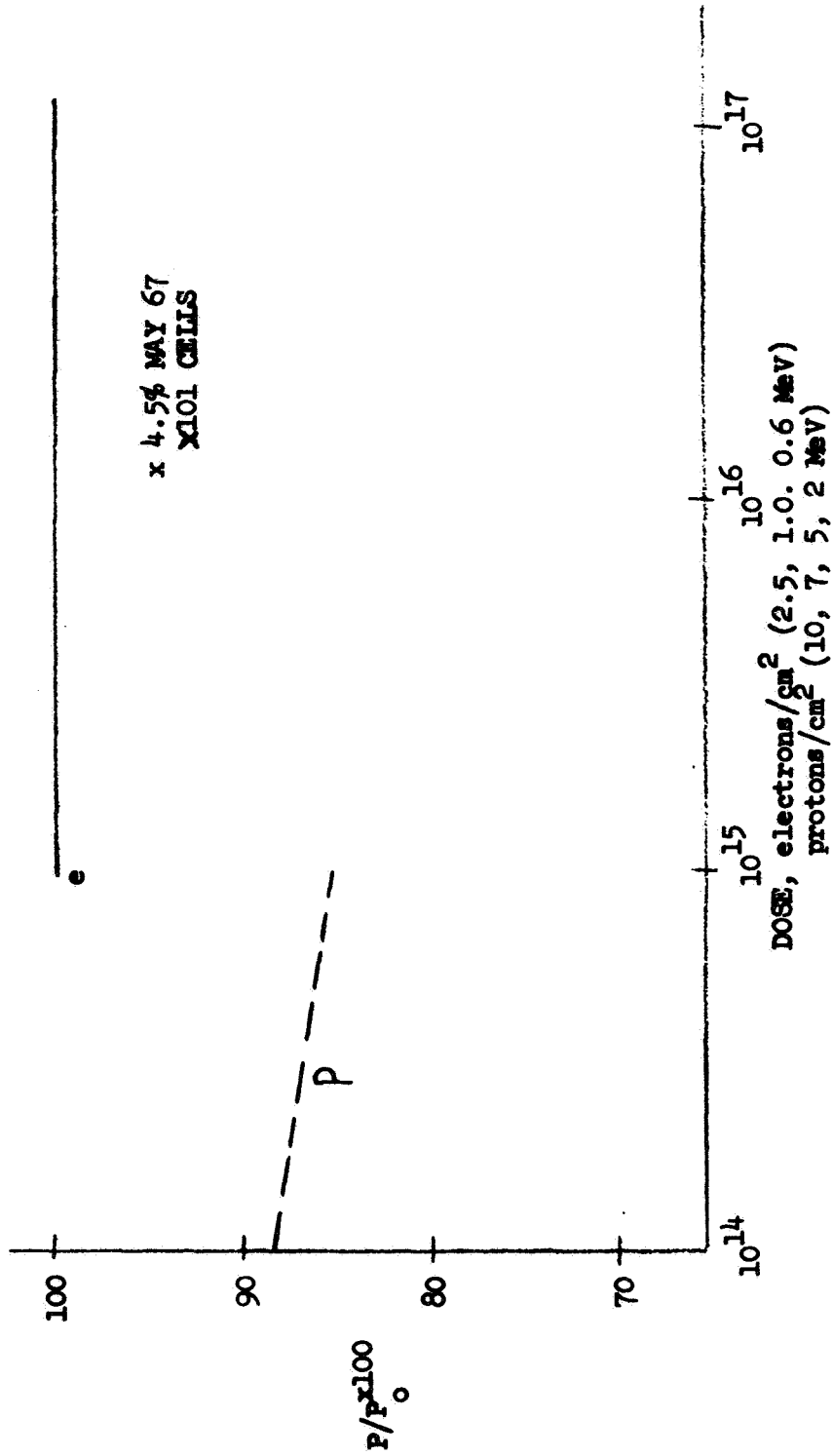to Cadmium Sulfide Solar Cells. NASA TN D-2932, 1965.

FIGURE 54. RADIATION STABILITY OF CdS CELLS

LOAD TESTS

A. F. Forestieri, NASA-Lewis

Another test showing the effect of loading on the performance of thin-film cells will be discussed. The cells were mounted on a temperature-controlled block under constant illumination with various loads. Periodically I-V curves were taken to follow the performance. In figure 55 the relative P_m (P/P_o) is followed for a cell held under a constant 100 mw/cm^2 illumination at 25° C. The cell is held at V_{oc} and the P/P_o degrades to 66 percent after approximately 70 hours. The load was then changed from V_{oc} to that equivalent to P_m. The P/P_o recovered to 86 percent in 20 hours. When the load was changed to short circuit conditions, the cell recovered to 95 percent. Finally, the cell recovered further when it was placed in darkness.

In figure 56 another cell is run at 65° C under a constant light of 100 mw/cm^2. After 50 hours at V_{oc}, the P/P_o had dropped to 59 percent. With the cell still at 65° C but held in the dark, a recovery to 93 percent was reached in 89 hours. In figure 57 a new cell is tested at the same conditions of light and temperature as before. The load conditions, however, are changed. First the cell is held at short circuit current and the P/P_o degrades to 90 percent in 24 hours. The light is then turned off with all other conditions held constant and the cell recovers to 95 percent. With the light back on at short circuit current the cell is down to 90 percent in 2 hours. At open circuit conditions the P/P_o degrades to 53 percent in the next 70 hours.
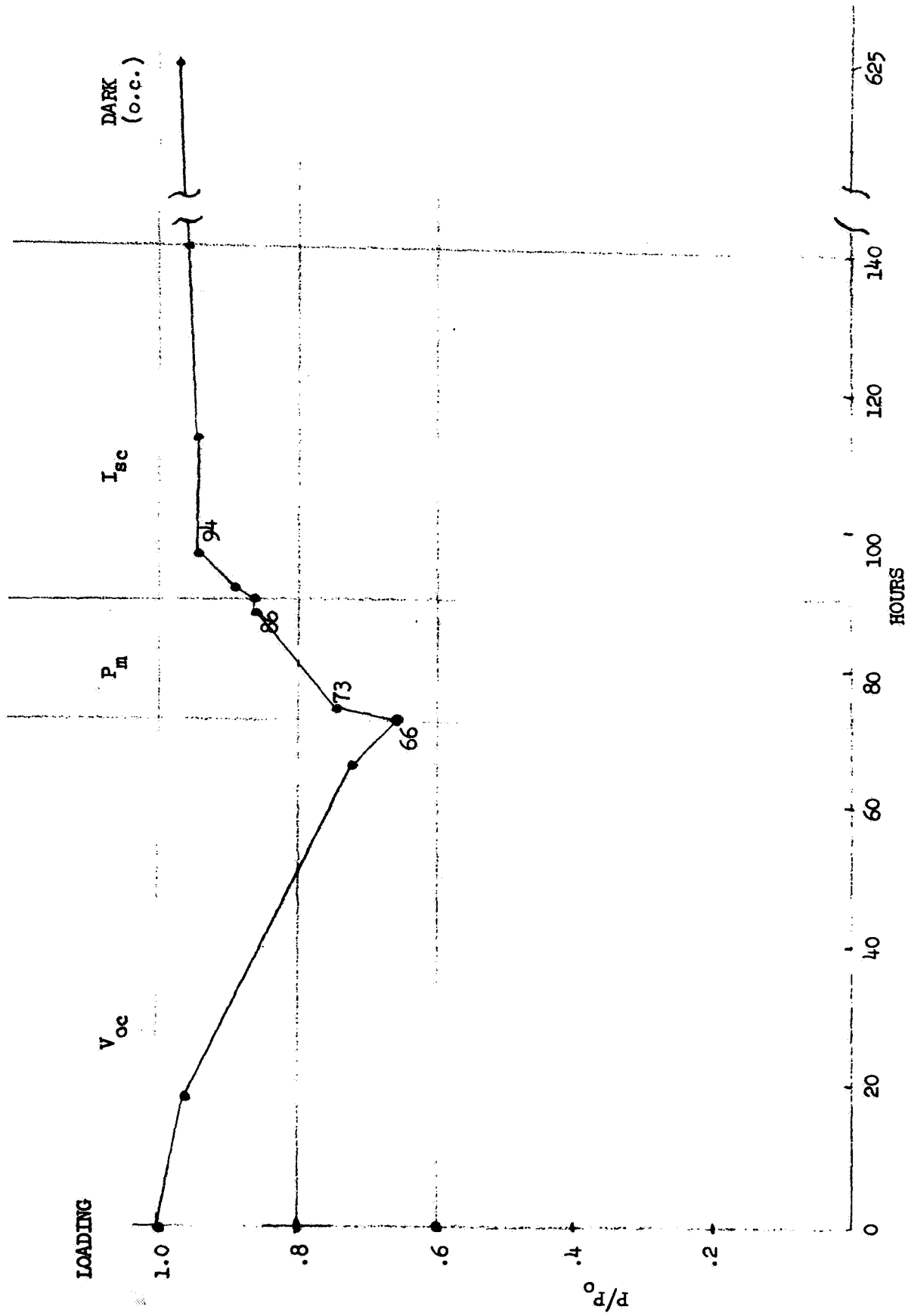
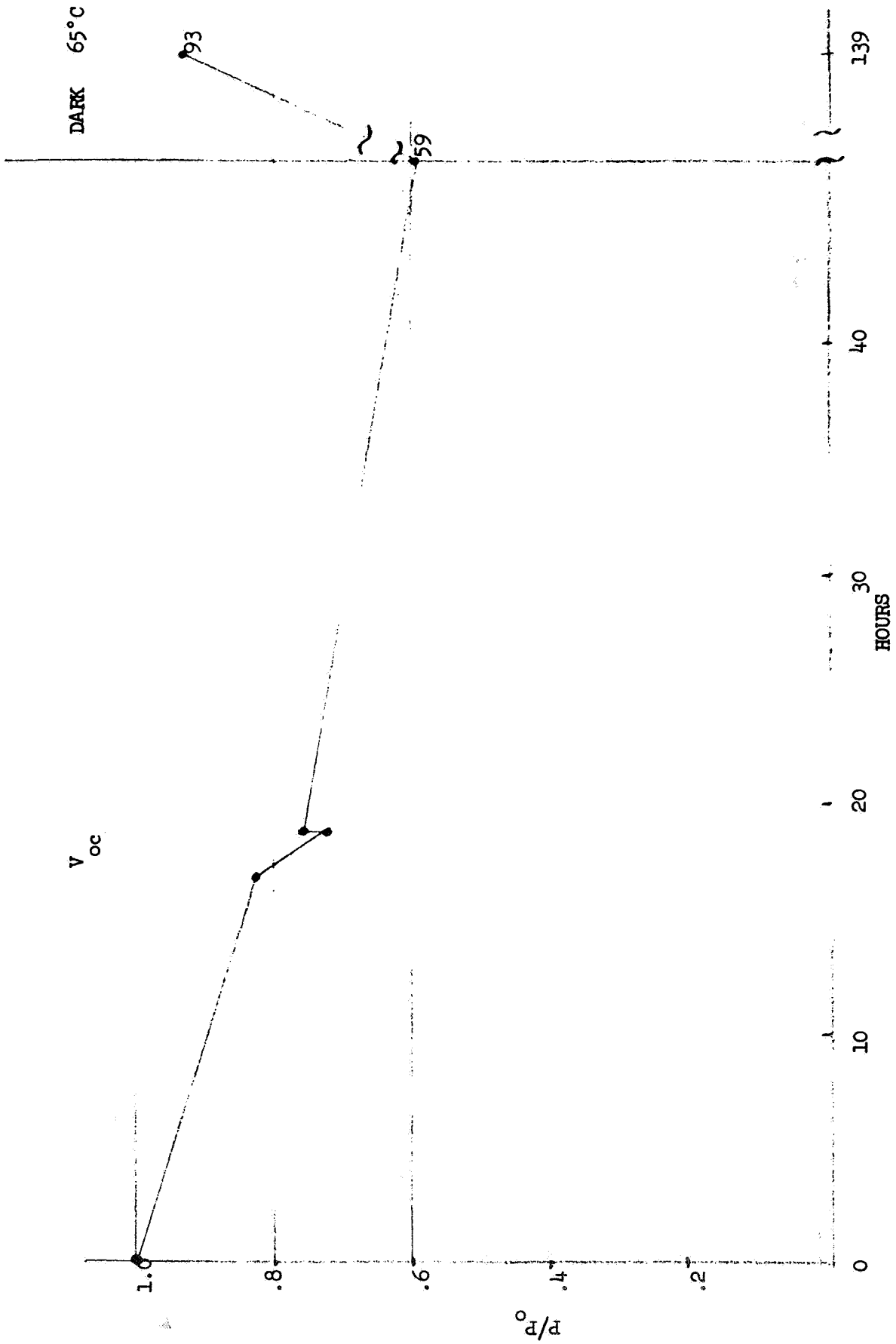FIGURE 55. CONSTANT ILLUMINATION   25°C   100 mw/cm^2

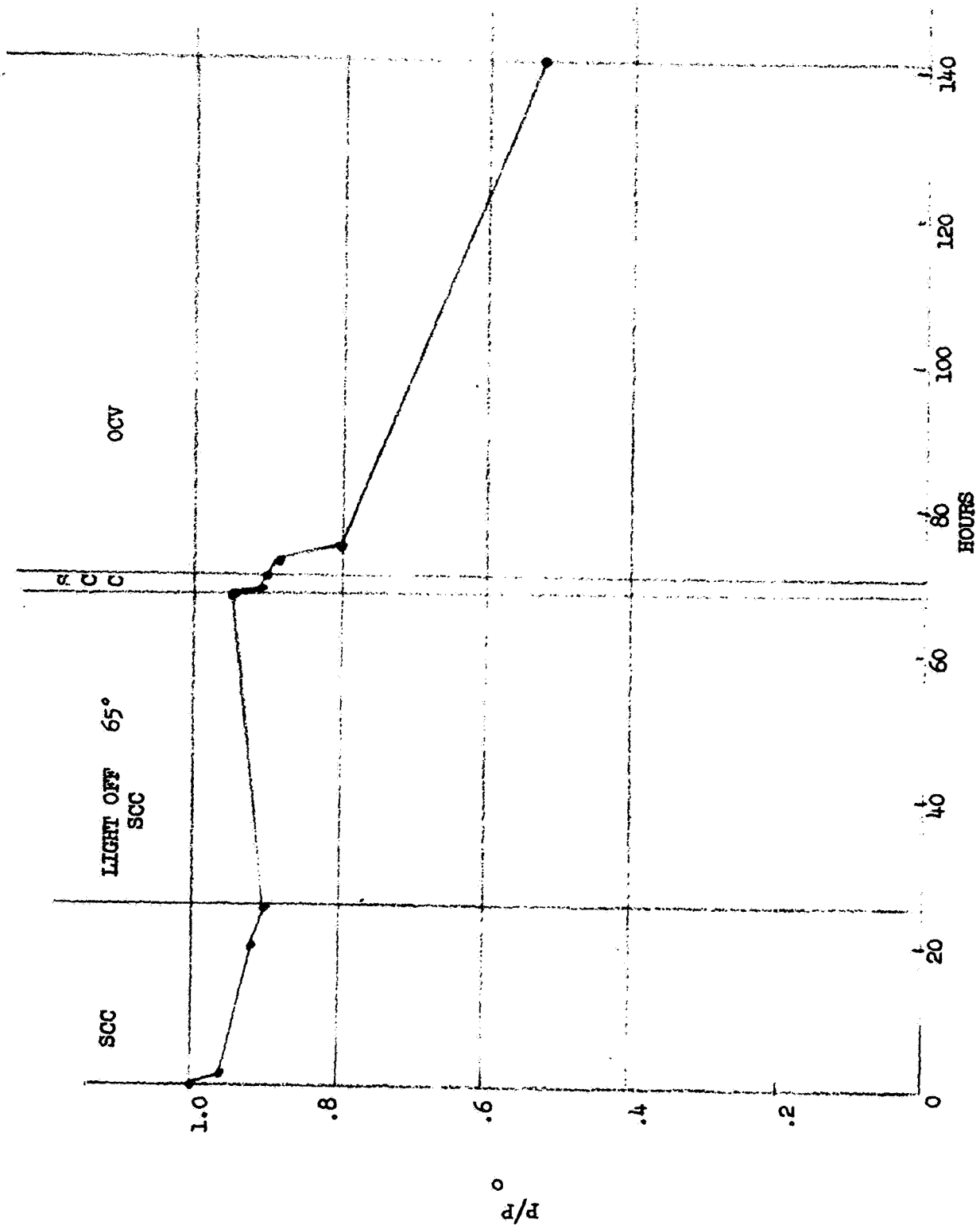FIGURE 56.   CONSTANT ILLUMINATION   65°C   100 mw/cm^2

FIGURE 57. CONSTANT ILLUMINATION   65°C   100 mw/cm²

AIR FORCE TEST RESULTS, EARLY FLIGHTS[1]

A. F. Forestieri, NASA-Lewis

The AFAPL had arranged to flight test a number of different experimental solar cells on a "piggy back" experiment in 1966 and 1967. The tests included the following types of cells:

1. Westinghouse dendritic Si cells.

2. Westinghouse dendritic Si drift field cells.

3. G.E. CdTe film cells.

4. Clevite CdS film cells.

5. Ion physics Si with junction formed by ion implantation.

The modules of each type of cell were composed of eight series connected 1 x 2 cm cells. The CdS cells for the 1966 flight had Mo substrates, pressure-held grids, and a nylon-Kapton cover. The cells for the 1967 flight had plastic substrates, grids cemented with conductive epoxy, and epoxy-cemented Kapton covers. The modules were delivered approximately a year prior to the launch date for testing and installation on the flight vehicle. The preflight tests, storage, and flight experiments suffered from a lack of controls and calibrated standards. For these reasons, although trends are clearly shown, the results remain in doubt. The results for the CdS cells are shown in figures 58 and 59.

---

[1] Massie, L. D.: A Status Report on the Results of the AFAPL Solar Cell Space Experiments. Rep. PIC-SOL 210.1/6, Pennsylvania Univ., Nov. 28, 1967.

8 - 1 x 2 cm cells in series
Moly substrate
Kapton cover
Nylon pressure contact
Delivered Sept. 1965
Flight - Aug. 19, 1966--Jan. 16, 1967
127 days

FLIGHT 1
Apogee   2007 NM
Perigee   1990 NM
Period   167.58 min.

Data near 50° incidence angle
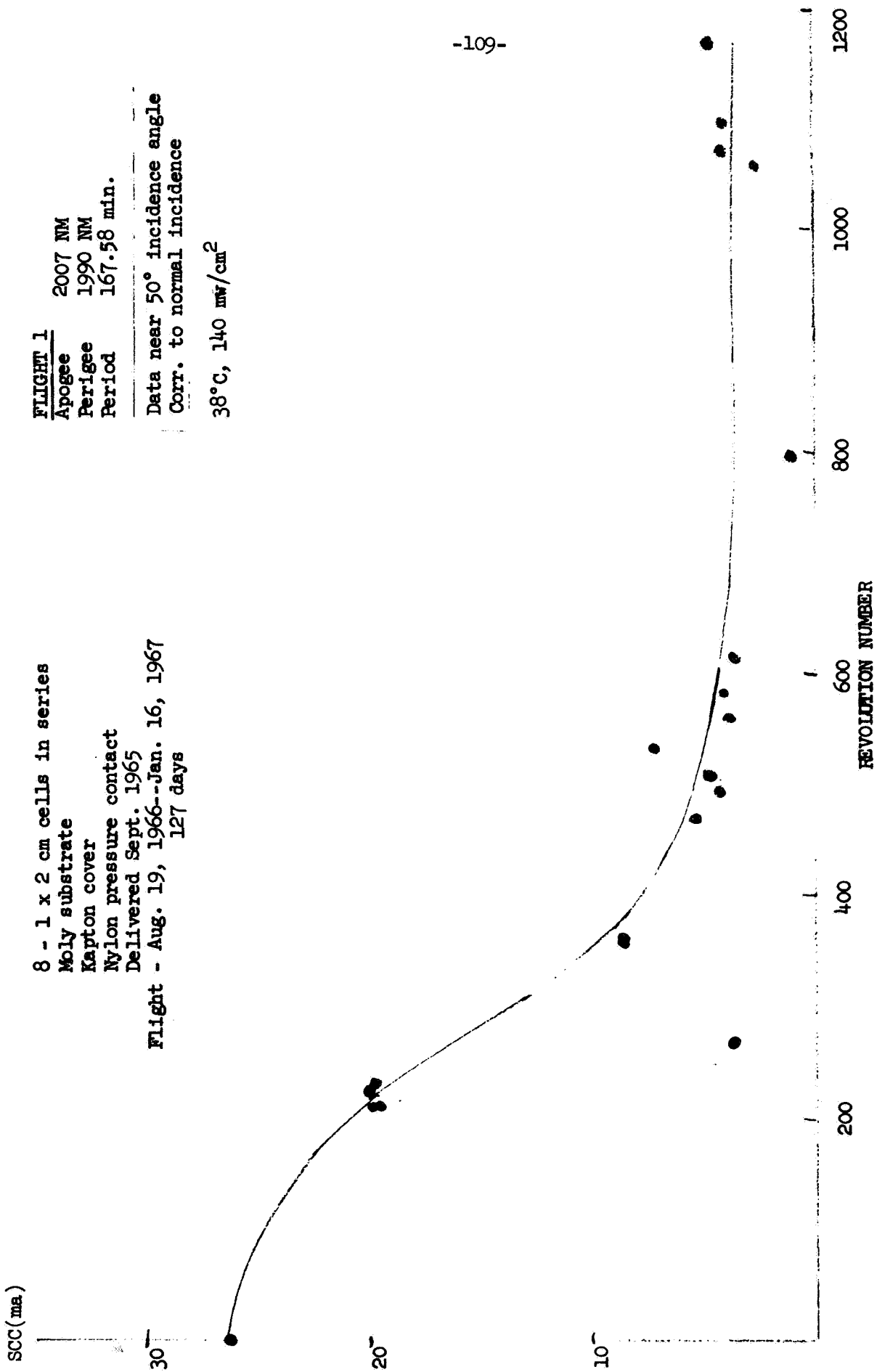Corr. to normal incidence

38°C, 140 mw/cm²
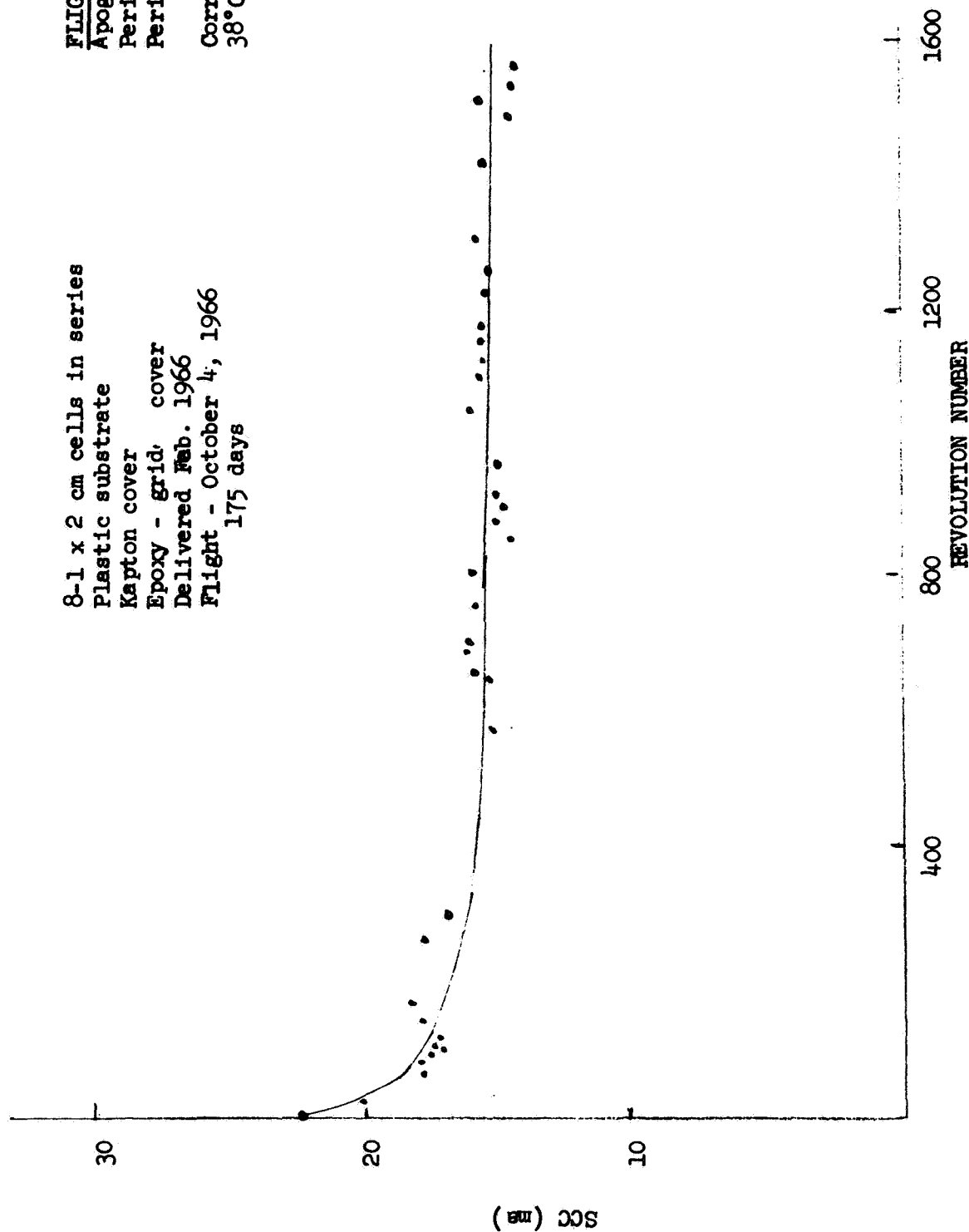
SCC(ma.)

FIGURE 58

FIGURE 59

AIR FORCE TEST RESULTS, ARX-701 FLIGHT PANELS[1]

H. Nastelin, Clevite

Four CdS panels were delivered to General Dynamics, San Diego, California, in April 1967. Two panels were to be selected for inclusion on the OVI-13 satellite. Each panel consisted of eight 1 x 1 inch cells connected in series. The standard plastic substrate design was used with a Kapton cover. They were fabricated in January 1967. The eight-cell array was attached to a Kapton backing film which, in turn, was attached to an aluminum frame. The panels are shown attached to the satellite in figures 60 and 61. The data taken included V_{oc}, I_{sc} (across a 1Ω load), power into a 40Ω load, temperature, angle of inclination, and the time. The satellite was launched April 4, 1968 into a polar orbit (perigee 300 NM, apogee 5000 NM) with a 200 minute orbit. The satellite was spinning at 8 rpm and the data was taken at the rate of one bit per second, continuously. Forty-five days after launch (319 orbits), the performance was very good. The biggest drop was the 39 mv loss of V_{oc} to 3.75 volts. Table XVI compares the results on a panel measured at Clevite and in an early orbit.

After 586 orbits (81 days) the I_{sc} is down 6 percent while the V_{oc} is unchanged. The temperature has increased about 10° C and the cells are now operating around 70° C. The voltage at the load point is following V_{oc}. Although it was intended that the load point be at P_m, the 40Ω point turned out to be on the V_{oc} side of P_m.

---

[1] Nastelin, H. E.; Hietanen, J. R.; and Shirland, F. A.: Fabrication of Cadmium Sulfide Thin Film Solar Cells for Space Vehicle Testing. Rep. 303280, Clevite Corp. (ARL-67-0282, DDC No. AD-666439), Dec. 1967.

TABLE XVI

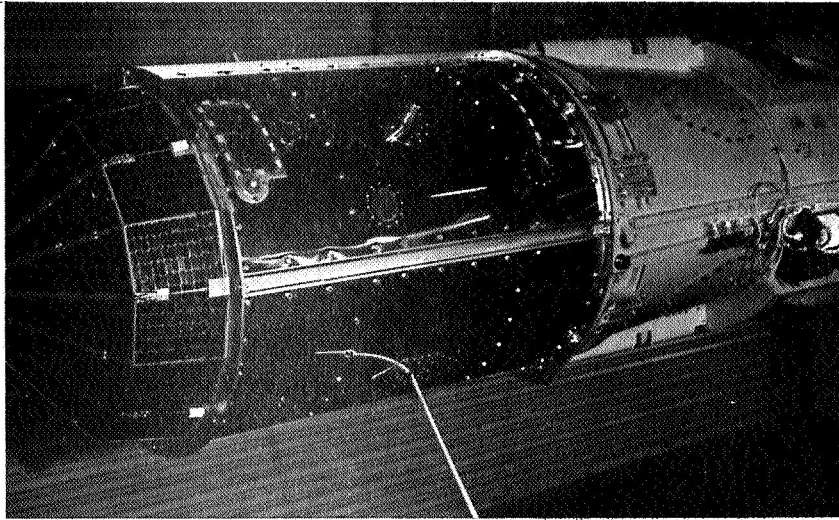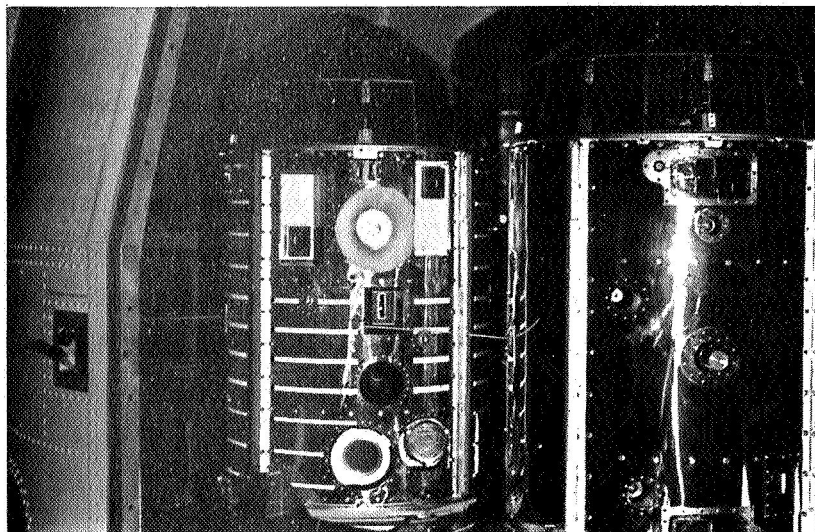|	Clevite AM1, 25° C	In orbit AM0, 62° C
V_{OC}, v	3.40	3.8
I_{SC}, a	0.860	0.982
$P_{40\Omega}$, mw	173	193

FIGURE 60

FIGURE 61

V. DIAGNOSTICS

PHOTOMICROGRAPHS, DARK CHARACTERISTICS

J. M. Bozek, NASA-Lewis

One of the diagnostic techniques used in characterizing the CdS thin-film solar cells is photomicrography. This technique was also used to determine if lateral cracks that had been observed in the CdS thin-film solar cells could be the cause for cell degradation. Figure 62 shows five different sample mounting techniques that were used. They include, from left to right, the large epoxy mount - the specimen is potted in a 2-inch diameter low shrinkage epoxy; the small epoxy mount - the sample is potted in a 1-1/4-inch diameter low shrinkage epoxy; the mechanical mount- the specimen is placed between two metal half cylinders and clamped firmly so that no movement of the sample can occur; the slab mount - the specimen is dipped into epoxy then removed and cured; the acrylic sandwich mount - similar to the mechanical mount except two acrylic half cylinders are used and held together by an adhesive.

Figure 63 shows a pair of photomicrographic cross sections of a CdS thin-film solar cell. The upper cross section shows a sample which was mounted using the slab technique. The lower cross section shows the same sample after it was potted in a small epoxy mount and polished. Lateral cracks are quite evident in the lower cross section. The cracks were caused by improper cell mounting and polishing techniques and not a result or cause of cell degradation. Of the five mounts discussed above, it was determined that the slab mount and mechanical mount are the ones which will result in undamaged cross sections. It is also important to polish the samples in a direction parallel to the sample to reduce the possibility of damage. The reason for failure of the other mounts is believed to be due to the shrinkage of the mount away from the sample thus allowing the sample to move during final polishing.

Dark characteristics of CdS thin-film solar cells were obtained in an attempt to correlate the characteristics with cell behavior. Figure 64 shows a composite dark I-V characteristic curve for eight different CdS thin-film solar cells. Of the eight cells, seven are standard metalized Kapton sub-

strate cells and one is a molybdenum substrate cell of earlier vintage.
The manufacturing date of the plastic substrate cells is also given. As
can be seen in figure 64, there is a large variation in the cells. Some
show good diode characteristics and others show poor diode characteristics.
The cells all had approximately the same efficiency.

From the data at hand, no correlation could be made between light
and dark characteristics. It is planned however to take the dark charac-
teristics before and after the cells have been thermally cycled or other-
wise degraded. It is hoped that this may prove to be a valuable diagnostic
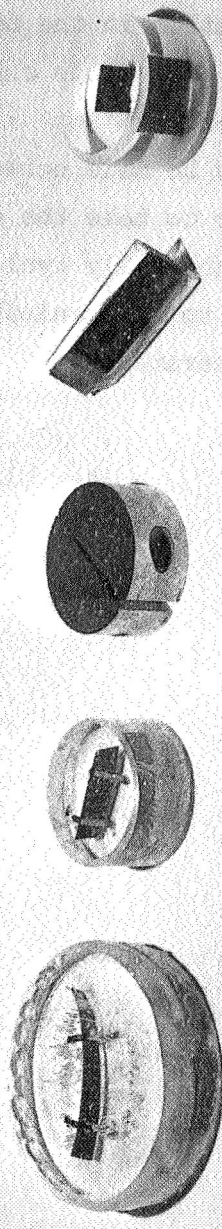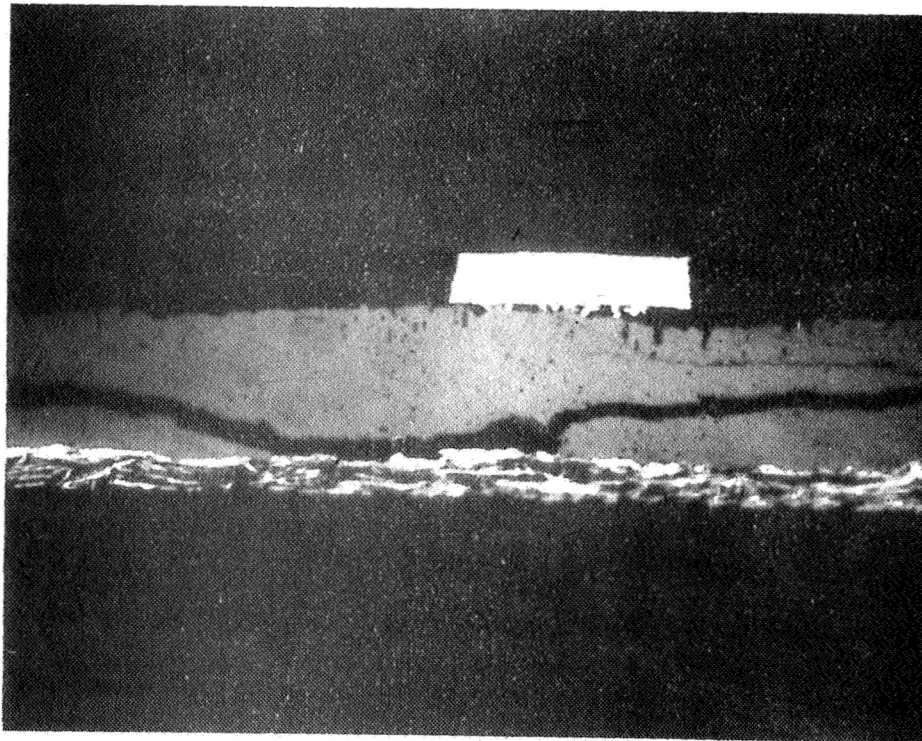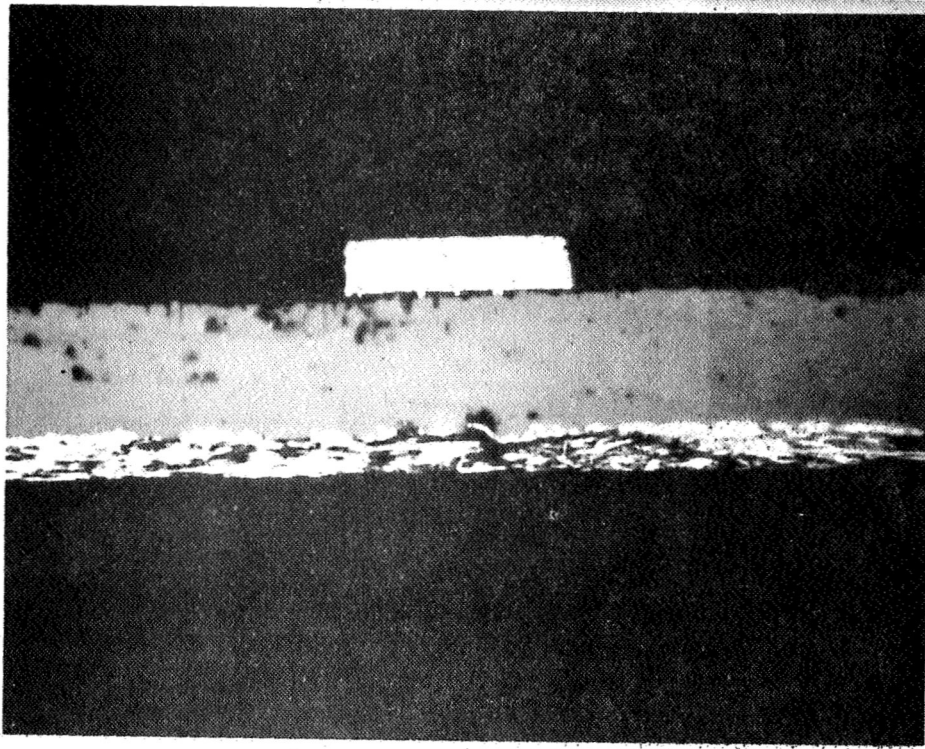technique to enable good and bad cells to be separated.
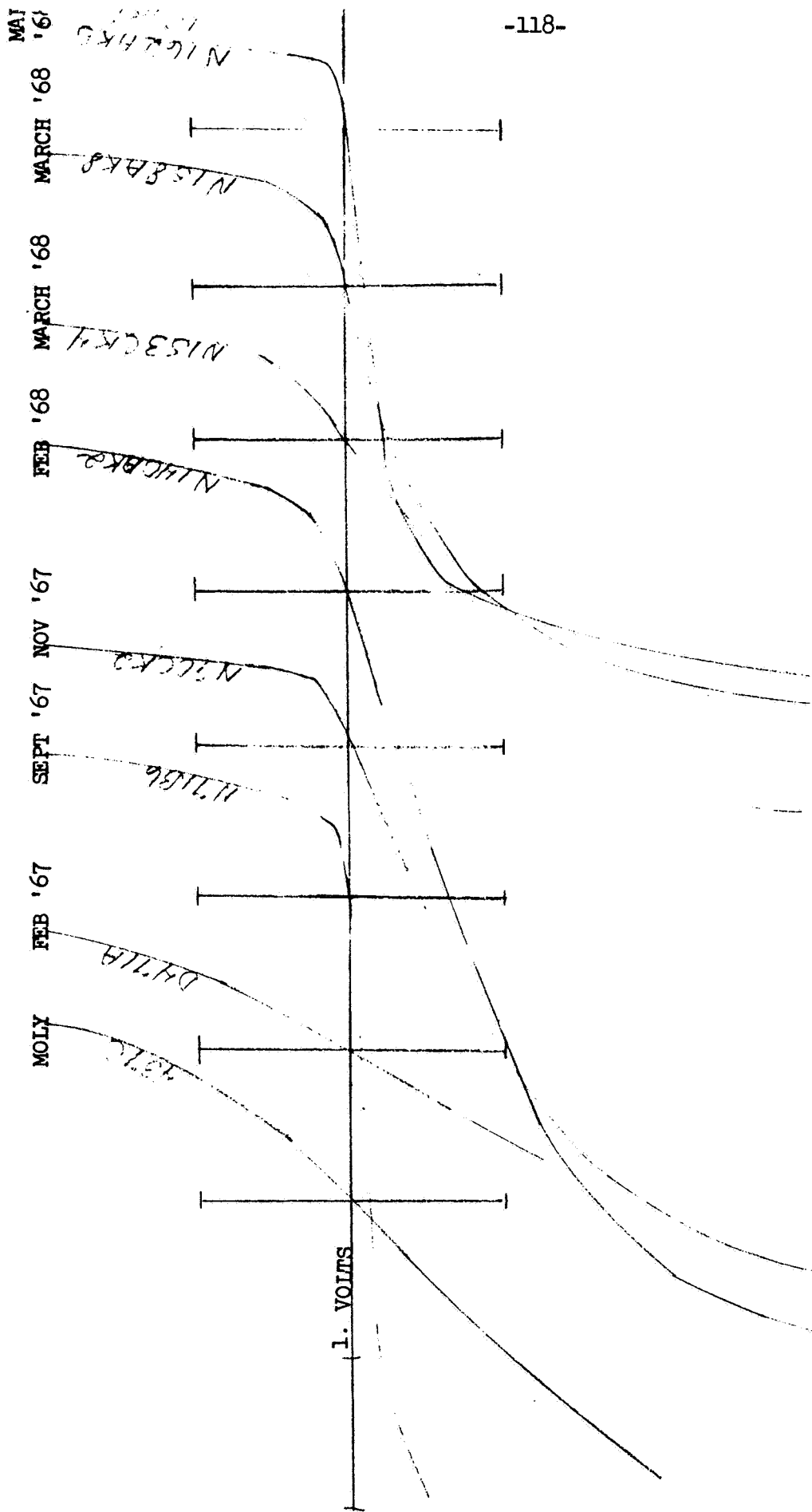
FIGURE 62

E-5000

FIGURE 63

FIGURE 64. DARK I-V PERFORMANCE

ULTRASONIC TESTING, THERMOGRAMS, LIQUID CRYSTALS

A. F. Forestieri, NASA-Lewis

Another diagnostic technique investigated was the use of ultrasonic testing. It was hoped that voids or delaminations in the cell package or poor contact between grid and barrier layer could be found. However, the technique did not prove to be feasible because of reflections from the metal grid.

A third diagnostic technique utilized was thermographic analysis of the solar cells. Thermograms were taken of solar cells before and after thermal cycling. Figure 65 shows a thermogram of a typical solar cell before thermal cycling. The temperature across the cell is seen to be rather uniform. In this case 1/2 ampere was passed through the cell in the forward direction. While the current is on, the surface of the cell is scanned with the thermographic system and the resulting thermogram is obtained. In the thermogram the cold areas appear darker than the warm areas. The temperature range from black to white is 2° C. Figure 66 shows a thermogram of a typical solar cell after thermal cycling. Again the temperature range from black to white is 2° C. A hot spot can be observed. In this case the hot spot was about 2° C hotter than the rest of the cell. It should be mentioned that even though the above case is typical, hot spots have been observed in cells as received without thermal cycling. Investigation of this phenomenon is continuing.

A technique closely associated with thermographic analysis is the use of liquid crystals to study the hot spots observed. A liquid crystal sensitive to temperature changes from 70° to 72° C is applied to either the front or back surface of a thin-film solar cell. Increasing current is then passed through the cell in the forward direction and a change in color of the liquid crystal is noted when the hot spot of the cell reaches the sensitive temperature. Under a microscope the spots can sometimes be resolved to areas about 0.001 inch in diameter. No correlation has yet been made on the location of the hot spots and anomolies in the cell.

E-5000

THERMOGRAMS OF TYPICAL CdS SOLAR CELLS
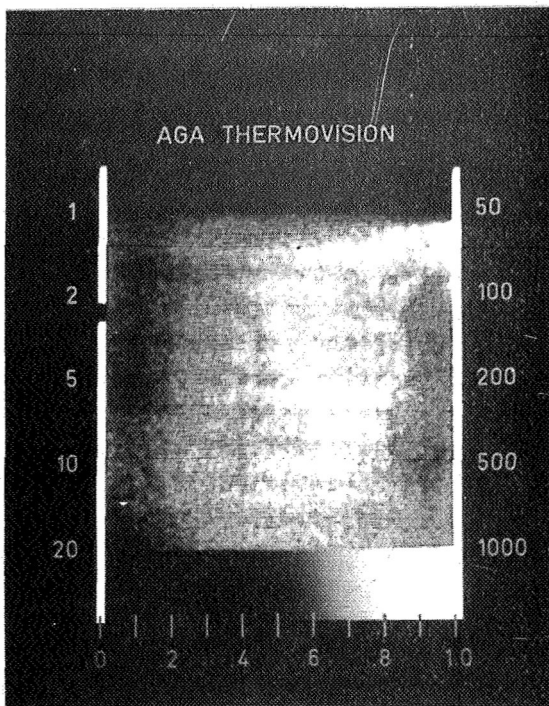SHOWING EFFECT OF THERMAL CYCLING

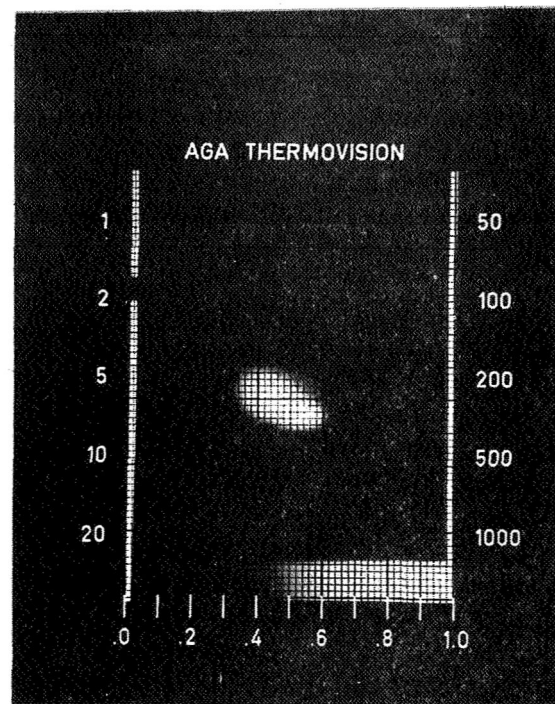FIGURE 65
BEFORE THERMAL CYCLING

FIGURE 66
AFTER THERMAL CYCLING

STRESS ANALYSIS, MAGNETIC MAPPING

F. J. Stenger, NASA-Lewis

A brief analysis was conducted on mechanical stresses in a thin-film solar cell. The results of this investigation are presented in figure 67. A thin two-layer structure labeled A and B with corresponding thickness t_A and t_B is shown. An equation relating the stress in the CdS layer or B layer to the thermal expansion coefficients, Young's modulus, thickness and temperature is given. For this investigation a value of 0.5 was fixed for the ratio of t_B/t_A. Two extremes for the Young's modulus of CdS were chosen, one the single crystal value of $E_B = 14 \times 10^6$ psi and the other a calculated value (for polycrystalline CdS) of $E_B = 0.8 \times 10^6$ psi. A plot of the E term, $(E_A/(E_A/E_B + t_B/t_A))$ versus the ratio E_A/E_B is shown. For $E_B = 0.8 \times 10^6$ psi the E term is essentially constant at about 0.8×10^6 psi for all values of E_A/E_B. These are shown as triangles on the plot. For $E_B = 14 \times 10^6$ psi the E term plotted as circles varies much more with E_A/E_B. Note also the break in the scale on the abcissa.

The table in figure 67 shows the stress in the CdS layer as a function of different materials for layer A. The table is made in two sections. In each section the materials for layer A are listed in order of increasing stress for layer B. The first section was determined for $E_B = 14 \times 10^6$ psi and the second section for $E_B = 0.8 \times 10^6$ psi. In both sections Kapton which is the substrate material for the standard CdS thin-film solar cell, produces a fairly low stress in CdS.

The results of this investigation were not meant to give a complete picture of the stresses involved in a thin-film solar cell. A complete stress analysis would be very time-consuming and difficult.

Another diagnostic technique developed at Lewis deals with mapping the normal component of the magnetic field that is produced by current flowing in a solar cell. Figure 68 is a block diagram of the apparatus used to obtain the magnetic maps. The apparatus consist of a pick-up coil mounted on the pen carriage of an x-y recorder which is controlled to scan in the x-direction and indexed to step in the y-direction. A 1000 Hz signal is

applied to an illuminated solar cell and the pick-up coil is tuned to this frequency. The signal is then amplified and applied as the input to another x-y recorder which is slaved to the scanning recorder. Figure 69 shows in detail how the solar cell is mounted. A metal foil shield conductor is shown in series with the solar cell. Any defect or anomaly in the current path of the solar cell sets up an unbalanced normal magnetic field which is detected by the pick-up coil. The recorder plots a trace of the variation of the signal. An undistorted trace means no unbalanced normal magnetic field is present.

Figure 70 shows a standard 3" x 3" CdS thin-film solar cell which was purposely damaged to test the apparatus. A large hole can be seen to the left of center in the cell. Figure 71 is a magnetic map of this cell. The outline of the cell including the tabs and aligning holes in the tabs is shown as a dotted line. The effect of the hole in the cell and the holes in the mounting tab on the current path through the cell are clearly seen. No current is passing through these areas and therefore an unbalanced normal magnetic field is produced. In the remainder of the cell the current passing through the cell is balanced by the current passing through the metal foil shield conductor and no resultant normal magnetic field is produced. Examination of the map also shows an expected slight unbalance at the edges of the cell.

Figure 72 is a magnetic map of another poor cell. In this cell grid separation from the positive lead tab was evident both on the magnetic map and visually. Figure 73 is a magnetic map of a relatively good cell. No major distortions in the traces are seen except where expected.

$$S_B = \left(\alpha_A - \alpha_B\right)\left(\frac{E_A}{\frac{E_A}{E_B} + \frac{t_B}{t_A}}\right)\Delta T$$

$$\frac{t_B}{t_A} = .5$$

$E_B = 14 \times 10^6 \, PSI$

$E_B = 0.8 \times 10^6$

MATERIAL	$(\alpha_A - \alpha_B)/C°$	(E TERM)	S_B FOR $\Delta T = 100$ °C
$E_B = 14 \times 10^6$			
TANTALUM	(6.5-6.0) .5×10⁶	11.11 ×10⁻⁶PSI	555 PSI
KAPTON	(20-6) 14	.575	805
MOLYBDENUM	(4.9-6.0) -1.1	12.14	-1336 (TENSION on cooling)
TITANIUM	(8.65-6.0) 2.65	9.57	2540
GOLD	(14.22-6.0) 8.22	8.85	7280
COPPER	(17.63-6.0) 11.63	9.92	11540
$E_B = 0.8 \times 10^6$			
TANTALUM	.5	.789	39.5
MOLYBDENUM	-1.1	.793	-87.2
TITANIUM	2.65	.779	206
KAPTON	14	.343	480
GOLD	8.22	.774	636
COPPER	11.63	.782	909

FIGURE 67.
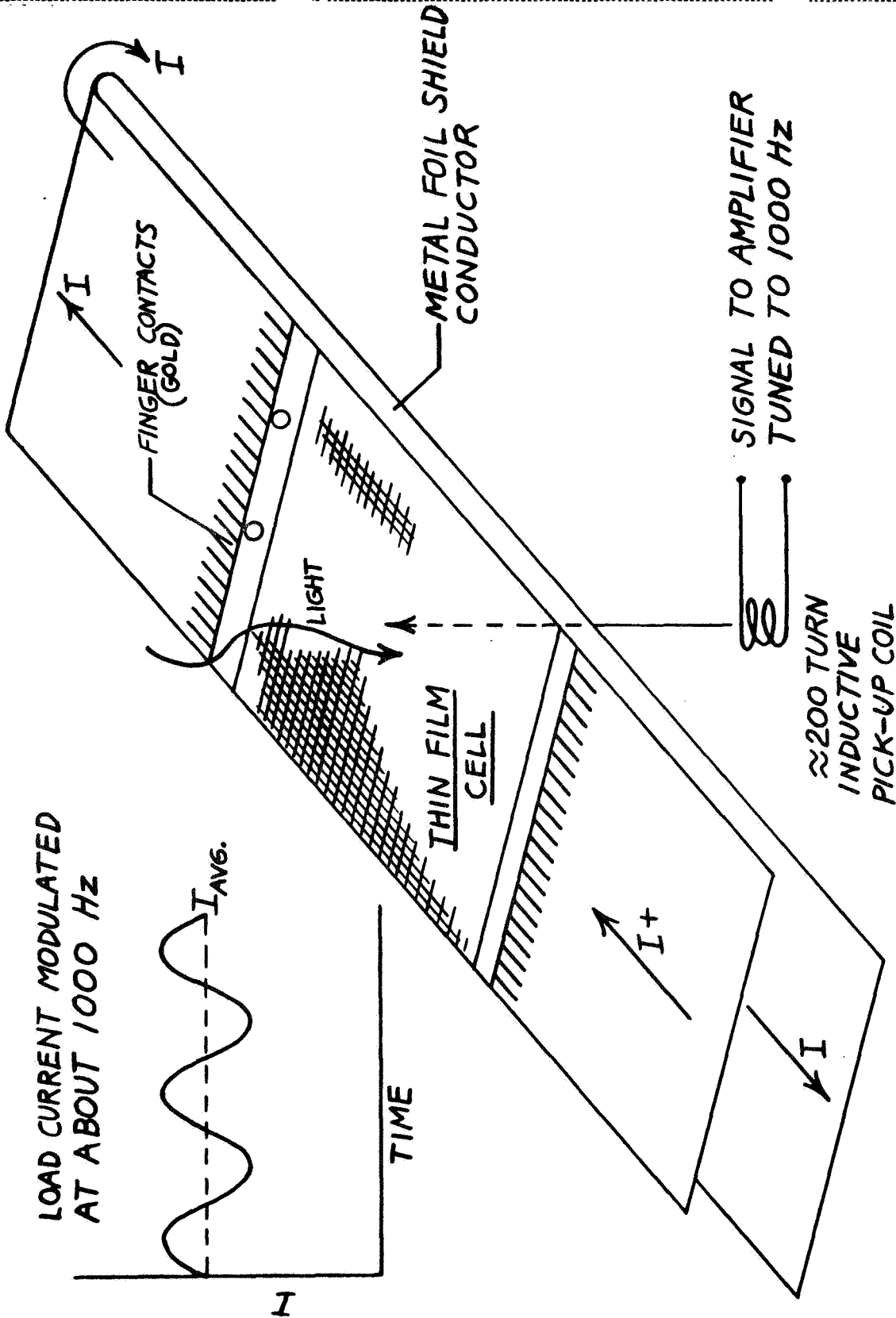
BLOCK DIAGRAM OF MAGNETIC
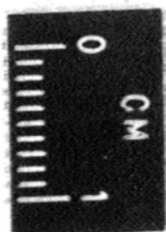MAPPING SYSTEM

FIGURE 68.

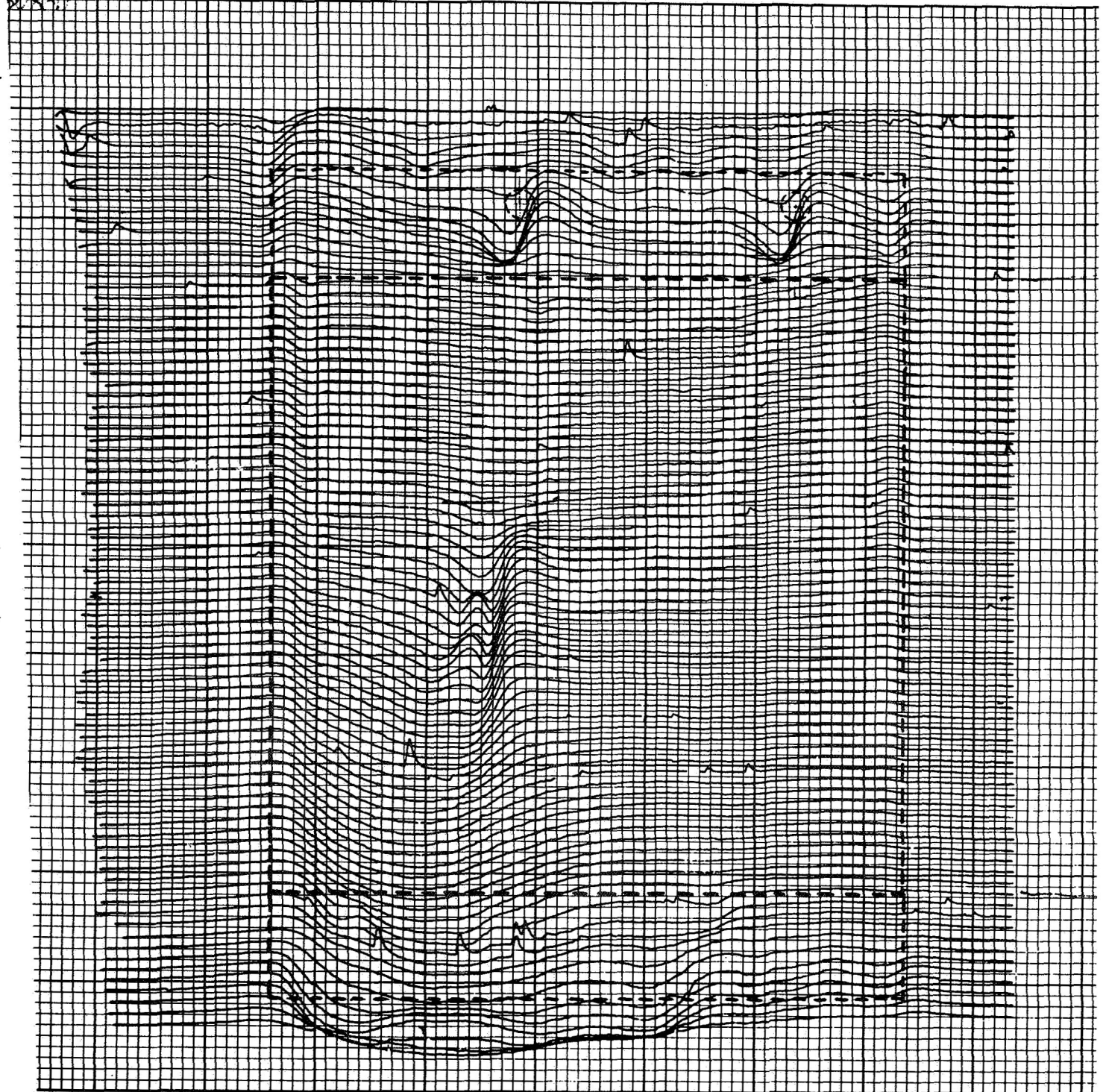FIGURE 69.

E-5000

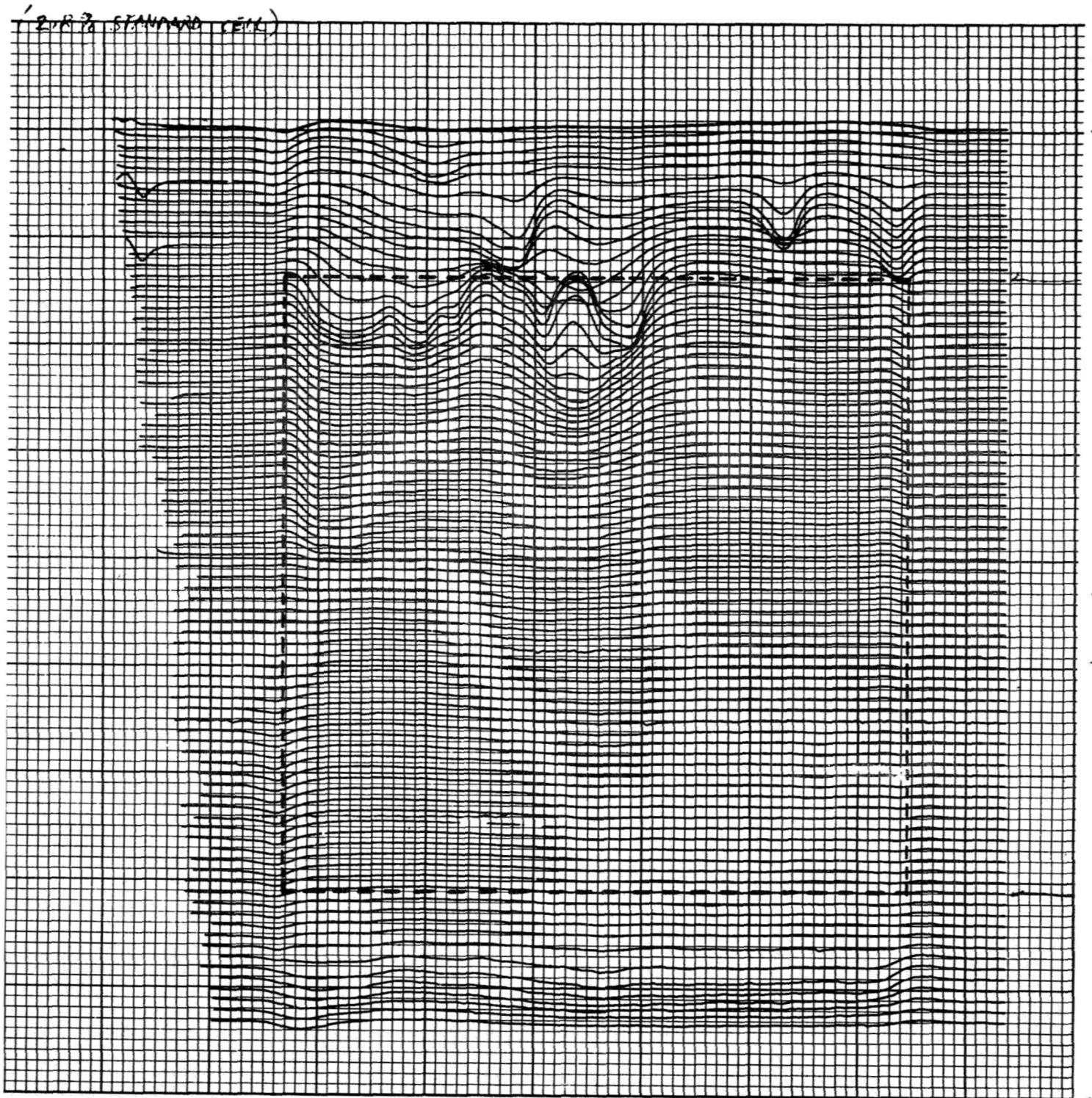FIGURE 70. CELL NO. D-616-CK

FIGURE 71.　D-616-CK

FIGURE 72. N 103 CK1   2.8%
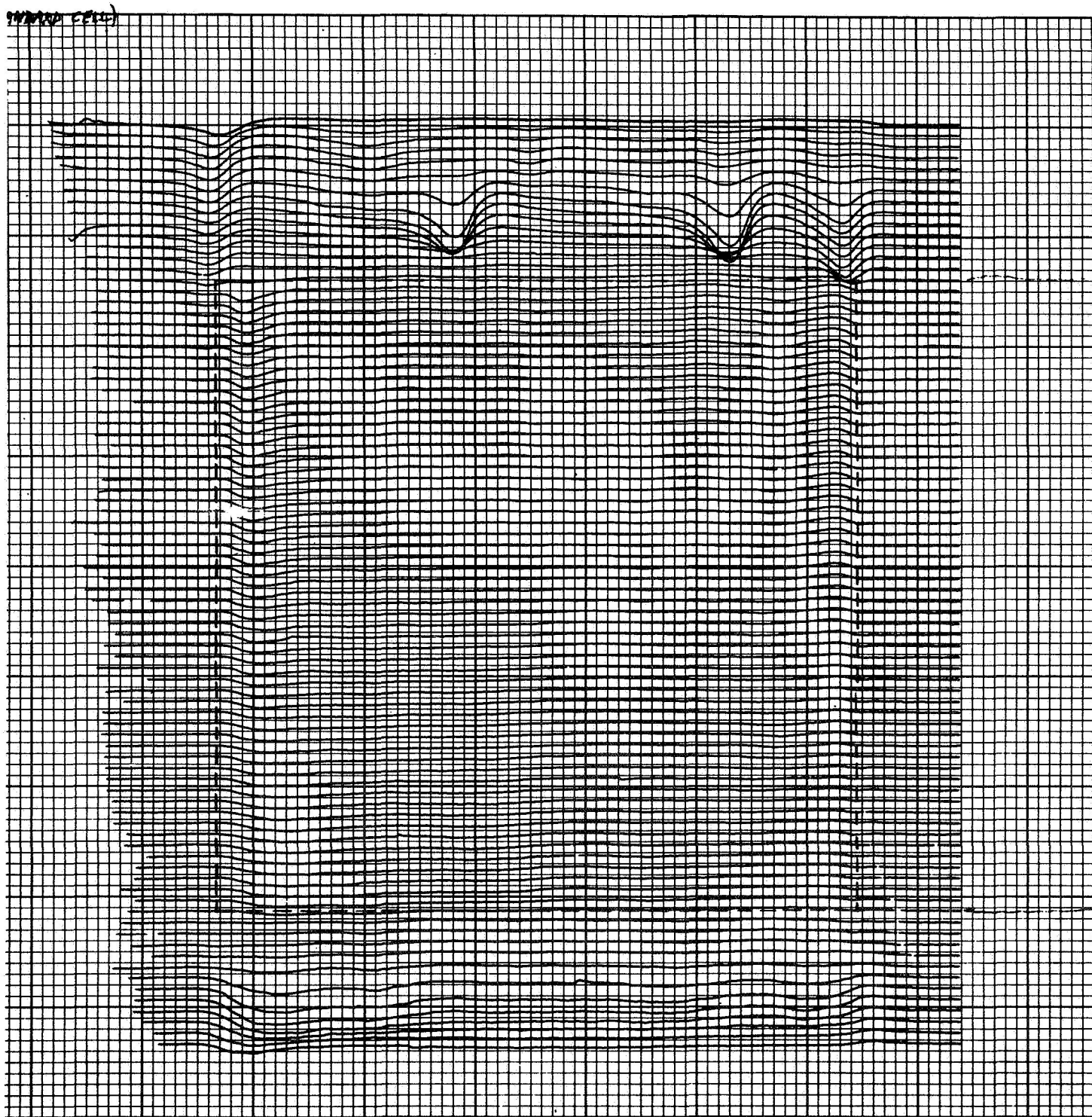
FIGURE 73. N 107 BK4   4.2%

VI. EXPERIMENTAL CELLS AND FABRICATION TECHNIQUES

SUBSTRATE, GRID, AND INTERLAYERS

R. Simonton, Clevite

The discussion will be limited to the substrate, grid, and interlayer portion of the CdS solar cell. Since these studies are adequately covered in Clevite reports, including the Interim Technical Report, NASA CR-72382, dated February 29, 1968, by Shirland, Bower, and Green, only a summary will be given here.

The problems associated with the substrates include:

1. Large thermal expansion of Kapton.

2. Poor conductivity.

3. High series resistance.

4. Pin holes in the CdS grown on both Kapton and molybdenum.

Using thicker layers of PML-Ag did not result in improvements. Other metals have been tried as substrates and although working cells have been obtained we have not had much luck in producing good cells. For example, Al foils give good adhesion of the CdS, but the cells are usually about 1 percent lower in efficiency.

Evaporated metals on plastics don't adhere too well especially when they are later subjected to the CdS evaporation temperatures. Sputtering metals on plastics usually results in an improved metal adherance. The characteristics of the CdS would be most important to know so that changes in the substrate could be evaluated. What the critical parameters are has not been determined. However, all metals tried gave the same 002 hexagonal structure of CdS.

Closely related to the substrate problem is that of the interlayer, since some of the difficulties associated with the substrate materials can be overcome by a judicious choice of the interlayer material. In the present cell Zn is plated onto the PML-Ag layer because it forms a good ohmic contact to the CdS. However, it has several drawbacks, such as:

1. High vapor pressure during CdS evaporation.

2. It will plate out Cu during the barrier formation, if exposed.

3. It may later migrate into the CdS.

4. Zn alloys with Ag.

This last area is being studied at Clevite. The Zn alloys with the Ag flake in the PML after plating to form the hexagonal $AgZn_3$. Very little of this phase is detected later since most goes to AgZn. CdS probably is evaporated onto the AgZn form. This area merits much more study.

Al and Cr have also been used as the interlayer. The Al makes good ohmic contact but the current and fill factor are lower than the standard cell.

Gridding of the cells is another area where improvements would be welcomed. The old Buckbee-mears solid Au grids have been replaced with the Hamilton Watch etched Cu foil grid. This grid is designed to carry more current and is much cheaper. The solid Au grid cost about $9 per 3" x 3" cell compared to under $1 per cell for the present Cu grid. Coarser grids have been examined with the objective of getting higher light transmission and perhaps even reducing the cost. Grid spacings from the present 60 to 50-40-30 lines per inch have been used. All were made with one mil wires. As the grid became coarser the series resistance of the cell increased and the fill factor dropped.

The method of attaching the grid to the top surface of the cell has been a problem. The pressure grid has given way to the present epoxied cemented grid. It has been suspected that some of the instability to thermal cycling is due to the method of grid attachment. New approaches to obtain improved adhesion are:

1. Evaporated Au grid.
2. Electroplated Au grid.
3. Printed grid.

The evaporated Au grid has very good adhesion but cannot be made heavy enough to carry the current load. To overcome this, a standard Au-plated Cu grid is cemented to the evaporated grid with an Au-filled epoxy cement. These cells have been very stable during environmental tests at Lewis and Boeing. One difficulty that still remains is to register the cemented grid over the evaporated grid. Thus far, an extra 10 percent of the active area is being lost because of the poor match. Several solutions are being evaluated. Small area cells (1 x 2 cm) with electroplated Au

grids and printed grids made by a silk-screening technique have been made with efficiencies of 3.5 percent. Samples will be sent to Lewis for evaluation.

THERMAL CYCLING OF SPECIAL CELLS

A. E. Spakowski, NASA-Lewis

Suggested improvements in the cell construction are considered from time to time to overcome suspected weaknesses. As a result, a series of special cells were obtained from Clevite in December 1967 and were subsequently thermal cycled in the space tank. The usual conditions prevailed for these tests. The results are shown in figure 74. This is a log-log plot with the actual degradation plotted as a function of the number of thermal cycles. The cells tested were:

1. Cu sub.: copper substrate cell.

2. Al layer: aluminum interlayer replacing the Zn.

3. Au grid: a solid gold grid used.

4. Low press: standard cells laminated at 10 psia.

5. Evapd. Au: standard cells that have a thin evaporated gold grid with the usual gold-plated copper grid epoxied on top.

None of the special cells showed spectacular gains and most were less stable than the standard cells. However, it must be kept in mind that these special cells were made by the standard process which has been optimized for the standard process steps. It can be speculated that the results might be different were the entire process optimized for the special cell.
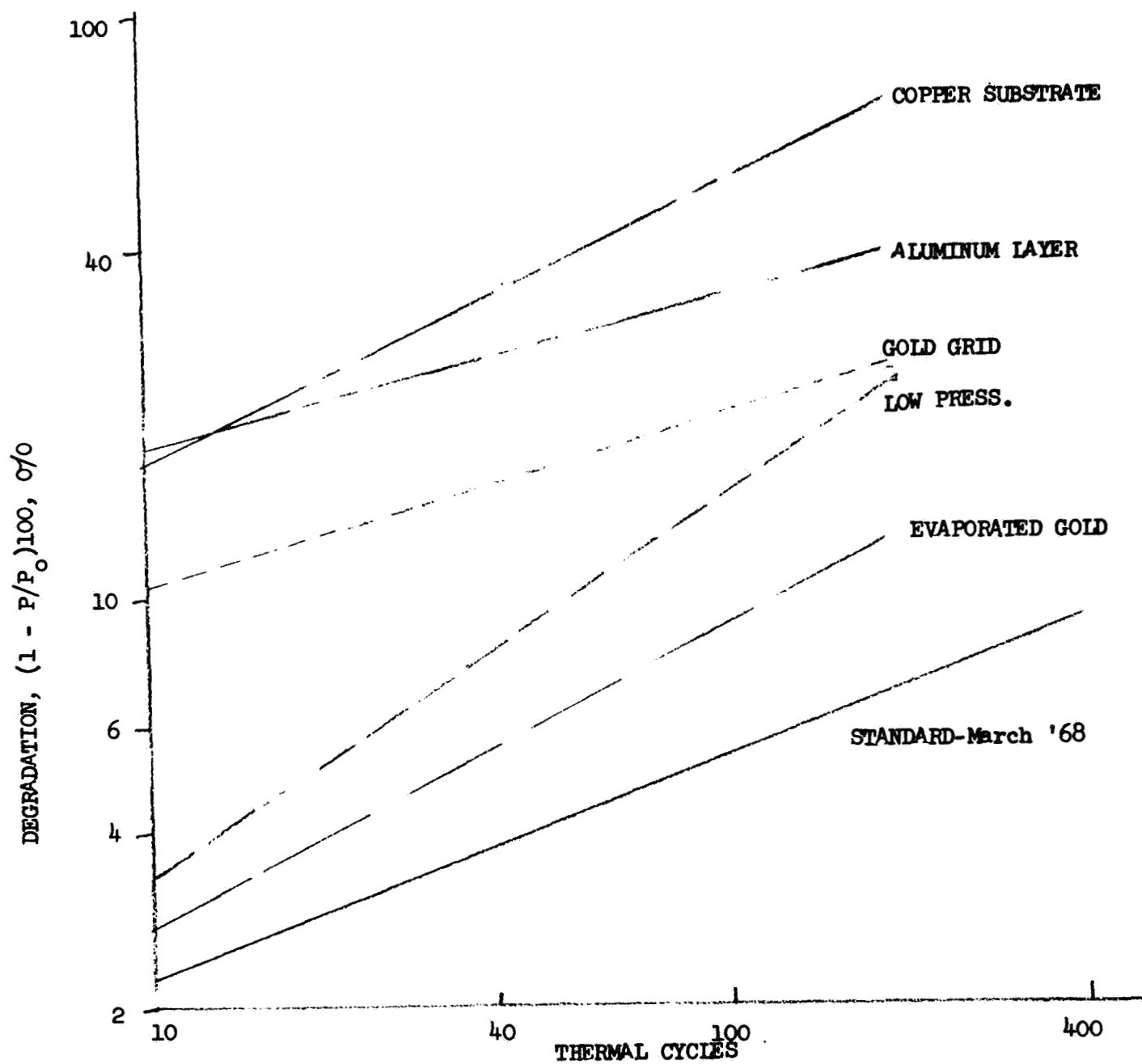
FIGURE 74. STABILITY OF SPECIAL CdS CELLS

COVER PLASTICS

A. E. Spakowski, NASA-Lewis

The evaluation of plastic materials has continued as they are brought to our attention. The primary environmental conditions under which the materials are tested are ultraviolet light and particulate radiation. In most space applications these are the most predominate sources of cover degradation. The two most recent plastics tested are Chemstrand's experimental PPT (polyphenylene tetrazode) and X101. In the next two figures the results from 1 MeV electrons and ultraviolet light exposure are presented as the ratio $T_P/T_{Mylar(reg)}$. T_P is the transmission of the plastic integrated against the solar spectrum at AMO over the wavelength range from 0.3 to 1.2 microns. All total transmissions are referenced to the total transmission of regular Mylar as delivered. Thus the percent total transmission of the #2 sample of X101 as received, compared to regular Mylar was 97 percent.

In figure 75 the results from exposure to 1 MeV electrons are shown. The tests were conducted in the Lewis Dynamitron as previously reported.[1] Weather-durable Mylar starts at 95 percent and drops to 83 percent after 10^{16} e/cm^2 while PPT and X101 (#1 sample) start at 92 and 89, respectively, and drop to 89 and 85, respectively, after 10^{16} e/cm^2. Recently a second sample of X101 (#2) was received with an initial relative transmission of 97 percent which we speculate should result in a 93 percent relative transmission after 10^{16} e/cm^2. Kapton is unaffected in our tests by electrons up to a fluence of 10^{17} e/cm^2, but has a relative transmission of 77 percent at the start of the test.

In figure 76 the results from exposure of the plastics to ultraviolet light are shown. Again the total transmission relative to regular Mylar are plotted against the time in the uv tank. The exposures were conducted at a pressure of 10^{-7} torr on a water-cooled plate held at 25° C. The uv light was from 10 lamps which produced 6 times the AMO radiation from below 0.4 micron at the test plane. As shown in the figure there is a

---

[1]Brandhorst, Henry W., Jr.; and Hart, Russell E., Jr.: Radiation Damage to Cadmium Sulfide Solar Cells. NASA TN D-2932, 1965.

cross over between Kapton and all the other plastics after approximately 600 hours. Thus with the exception of Kapton, all plastics tested are discolored by uv and in some cases even become brittle. One obvious solution is to use thinner Kapton, e.g., 1/2 or 1/4 mil, to increase the total transmission.
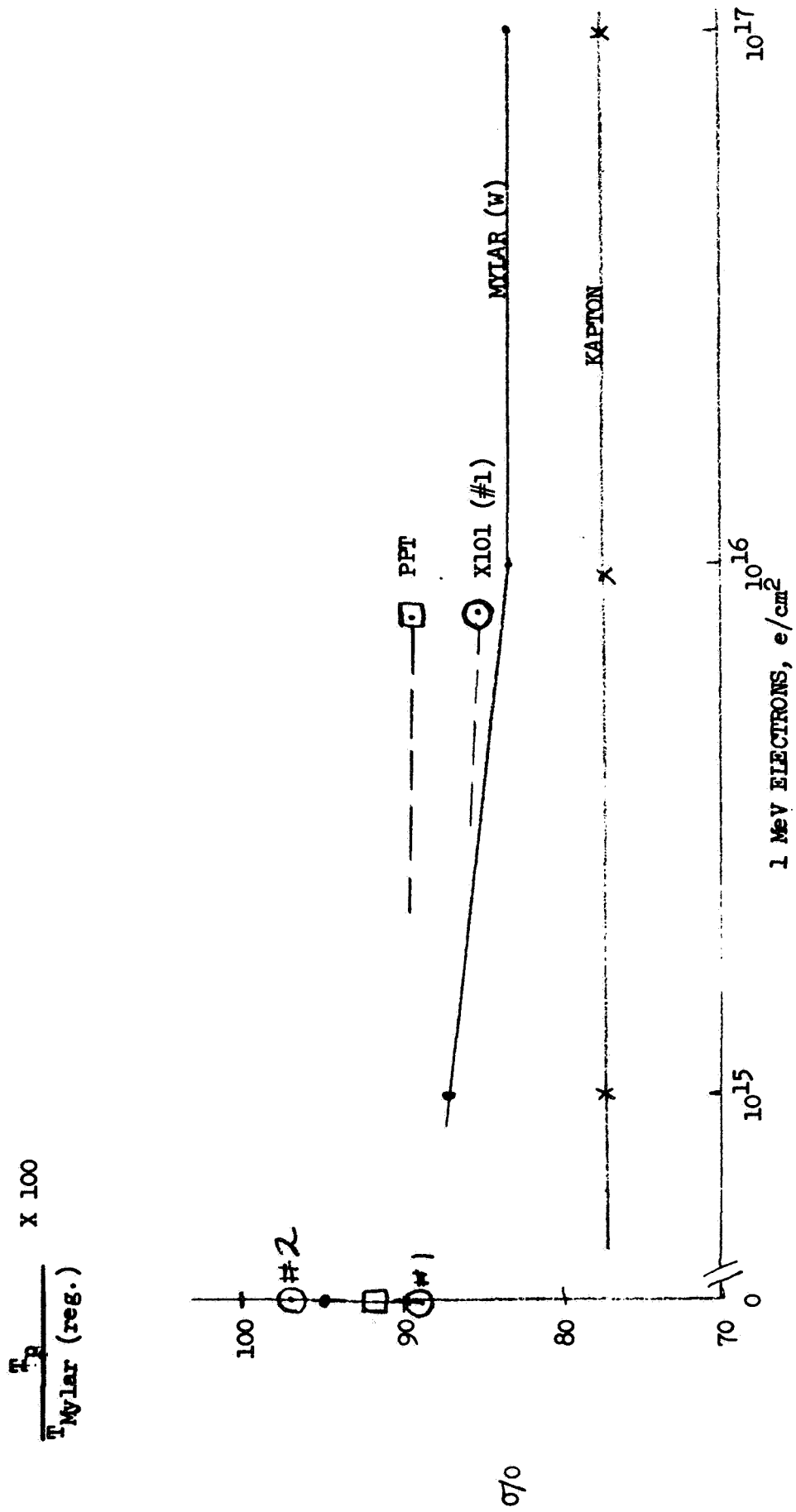
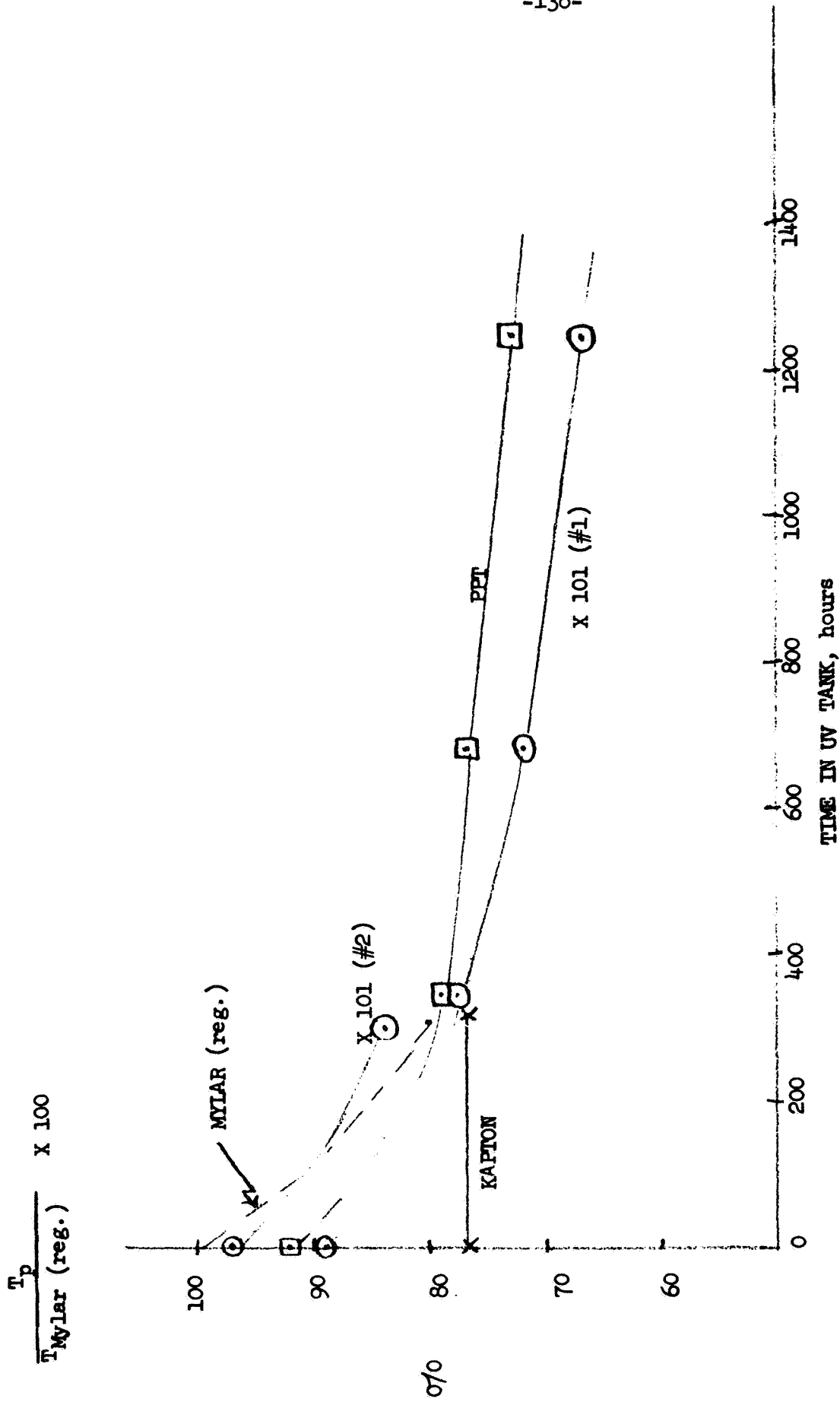FIGURE 75.   DEGRADATION OF PLASTICS BY 1 MeV ELECTRONS

FIGURE 76. DEGRADATION OF TRANSMISSION BY UV

COATINGS

J. M. Bozek, NASA-Lewis

A study was made to determine how various coatings applied to the front and back surfaces of the CdS solar cell would affect its equilibrium temperature in space. In figure 77 the absorptance as a function of the wavelength of light is shown for a CdS cell with a zinc oxide coating on the back surface of the cell. Also shown are the extent of the sun's spectrum, the radiation from a 300° K black body, and the extent of the spectral response of the CdS cell with the arrows designating the peak response. The dotted curve is the transmittance of the OCLI coating which cuts out the uv and is transparent to ir thereby permitting maximum absorption in the range of the cell's response and maximum emittance in the infrared region.

Table XVII shows the equilibrium temperatures attained by a CdS solar cell with various coatings on the front and back. The standard Mylar covered cell (Kapton on the back side) reaches a temperature of 58° C and has an efficiency of 4.0 percent. The 4.0 percent efficiency is 20 percent greater than for a similar Kapton covered cell. If the back of the cell is coated with ZnO, the cell temperature drops to 50° C and as a consequence the efficiency increases to 4.0 percent. If the OCLI (uv) coating is applied to the front and the ZnO to the back, the cell temperature drops to 34° C increasing the η to 4.5 percent. However, since the OCLI coating absorbs some light the corrected η is 4.2 percent. This coating is made up of 16 different layers which should have some bearing on the cost. The best front coating (theoretical) and the ZnO back coating would lower the cell temperature to 17° C and raise the η to 4.8 percent. If it were 100 percent transparent, no loss of η would result. A 41 layer OCLI coating reported in the literature plus the ZnO on the back would result in a cell temperature of 20° C. However, the absorptance of this coating is such as to lower the efficiency to 4.0 percent. Therefore no gain in η over the standard Mylar cell would result. Before these types of coatings can be completely dismissed they should be evaluated in uv and ionizing radiation and any improvement in stability ascertained.

Also shown in Table XVII are a number of antireflection coatings applied to several substrates. These coatings were taken from the literature. Very little improvement is indicated.

TABLE XVII

Temperature Coatings

Type	Temp.	Efficiency (Temp.)	Efficiency (Temp., Trans.)	Comments
Mylar	58°C	4.0%	4.0%	$\sim$ 20% increase over Kapton
ZnO	50°C	4.1%	4.1%	Painted on back
OCLI (U.V) + ZnO	34°C	4.5%	4.2%	$\sim$ 16 layers
Best + ZnO	17°C	4.8%	4.8%	$\sim$ 100% trans.
OCLI (U.V., I.R) + ZnO	20°C	4.7%	4.0%	$\sim$ 41 layers

Antireflection Direct Coatings

Coating	Substrate	Comments
SiO + MgF_2	Mylar	no improvement
SiO + MgF_2	CdS	some moisture degradation
MgF_2	CdS	cracking and moisture degradation
MgF_2	GaAs	little improvement
SiO	GaAs	some improvement
SiO	Si	40% improvement
BaF_2	CdS	soluble in water
CaF_2	CdS	soluble in water
LiF	CdS	radiation damage
$CaCO_3$	CdS	decomposes when heated
Al_2O_3	CdS	decomposes when heated

FIGURE 77. SPECTRAL CHARACTERISTICS OF THE CdS SOLAR CELL

ATTENDEES AT

CADMIUM SULFIDE THIN-FILM SOLAR CELL REVIEW

June 11-12, 1968

Miss E. Anagnostou	-- NASA Lewis Research Center
Dr. S. J. Begun	-- Clevite Corporation
Mr. D. T. Bernatowicz	-- NASA Lewis Research Center (Chairman)
Mr. J. M. Bozek	-- NASA Lewis Research Center
Dr. H. W. Brandhorst	-- NASA Lewis Research Center
Mr. W. Dunn	-- Clevite Corporation
Mr. A. F. Forestieri	-- NASA Lewis Research Center
Mr. M. P. Godlewski	-- NASA Lewis Research Center
Dr. H. Jaffe	-- Clevite Corporation
Mr. T. M. Klucher	-- NASA Lewis Research Center
Mr. C. H. Liebert	-- NASA Lewis Research Center
Dr. B. Lubarsky	-- NASA Lewis Research Center
Mr. R. M. Masters	-- NASA Lewis Research Center
Mr. H. Nastelin	-- Clevite Corporation
Mr. A. F. Ratajczak	-- NASA Lewis Research Center
Dr. L. Rosenblum	-- NASA Lewis Research Center
Mr. F. Sauerland	-- Clevite Corporation
Miss R. Schalla	-- NASA Lewis Research Center
Mr. L. R. Scudder	-- NASA Lewis Research Center
Mr. L. Shiozawa	-- Clevite Corporation
Mr. F. Shirland	-- Clevite Corporation
Mr. R. Simonton	-- Clevite Corporation
Mr. J. J. Smithrick	-- NASA Lewis Research Center
Mr. A. E. Spakowski	-- NASA Lewis Research Center
Dr. A. Stanley	-- Lincoln Laboratories
Mr. F. J. Stenger	-- NASA Lewis Research Center